Plant Design Report Series
Tehdassuunnittelun raporttisarja No. 76
Espoo 2004

PARTICLE PRODUCTION BY SUPERCRITICAL ANTISOLVENT PROCESSING TECHNIQUES

Markku Rantakylä

TEKNILLINEN KORKEAKOULU
TEKNISKA HÖGSKOLAN
HELSINKI UNIVERSITY OF TECHNOLOGY
TECHNISCHE UNIVERSITÄT HELSINKI
UNIVERSITE DE TECHNOLOGIE D'HELSINKI

Plant Design Report Series
Tehdassuunnittelun raporttisarja No. 76
Espoo 2004

PARTICLE PRODUCTION BY SUPERCRITICAL ANTISOLVENT PROCESSING TECHNIQUES

Markku Rantakylä

Dissertation for the degree of Doctor of Technology to be presented with due permission for public examination and debate in Auditorium Ke2 at Helsinki University of Technology (Espoo, Finland) on the 11th of December, 2004, at 12 o'clock noon.

Helsinki University of Technology
Department of Chemical Technology
Laboratory of Chemical Engineering and Plant Design

Teknillinen korkeakoulu
Kemian tekniikan osasto
Kemian laitetekniikan ja tehdassuunnittelun laboratorio

Distribution:
Helsinki University of Technology
Laboratory of Chemical Engineering and Plant Design
P.O. Box 6100
FIN-02015 HUT
Tel. +358-9-451 2634
Fax. +358-9-451 2694
E-mail: markku.rantakyla@helia.fi

ISBN 951-22-7400-0 (print), ISBN 951-22-7401-9 (pdf, available at http://lib.hut.fi/Diss/)
ISSN 0358-0776

Espoo 2004

Rantakylä, M., *Particle Production by Supercritical Antisolvent Processing Techniques*. Helsinki University of Technology, Plant Design Report Series No 76, ISBN 951-22-7400-0, ISSN 0358-0776

Keywords: Supercritical antisolvent processing, SAS, particle production, modelling, feasibility, capital and manufacturing cost.

ABSTRACT

This thesis discusses particle production by supercritical antisolvent processing (SAS) techniques by looking the fundamentals and applications of the method with some case studies. The final aim of this work is however to consider the SAS particle production process feasibility. In the process studied the solid is dissolved in a conventional solvent and the solution is sprayed continuously through a nozzle into the subcritical or supercritical fluid. The dispersion of solution in the fluid leads to an expansion of the droplets and at the same time an extraction of the liquid into the fluid occurs. The solvent power of the conventional solvent decreases dramatically and supersaturation leads to the precipitation of particles.

A static variable volume view cell (VVV-cell) is a useful and fast way to find out the appropriate combinations of the solvent and the gaseous antisolvent for a given solid. Often pharmaceutical materials are expensive and not available in large amounts, which makes it impossible to make phase separation studies with laboratory or production scale SAS equipment. However in VVV-cell experiments it is possible to use small amounts of materials and fast examine the influence of recrystallization temperature, pressure and concentration. But it is not possible to conclude by using only VVV-cell experiments, what kind of particles (size distribution, crystal habit and morphology) there will be produced in SAS process, because of the different formation dynamics and residence times.

The present study showed that in the supercritical state the variables, such as density of CO_2 and temperature, have a greater effect on the particle size than the model of droplets predicts. The liquid side mass transfer seems to control the studied polymer material particle size. In poly(L-lactic acid) particle formation with dichloromethane solvent and CO_2 antisolvent by SAS technique it is advantageous to use low temperature and high pressure, in which conditions the mass transfer effect and volumetric expansion of droplets to produce high supersaturation will be favourable. In SAS process it is not possible to influence the initial droplet size by varying process variables (temperature, pressure and flow rate) in a typical operating range with a similar nozzle. Therefore the mass transfer coefficient of the liquid phase should be maximized to produce a high supersaturation fast when a small particle size is needed.

Supercritical fluid technology is considered to be an innovative and promising way to design particles. In this thesis the applicability of two special supercritical precipitation techniques was studied. In the first case the results show, that it is possible to produce completely amorphous particles by spraying a methanol solution of sodium cromoglycate into supercritical carbon dioxide. The most significant parameter affecting the crystallinity was the residual methanol

concentration in the particles. In the second case the results show, that cholesterol can be selectively extracted / crystallized at high purity, from a one phase mixture which contains lipids and cholesterol dissolved in pressured CO_2. In this simple cholesterol production process no liquid solvents are needed. The egg yolk phospholipid was the most suitable raw material for the tested method. Because the concentration of cholesterol in the fluid stream is low, this method is not economically viable in industrial scale

The work clearly demonstrated that to recrystallize fine particles with SAS techniques in an industrial scale the price of the products must be high. These products would be chemical intermediates, biological and pharmaceutical compounds. On the other hand, if the compound properties are waxy or soft or the products are thermally unstable compounds, it may be feasible to use antisolvent formation techniques also for less expensive products, if the method makes the production possible. The manufacturing cost of SAS process is capital intensive. An estimated manufacturing cost for a new GMP plant is around 50-300 Euro/kg product without a feedstock price. This is for a 4000 to 8000 kg/year production rate and 5-10 wt% feed concentration of the starting material in an organic solvent. An effective way to decrease the manufacturing cost is to increase the raw material concentration in solvent. It is favourable to design a process for production rate over 2000-3000 kg/year and to use over 5 wt% feed concentration. Below those values the manufacturing cost increases dramatically.

Preface

The research in this thesis was done at the Processes of the Technical Research Centre of Finland (VTT). Most of the work was carried out during the years 1995-2003 within the TEKES-projects; Particle tailoring with supercritical fluids (1995-1999) and Drug 2000, Supercritical fluid techniques in microparticle formation (2000-2006).

I am most grateful to my supervisor, Prof. Markku Hurme for his invaluable guidance in the course of this work. Likewise I am most grateful to my chief Olli Aaltonen for his support and encouragement during this work.

To my many colleagues and co-workers I extend thanks for mutual effort, pleasant co-operation and hard work carried out together. Special thanks go to my colleague Matti Jäntti at VTT Processes for programming the mathematical model to a computer. Warm thanks are due to my colleagues Martti Alkio, Antero Laitinen and Susanna Jaarmo, at VTT Processes for valuable help for this research work. I wish also thanks to Jouko Rakkolainen at VTT Processes for his excellent technical assistance.

Financial assistance of this project from TEKES and Orion Corporation Orion Pharma is gratefully acknowledged.

My most sincere thanks are due to my family, my parents, by brothers and my friends for their unselfish support during this work. Finally, I would like to dedicate this thesis to my children Julia and Heini.

Helsinki, on the 21th of November, 2004

Markku Rantakylä

Contents

Symbols and abbreviations

Symbols

A_d	droplet surface, m^2
BC	total battery limits capital cost, million Euro
C_{drag}	drag coefficient
ΔC_i	concentration gradient of component i between gas-liquid interface, kg m^{-3}
D	diffusion coefficient, m^2 s^{-1}
D_{11}	self-diffusion coefficient of component i, m^2 s^{-1}
D_{12}	diffusion coefficient of the CO_2 molecule in liquid solvent, m^2 s^{-1}
D_{21}	diffusion coefficient of the liquid solvent molecule in CO_2 phase, m^2 s^{-1}
D_{32}	diffusion coefficient of the heavy solute molecule in liquid solvent, $m^2 s^{-1}$
d_d	droplet diameter, m
$d_{d\max}$	maximum droplet diameter produced, m
d_{nozzle}	diameter of the air discharge, m
d_p	particle diameter, m
d_{pipe}	diameter of pipe, m
d_{32}	droplet with the same surface-to-volume ratio as the total droplet population (Sauter mean diameter), m
G	gas or fluid mass flow rate, kg s^{-1}
Gr	dimensionless Grashof number
g	gravity acceleration, 9.81 m s^{-2}
K_i	component i equilibrium constant
K_G	overall mass transfer coefficient in gas phase, m s^{-1}
K_L	overall mass transfer coefficient in liquid phase, m s^{-1}
K_x	overall mass transfer coefficient, m s^{-1}
k	mixture parameter describing the intermolecular interaction between the unlike molecules
k_G	mass transfer coefficient in gas phase, m s^{-1}
k_L	effective internal mass transfer coefficient in liquid phase, m s^{-1}
L	liquid mass flow rate, kg s^{-1}
M	molecular weight, g mol^{-1}
M_n	number average molecular weight, g mol^{-1}
M_1	molecular weight of CO_2, g mol^{-1}
M_2	molecular weight of liquid, g mol^{-1}
M_3	molecular weight of heavy solute, g mol^{-1}
MP	melting point, K
m	slope of equilibrium curve
m_j	number of droplets of size d_j
m'_j	number of droplets for volume feed V
N_i	mass transfer rate of component i, kg s^{-1}
n	particle size distribution function
n_i	number of particles or droplets in size interval i
P	pressure, Pa
P_c	critical pressure, Pa
P^{Sat}	saturation pressure, Pa
R	universal gas constant, 8.314 J mol^{-1} K^{-1}

Re	dimensionless Reynolds number
Re_d	droplet Reynolds number
Re_n	nozzle Reynolds number
Sc	dimensionless Schmidt number
Sh	dimensionless Sherwood number
T	temperature, K
T_c	critical temperature, K
T_R	reduced temperature (T/T_c)
t	time, *s*
t_c	contact time between the two phase, s
U	velocity, m s^{-1}
U_d	droplet velocity, m s^{-1}
U_G	gas velocity, m s^{-1}
U_{GL}	relative velocity between gas and liquid, m s^{-1}
V	volume, m^3
V_0	volume of pure liquid phase at atmospheric pressure, m^3
ΔV_E	relative volume expansion
We	dimensionless Weber number
x	mole fraction
x_i	component *i* mole fraction in liquid phase
y_i	component *i* mole fraction in gas phase

Greek letters

ϕ	association factor for the solvent
η	stand for the effect of the different size and structure of unlike components
φ	fugacity coefficient
φ_i^G	fugacity coefficient of *i* in gas phase
φ_i^L	fugacity coefficient of *i* in liquid phase
μ	dynamic viscosity, Pa s
μ_G	gas or fluid viscosity, Pa s
μ_{CO_2}	CO_2 viscosity, Pa s
μ_L	liquid viscosity, Pa s
μ_{0,CO_2}	CO_2 low-pressure viscosity, Pa s
ν	molar volume, cm^3 mol^{-1}
ν^{OS}	molar volume of pure solid, cm^3 mol^{-1}
ρ	density, kg m^{-3}
ρ_c	critical density, kg m^{-3}
ρ_d	droplet density, kg m^{-3}
ρ_G	gas density, kg m^{-3}
ρ_L	liquid density, kg m^{-3}
ρ_R	reduced density (ρ/ρ_c)
$\Delta\rho$	density difference at the solid surface as compared to the bulk, kg m^{-3}
σ	interfacial tension, N m^{-1}
σ_{lnd}	standard deviation
ω	acentric factor

Subscripts

c	critical value
d	droplet
G	gas or fluid phase
L	liquid phase
n	number of molecules
p	particle
S	solid phase
V	vapour phase
0	pure solvent or antisolvent
1	supercritical antisolvent (CO_2)
2	organic solvent (dichloromethane)
3	heavy solute (polymer)

Abbreviations

ASES	aerosol solvent extraction system
CE	capital cost of equipment
CHO	cholesterol
CP	critical point
DC	dielectric constant
DCM	dichloromethane
DMF	N,N-dimethyl formamide
DMSO	dimethyl sulfoxide
EOS	equations of state
GAS	gas anti-solvent system
GMP	good manufacturing practice
GPC	gel permeation chromatography
HPLC	high pressure liquid chromatography
ID	inner diameter
LCEP	lower critical end point
L-PLA	poly(L-lactic acid)
NCL	near-critical liquid
NEP	number of experiment
PGSS	particles from gas saturated solutions
PL	phospholipid
PVT	pressure-volume-temperature
RESS	rapid expansion of supercritical solution
SAS	supercritical antisolvent precipitation
SC	equipment's capacity
SCF	supercritical fluid
SEDS	solution enhanced dispersion by supercritical fluids
SEM	scanning electron microscopy
SF	minimizing function of the Simplex search method
SFC	supercritical fluid chromatography
SFE	supercritical fluid extraction
SFF	supercritical fluid fractionation
SFN	supercritical fluid nucleation

TG	triglycerides
THF	tetrahydrofuran
TP	triple point
TPH	threshold pressure
UCEP	upper critical end point
VTT	Technical Research Centre of Finland
VVVC	variable volume view cell

1. INTRODUCTION

Micrometer range organic particles with narrow size distributions are needed, for example, in the pharmaceutical industry. The conventional techniques such as milling, spray drying and solvent evaporation are not always suitable for producing fine and pure particles. There are practical problems associated with many of the above processes. Spray drying can thermally denature compounds, milling produces broad size distribution and solvent/emulsion evaporation techniques often leave residual solvents that are difficult to remove [1]. Certain dyes, chemical intermediates, biological and pharmaceutical compounds which are "waxy" or "soft", certain specialty polymers, and explosives are a few categories of difficult to process materials [2]. Crystallization with compressed gases or supercritical fluids seems to be a promising new technique. The use of near critical or supercritical fluids as solvents or antisolvents in particle production has been shown by numerous researchers to be useful in modifying particle properties such as particle size, size distribution, crystal habit and morphology [3]. Supercritical fluid nucleation can be an attractive recrystallizing method for many solids, especially for some difficult to comminute or recrystallize materials such as pharmaceuticals used in dermal salves, injectable solutions, and ophthalmological preparations, which require ultra-fine and uniform particles. The use of supercritical fluids allows a precise control of the crystallization process and is capable of generating very small and uniform particles. Another advantage is the easy separation of the antisolvent from the particles after precipitation. It is therefore possible to avoid large amounts of solvent by-products and offer a potentially advantageous circulation of the solvent and antisolvent [4].

Several processes of applying supercritical fluids in spraying devices have been proposed and investigated, as reviewed by Jung and Perrut [5]. Generally the three basic techniques are distinguished [6]. The earlier process is known as Rapid Expansion of Supercritical Solution (RESS). A solid is dissolved in a supercritical fluid, which is expanded adiabatically within a capillary nozzle to gaseous condition creating high supersaturation and thereby causing rapid nucleation and precipitation of the desired product as fine particles. In the Particles from Gas Saturated Solutions (PGSS) techniques the supercritical fluid is used for formation of particles from gas saturated solutions.

The other technique is currently called Gas Anti-Solvent system (GAS). In one version of this technique the supercritical fluid is used in batch mode. The solid is dissolved in a conventional solvent. The solution is introduced into a supercritical fluid (antisolvent) leading to a rapid volume expansion of the solution. As a result, the solvent power of the conventional solvent decreases and supersaturation triggers off the precipitation of particles. After the solid has precipitated out fresh antisolvent is added to flush away the solvent.

The semi-continuous and continuous gas anti-solvent techniques are known as Aerosol Solvent Extraction System (ASES) [1,7], Supercritical Antisolvent Precipitation SAS [8,9] and Solution Enhanced Dispersion by Supercritical fluids

(SEDS) [10,33]. The general aim of using supercritical technique is to improve mass transfer by generating fine drops with a high surface area [11] and thereby to increase mass transfer between a drop and drying medium. In the continuous GAS technique mass transfer occurs between the dispersed drops and the surrounding gas phase. In the ASES and SAS techniques the solid is dissolved in a conventional solvent and the solution is sprayed continuously through a nozzle into the supercritical fluid. The dispersion of solution in the supercritical fluid leads to an expansion of the droplets and at the same time an extraction of the liquid into the fluid occurs. The solvent power of the conventional solvent decreases dramatically and supersaturation leads to the precipitation of particles. The SEDS technique resembles ASES and SAS techniques, but in SEDS the solution is sprayed continuously with a compressed gas or supercritical fluid antisolvent through a two-fluid nozzle.

The thesis aims at solving four problems:
1) Generally the problem in gas antisolvent processing is to find for a given solid the appropriate combinations of the solvent and the gaseous antisolvent. The gas (antisolvent) must be totally miscible with the solvent in the desired temperature and pressure range. The variable volume view –cell (VVV-cell) is mainly used for the solubility measurements of compounds. Also in this work the VVV-cell is used for finding the feasible operating conditions for particle formation.

2) Before successful particles formation can be started, it is necessary to understand the mechanism, which controls particle sizes in the near critical and supercritical regions. In this work is a simple particle size model for the continuous Gas Antisolvent technique is developed. Also the phenomena, which control particle size in the near critical and supercritical regions, are examined. The proposed mean particle size control mechanisms are mass transfer, jet break up and hydrodynamics. The mathematical model developed includes a model of initial droplet size at exit of nozzle, model of ternary fluid phase equilibrium inside the droplet and a model of mass transfer between a drying droplet and the drying medium as a function of time. The model was tested with experimental results from spraying poly(L-lactic acid) in dichloromethane into carbon dioxide. The values of experiments and the calculated particle sizes were compared.

3) Supercritical fluid technology is considered to be an innovative and promising way to design particles [5]. In this thesis two special applications of the supercritical precipitation technique are shown; amorphous pharmaceutical particle production with supercritical antisolvent precipitation (SAS) and selective extraction/crystallization of cholesterol from supercritical CO_2. The later crystallization process is not antisolvent technique, but it is an interesting way to produce pharmaceutical products, where no liquid solvents are needed.

4) Economic considerations are obviously the major constraint of any engineering design. A limited number of papers have been published on the economic issues of supercritical fluid processes. In this thesis a quick calculation tool for estimating the total battery limit capital costs of an SAS process is developed. A further aim is to study the effect of production rate and feed concentration on the

capital cost. Also a cost calculation tool is developed to study the micronization costs of particles in a large semi-continuous SAS process.

1.1. SUPERCRITICAL FLUID TECHNOLOGY IN PHARMACEUTICAL APPLICATIONS

It has been know for more than a century that supercritical carbon dioxide can dissolve non-volatile solvent. Supercritical fluid technology has applications in the food industry separations, chemical processing, pharmaceuticals polymers and environmental, textile, forest product industries and in the cleaning of precious parts. In the 1980's many supercritical fluid industrial applications were studied, including the purification of surfactants and pharmaceuticals, fractionation of polymeric materials and chemical reactions and polymerization's. In the same period, interest in using supercritical fluids for precipitation and crystallization process was developing for pharmaceutical materials and this activity has steadily increased over recent years [28].

The supercritical fluids are extremely useful in designing stable protein formulations. They offer viable alternatives to process peptides and proteins without affecting the pharmacological activity [28]. Several applications of supercritical fluid technology in pharmaceutical industry are experienced, such as:

Supercritical fluid extraction (SFE):
SFE is extensively used in industries such as petroleum, chemical, textile industries and as to produce high quality extracts from natural raw materials for the food industry. In the pharmaceutical industry this is more challenging because the standards for recovery and reproducibility are more rigorous than for other applications [28]. It is known that some of plants, used as origin for supercritical extracts contain pharmaceutical active substances, which are extractable by supercritical carbon dioxide. Nutraceuticals for instance contain such substances such as gamma ionolein acid, which has a healthy effect. Plant seeds from black currant, grape, borage, saw palmetto are extracted in production scale to recover this nutritional components even for use in pharmaceutics [12].

Chemical reactions:
Several chemical reactions, such as oxygenation, hydroformulation, and alkylation have been studied in supercritical fluids [13]. Supercritical fluid acts as ideal medium for enzyme-mediated reactions as enzymes retain their activity when exposed to supercritical fluids. Depending reaction they provide efficient processes with increased yields and increased selectivity [14,15]. Review articles concerning enzymatic catalysis in supercritical fluids are available [16,17,79].

Supercritical fluid chromatography (SFC):
SFC is one of the most successful areas of supercritical fluids and has become a commonly used analytical technique for the separation and analysis of drug molecules [28]. Preparative SFC can be used for separation of high pressure extract or for cleaning of product mixtures from reactions. It is also possible to concentrate an extract by removing impurities or unwanted by-products [12].

Industrial development is now restricted to purification of polyunsaturated fatty acids and enantiomers [196]. Preparative SFC is a technically feasible process for purifying a polypeptide from other peptides and from other constituents obtained from fermentation. Example cyclosporin A can be separated from mycelial extracts by SFC and purified by subsequent crystallization to meet the US Pharmacopoeia purity specifications. An industrial-scale SFC plant for the production of up to 1000 kg/year purified cyclosporin A was built and successfully tested [18,19]. Also SFE with SFC are successfully coupled to achieve up to a 50 %-enriched nutraceutical concentrate containing sterolester and phospholipids [20].

Supercritical fluid fractionation (SFF):
Industrial SCF applications are designed to profit from continuous operation: polymer fractionation such as specialty lubricants and pharmaceuticals, aromas production from fermented and distilled beverages, polyunsaturated fatty acids, active compounds from fermentation broth etc. Several coupled SFE/SFF applications for phytopharmaceuticals preparation and for spices and aromas extraction on site of large agricultural productions are constructed [196].

Polymer processing:
In some applications it is difficult or impossible to produce polymers with narrow molecular weight distributions by traditional methods. The solubility parameter of supercritical fluids can be varied carefully and systematically by pressure and temperature (i.e. density) to fractionate materials according to molecular weight, because the solubility varies according to the molecular weight or chain length. Therefore selective extraction and fractionation are possible from a multi-component mixture [28].

Particle coating or encapsulation:
In the last years the attention of many researches was focused on biodegradable polymeric systems for drug delivery to enhance the therapeutic properties of drugs and patient compliance [21]. Conventional pharmaceuticals methods for the production of protein-loaded microparticles include emulsion or double-emulsion and solvent extraction, spray drying and freeze-drying. Often these techniques use organic solvent, which may cause the drug inactivation, lead to high residual contents of them in the final product and low drugs encapsulation efficiencies [22].

Supercritical fluids can be used to coat tablets and particles of active substance, which have the desired size, with a coating agent. Several processes are under investigation and development for coating. Tablets can coated by classical means, using a solution of coating agent in an organic solvent, and then subjected to extraction with a supercritical fluid. The precipitation methods such as GAS RESS, PGSS, SAS, SEDS, ASES and thermal degradation have been developed for particle coating [5]. Also high pressure fluidized bed techniques with the precipitation method were successful used to create coating. Elvassore et al. [22] and Wang et al. [23] have presented excellently the applications of particles coating/encapsulation.

Particle size formation:
Fine particles with defined grain size distribution are of interest for the pharmaceutical industry. Particle size is a critical parameter that determines the rate of dissolution of a drug in biological fluids and thus has significant effect on bioavailability. Particle design is presently a major development of supercritical fluids applications, mainly in the pharmaceutical [5,24], nutraceutical, cosmetic and specialty chemistry industries [5]. Next chapters discuss in more detail particle production by supercritical antisolvent techniques.

1.2. SUPERCRITICAL FLUID RECRYSTALLIZATION TECHNIQUES

The conventional methods for size reduction include mechanical techniques and equilibrium controlled techniques. The mechanical methods for particle size redistribution are crushing and grinding, which for some applications are carried out at cryogenic temperatures, by ball milling with or without milling aids and by air micronization (also called jet impingement or fluid energy milling). The equilibrium techniques are sublimation and recrystallization from solution. The recrystallization from solution can be carried out by thermal a method using the temperature dependency of solubility and anti-solvent methods using a non-solvent to decrease the solubility of a solid, which is dissolved in a solvent [2]. One of the techniques is spray drying, where solution is sprayed into a vessel through which a stream of hot gases is passing. By these means a large interfacial area is produced and consequently a high rate of evaporation is obtained.

The use of near critical or supercritical solvents for recrystallization has been shown to be useful in improving particle characteristics such as size, size distribution, crystal form and morphology. To the date three main methods have been used to carry out recrystallization in supercritical fluids: In the first, particles are formed as a result of the rapid expansion of a supercritical fluid (RESS). In the second, the supercritical fluid is used to form particles from gas-saturated solutions (PGSS). In the third, the supercritical fluid is used as an anti-solvent that causes particle precipitation from a liquid solution (example GAS, SAS, SEDS, SAS). There are several variations of gas antisolvent recrystallization techniques. Table I compares supercritical fluids recrystallization techniques and conventional methods for particle size redistribution.

The disadvantages of conventional methods for size reduction by mechanical techniques are, that

- due to heat generation during size reduction; not feasible for thermolabile drugs
- not appropriate for drugs capable of degrading on exposure to atmosphere
- electrostatically charged particles are obtained after fluid energy grinding;
  difficult to obtain mono-disperse particles.

The disadvantage of conventional methods for size reduction with equilibrium controlled techniques such as liquid phase crystallization is that, it is based on the fact that a compound's solubility depends on temperature and mixture composition. By changing temperature, adding anti-solvent or carrying chemical reaction, the desired material can be precipitated. Further disadvantages are: product contamination by solvent and other solutes, high energy requirement and generation of large volumes of waste, low yield due to multiple crystallization steps and difficulty to obtain monodisperse particles.

Table I *Supercritical fluids recrystallization techniques and conventional methods for some particle size redistribution ranges [25].*

	Particle size (μm)					
Techniques	500-1000	150-500	50-150	10-50	< 10	< 1
Cutting mills	Yes	Yes	No	No	No	No
Crusher	Yes	No	No	No	No	No
Universal and pin mills	Yes	Yes	Yes	Yes	No	No
Hammer mill	Yes	Yes	Yes	Yes	No	No
Mechanical mills with internal classifier	No	Yes	Yes	Yes	No	No
High-compression roller mills and table roller mills	No	No	No	Yes	Yes	No
Jet mills	No	No	No	Yes	Yes	No
Dry-media mills	No	No	No	Yes	Yes	No
Wet-media mills	No	No	No	No	Yes	Yes
Recrystallization from solutions	Yes	Yes	Yes	Yes	Yes	Yes
Spray drying	-	-	-	-	Yes	Yes
Supercritical fluid techniques 1)	Yes	Yes	Yes	Yes	Yes	Yes

1) See Table II

1.2.1 RAPID EXPANSION OF SUPERCRITICAL FLUIDS (RESS)

The technique is known as Rapid Expansion of Supercritical Solutions (RESS), first proposed by Matson et al. [26,27]. This process is also known as supercritical fluid nucleation (SFN) [28]. A schematic illustration of the RESS techniques is shown in Fig. 1.

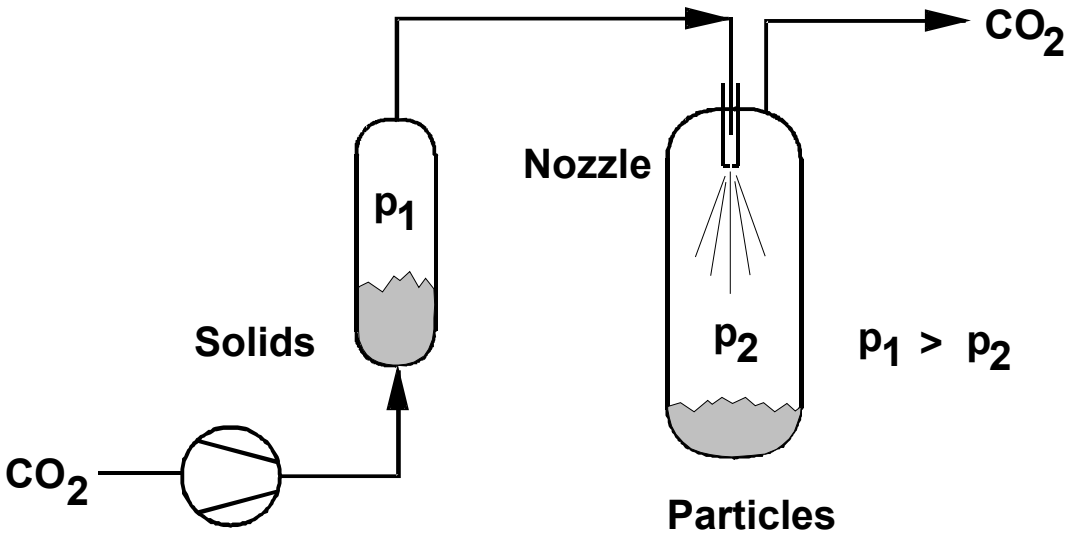

Fig. 1. *A schematic illustration of the Rapid Expansion of Supercritical Solutions (RESS) techniques.*

In this technique the solute is dissolved in a supercritical fluid and the resulting solution is expanded through a restriction (silica tubing inner diameter 30-70 μm and length/diameter 100-1000) or an orifice (inner diameter 25-30 μm and length ≤10*diameter). The resulting pressure drop causes the solvent power (density) of the supercritical solvent to decrease rapidly ($<10^{-5}$ s), leading to an appreciable supersaturation and hence bringing about precipitation of the solute. The combination of large supersaturations and uniform conditions is a distinguishing feature of the RESS process, which cans thus in principal produce very small and monodisperse particles. RESS is usually carried out at steady state conditions.

The morphology and size distribution of the precipitated material is a function of its pre-expansion concentration and expansion conditions. The pre-expansion concentration is dependent on the nature of supercritical fluid and solute, addition of cosolvent, operating pressure and temperature. The higher the pre-expansion concentration, the smaller the particles will be and the narrower the particle size range [28].

Applications of RESS techniques are depicted by Tom and Debenedetti [29]. The applications of RESS techniques are for examples inorganics and ceramics materials (SiO_2, Al_2O_3), organics and pharmaceuticals materials (Lovastain, Phenanthrene, β-Carotene, β-Estaradiol, Navy blue dye) and polymers materials (Polystyrene, Cellulose acetate and Polycaprolactone) and two-solute systems (Polyvinyl chloride/KI and SiO_2/NaCl). The application of RESS is limited by the low solubility of polar compounds and drugs in carbon dioxide. The others used supercritical fluids used are ethylene, water, ethanol, pentane and trifluoromethane.

The advantages of RESS technique are very fine particles (<1 μm) with desired particle size distribution and the solvent-free product obtained. No surfactant or nucleating media is required to trigger the nucleation and one can operate at a moderate temperature. The solvent (supercritical gas) is removed by simple mechanical separation and controlling the pressure in the post-expansion chamber can lower the pumping cost. The disadvantages are the high ratios of gas/substance due to the low solubility of the substance, the high pressures (supercritical conditions) and sometimes temperatures and separation of submicron particles from large volumes of gas is difficult on industrial scale. The limitations can be partly overcome by using more polar co-solvents in the supercritical fluid [30], but then one has given up the solvent-free processes.

1.2.2. PARTICLES FROM GAS SATURATED SOLUTIONS (PGSS)

The solubility of compressed gases in liquids is usually quite high. Dependent on pressure and temperature concentrations of highly compressible media between 5-50 % by weight can be dissolved in the solute (liquid). Due to the solubility of the gas the properties of the liquid are changed. Gas saturated solutions process lower viscosity (e.g. they are in the region of the viscosity of water). The surface tension between gas and liquid phase is also lowered. By expansion of such a gas saturated solution through a nozzle or other expansion device the compressed medium is set free, due to its high vapor pressure. Therefore the solution will be cooled. At the same time high supersaturation occurs and fine particles are formed. This technique is called the Particles from Gas Saturated Solutions (PGSS) technique. The crystallinity, particles size and particle size distribution (1-50 μm) can be influenced by the process parameters temperature, nozzle dimensions and supercritical fluids addition [31]. The schematic illustration of the PGSS techniques is shown in Fig. 2.

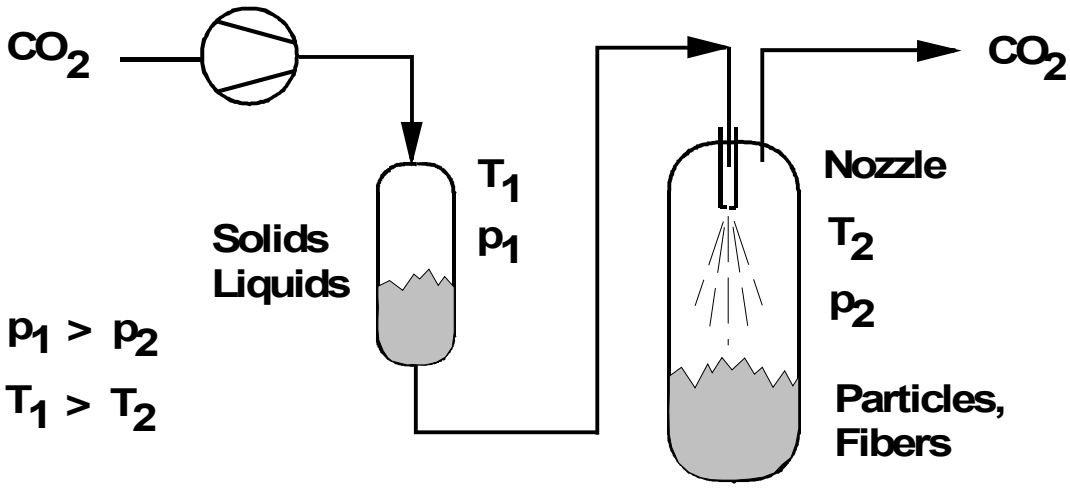

Fig. 2. *The schematic illustration of the Particles from Gas Saturated Solutions (PGSS) techniques.*

Carbon dioxide and propane are used as supercritical fluids. The produced materials are pharmaceutical preparations (calcium antagonist-difedipine) and polymers (polyethyleneglycols) [31,32]. Through the choice of an appropriate combination of solvent and operating conditions suitable for a particular compound, PGSS can eliminate some of the disadvantages of traditional methods of particle size redistribution in materials processing. The advantage of PGSS is the lower pressure compared to that of RESS, lower consumption of gas due to the lower ratios of gas/liquid than in RESS. The solvent can be recycled after its purely mechanical separation from the solutes. There are no waste streams. The product is free from solvents and the process can be applied to thermal unstable compounds because no hot streams are used in the evaporation of the gaseous solvent and there is no danger of explosion if inert gases are used [32].

1.2.3. BATCH GAS ANTISOLVENT TECHNIQUES (GAS)

Two basic techniques are distinguished if the gas antisolvent techniques; namely the batch and continuous techniques. In both processes the particle formation is based on the anti-solvent effect.

In batch GAS technique a sub- and near critical fluid is used as an anti-solvent that causes the precipitation of solids. The solids are first dissolved in a liquid, and a fluid (having a low solvent power with the liquid) is added to precipitate the solids. The rapid addition of fluid results in a sudden reduction of the liquid density and a volumetric expansion of liquid, a sharp rise in the supersaturation in the liquid mixture, and a consequent formation of small and uniform particles. The schematic illustration of the batch GAS techniques is shown in Fig. 3.

The advantages are, that the particle size can be easily controlled by the addition rate of anti-solvent, by the initial concentration of formed material in solutions and by temperature. In the batch process the volumetric liquid expansion profile is a function of the temperature, the pressure profile, type of solvent and antisolvent gas and the stirring power. The volumetric liquid expansion profile as a function of the process time determines the ratio of supersaturation build-up in the solvent. The particle size distribution is expected to be influenced by the volumetric expansion profile [38]. In the literature it is shown that the particle sizes range from 0.5 to 500 μm (See Table II).

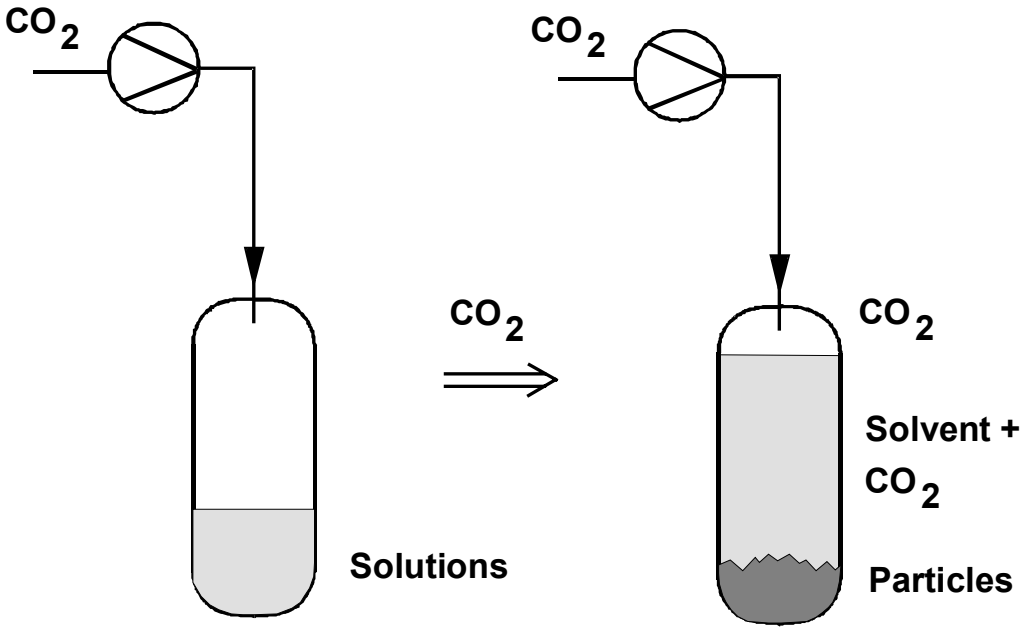

Fig. 3. *The schematic illustration of the batch GAS techniques. The CO_2 is used as anti-solvent.*

The limiting factor of the GAS process is that it is essentially a batch operation and it is associated with problems of solvent removal [33]. A disadvantage of GAS is also, that it uses organic solvents. Various microparticles have been produced by batch GAS process including explosives [45], organic acids [46], and proteins [1,34,61]. The applications of the batch GAS processes are shown in Table II.

1.2.4 CONTINUOUS GAS ANTI-SOLVENT TECHNIQUES

In the batch GAS operation, the liquid phase cannot, in general, be completely removed, which calls for an additional processing step before a dry product can be recovered. Therefore many continuous GAS techniques have been developed. In the continuous GAS techniques, such as Supercritical Antisolvent (SAS) processing and Aerosol Solvent Extraction Systems (ASES), the liquid and supercritical phases are fed continuously into a precipitator. The above depicted techniques have the same principle. Very small, sub-millimeter liquid droplets are contacted with an excess of supercritical fluid. The schematic illustration of a typical continuous GAS operation is shown in Fig. 4.

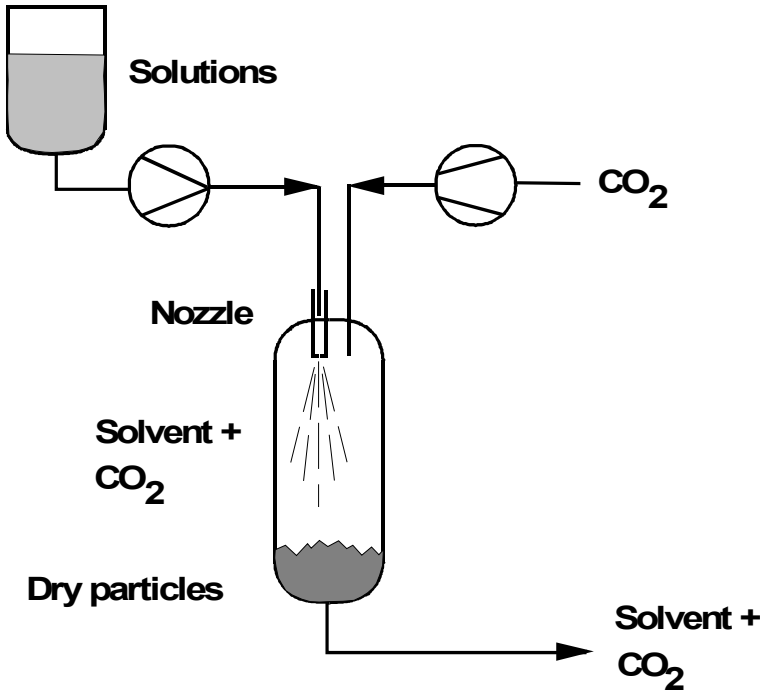

Fig. 4. *Schematic illustration of a typical continuous gas anti-solvent operation.*

To produce small liquid droplets in the nozzle, the liquid solution is pumped at a pressure of ca. 20 bar higher than the crystallizer operating pressure. The nozzle (in the example ca 20-50 μm in diameter, 0.24-0.80 mm in thickness) or capillary tubing (of 75 μm inner diameter), is installed at the top of the crystallizer, so that both the solution and supercritical anti-solvent flow continuously and in downward concurrent mode through the crystallizer. Also the nozzle is vibrated at 120 kHz to produce a narrow, cylindrically shaped spray [10]. Sub-millimeter liquid droplets are sprayed into a continuum of supercritical anti-solvent.

Dry particles are produced through the expansion of the organic solvent by anti-solvent diffusion and evaporation of the organic solvent into the anti solvent [6,9,59]. A particle size range of 0.1 μm to 250 μm is produced, mainly of the size of 1-10 μm (See Table II). In the continuous gas anti-solvent operation the effect of processing variables such as temperature, pressure, concentration of the injection solution, rate and temperature of the carrier solution, nature of liquid solvents, and choice of the supercritical fluid on the physical properties of the end product are to be studied and optimized for any product [28].

The above process has been further developed to achieve a smaller droplet size and intensify mixing to increase mass transfer rates with Solution Enhanced Dispersion by Supercritical fluids (SEDS). This process was originally named by Hanna and York [35]. The schematic illustration of the SEDS technique and co-axial nozzle is shown in Fig. 5.

Essentially, a flow of supercritical fluid (anti-solvent) disperses and extracts streams of solution passing through a specially designed nozzle into a particle

formation vessel at a constant temperature and pressure. The solution and the supercritical fluid are introduced simultaneously into the particle formation vessel using a co-axial nozzle arrangement causing rapid dispersion, mixing and extraction of the solution solvent by supercritical fluid leading to very high supersaturation ratios. Because of the construction of nozzle, the pressure drop over the nozzle is small. The temperature and pressure together with accurate metering of flow rates of solution and supercritical fluid through nozzle provide uniform conditions for particle formation. This helps to control the particle size of the product. In this way and by choosing an appropriate liquid solvent, it is possible to manipulate the particle morphology [28].

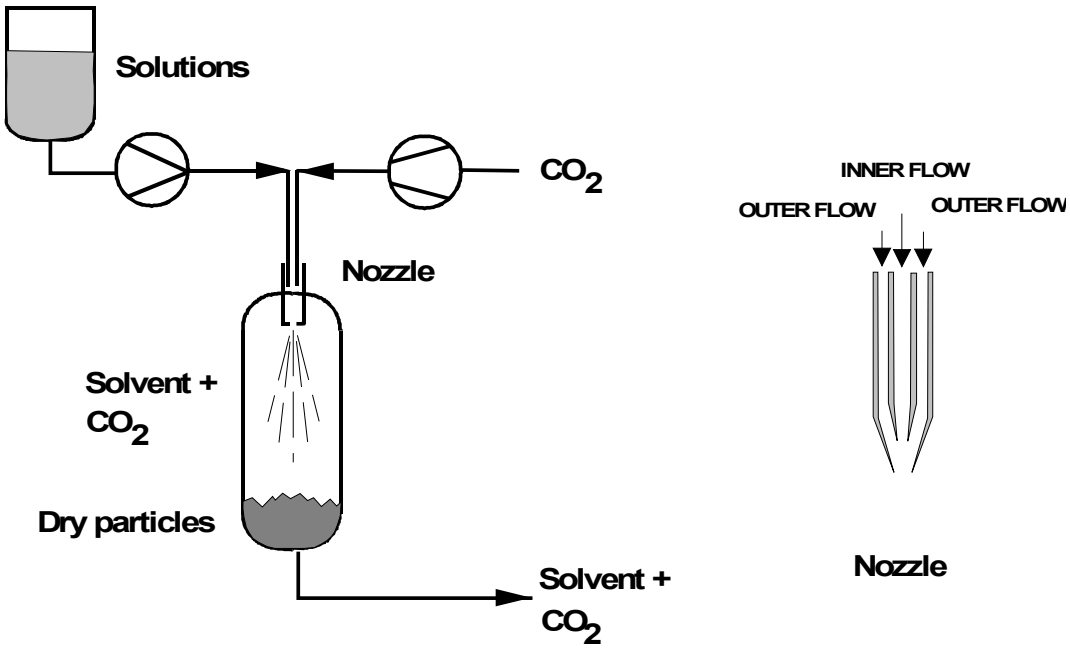

Fig. 5. *The schematic illustration of the solution enhanced dispersion by supercritical fluids (SEDS) techniques and co-axial nozzle.*

Preferably, the opening at the outlet end (tip) of the nozzle will have a diameter in the range of 0.05 to 2 mm, more preferably between 0.1 and 0.3 mm. The angle of taper will be in the range about 20 ° to 40 °, typically 30 °. Anti-solvent is usually introduced through the inner tube. In one embodiment of the application, the nozzle has two co-axial passages, an inner and outer. In another, the nozzle has three co-axial passages, an inner, an intermediate and outer. However, the nozzle may have any appropriate number of co-axial passages. Improved dispersion and finer particles can also be obtained if such a nozzle is used to introduce a flow through the vehicle sandwiched between an inner and an outer flow of the supercritical fluid, since this ensures that both sides of the vehicle are exposed to the supercritical fluid. Changes in the process conditions (e.g. pressure, temperature, flow rates and solvent) allow the particle properties to be controlled [78,70].

The applications of continuous supercritical antisolvent techniques are depicted for example by Reverchon [3], Sze et al. [36] and Weber et al. [4]. In Table II the selected applications of supercritical antisolvent techniques are shown.

Table II *The selected applications of supercritical antisolvent techniques.*

Supercritical Fluid	**Compounds Solute**	**Particle types**	**Particle size**	**References**
GAS (BATCH)				
CO_2	Insulin+DMSO Insulin+DMFA	Powders	< 4 μm	Yeo et al. 1994 [37]
CO_2	Phenanthrene+ Toluene	Particles	160-540 μm	Berends et al. 1994 [38, 39]
CO_2	Triamcinolone Acetonide+THF	Individual particles	5-10 μm, some 20-30 μm	Schmitt, 1990 [40]
CO_2	Poly(L-lactide acid) + Methylen chlodide	Particles	0.5-3 μm	Randolph et al. 1993 [10]
CO_2	Nitroguanidine-DMF	Separate Particles	Micron	Gallagher et al. 1988 [41]
CO_2	RDX and HMX + Acetone	Free crystals of RDX	200 μm	Gallagher et al. 1988 [42]
CO_2 (Batch and Continuous GAS)	Pigments: Red Lake C, C. I. Yellow and C. I. Blue+ Acetone	Fibers Particles	< 0.6 μm	Gao et al. 1997 [43]
CO_2	Acetaminophen+ Ethanol	Particles	---	Wubbolts at al. 1998 [44]
CO_2	β-HMX explosive material	Particles	2-5 μm	Cai et al. 1997 [45]
CO_2	Two key pharmaceuticals compounds	Needle crystals	Length 3-5 μm Diameter 0.5-2 μm	Robertson et al. 1997 [46]
CO_2 Chlorodifluoro-methane (CFC-22) Dichlorodifluoro methane (CFC-12)	Nitroguanine (NG) + N,N-dimethyl formamide (DMF) or N-methylpyrrolidone (NMP)	Particles Crystals Agglomeratas	5-500 μm 1-100 μm	Gallagher et. al. 1989 [2]

Table II *continues*

Supercritical Fluid	**Compounds Solute**	**Particle types**	**Particle size**	**References**
CF_3CH_2F	Polystyrene + Tolune	Uniform microspheres Agglomerated particles	About 1-5 μm	Tan et al. 1998 [47]
SAS+SEDS+ ASES CO_2	Yttrium acetate, Samarium acetate and Neodymium acetate + DMSO	Particles	About 100 μm	Reverchon et al. 1998 [48]
CO_2	N,N-dimethylformamide + DMSO	Particles	1-10 μm	Yeo et al. 1993 [49]
CO_2	Poly(L-lactic acid) + Methylene chloride	Particles	0.4-2 μm	Randolph et al., 1993 [50]
CO_2	Polystyrene + Toluene	Fibers Agglomerated particles	0.1-20 μm	Dixon et al. 1993 [51]
CO_2	Salmeterol xinafoate + Ethanol, Methanol and Acetone	Particles, Blade like shape particles	1-10 μm	York and Hanna 1995, 1996 [78,52, 53]
CO_2	Hydroquinone + Acetone	Particles Crystals	50-250 μm	Wubbolts et al. 1997 [54]
CO_2 (SEDS)	Sodium cromoglycate + Methanol	Particles Amorphous	0.1-20 μm	Jaarmo et al. 1997 [55]
CO_2 (ASES)	Poly(L-lactid acid) and hyoscine butylbromide + Methylene chloride/Methanol (85:15)	Particles	1-10 μm 10-30 μm	Bleich et al. 1993 [7]
CO_2	Insulin + DMSO or DMFA	Particles	2-3 μm	Yeo et al. 1993, 1994 [34,56]
CO_2 (Batch and continuous)	Polyamides Modified aramids (PPTA)+ DMSO, DMFA and DMA	Polycrystalline spherulites	1-10 μm	Yeo et al. 1995 [57]

Table II *continues*

Supercritical Fluid	Compounds Solute	Particle types	Particle size	References
CO_2 (ASES)	Ethyl cellulose, Poly(methyl methacrylate), Poly(ε-caprolactone), Poly(L-lactide), Poly(DL-lactide-glycolide) + Methylene chloride + Chlororpheniramine maleate, Indomethacin	Unchanged Agglomerated Fibers Particles	< 1 μm 1-5 μm	Bodmeier et al. 1995 [58]
CO_2	Poly(lactide-co-glycolide)+ Acetone	Particles	< 50 μm	Dillow et al. 1997 [59]
CO_2 (SEDS)	Poly(L-lactid acid) + Methylene chloride	Particles	1-30 μm	Rantakylä et al. 1998 [60]
CO_2 (Spray extraction)	Coffee oil	Instant powder	---	Eggers et al. 1996 [11]
CO_2	Insulin+ Ethanol-Water mixture	Powder Spherical or rectangular particles Thick needles	About 1 μm About 5 μm	Tom et al. 1992, 1993, 1994 [61,6, 62]
CO_2	Poly acrylonitrile (PAN)+ DMFA Polyrstyrene+ Toluene	Fibers Micro-fibrils	About 0.3 μm	Johnston et al. 1994 [63] Luna-Barcenas et al. 1995 [64]
CO_2	Polymeric hyaluronic acid methyl ester (HYAFF-11)+ DMSO	Aggregated structures Spherical particles		Benedetti et al. 1997 [65]
CO_2 or Ethane	Methylprednisolone+ THF	Crystal patrticle	About 5 μm	Schmitt et al. 1995 [66]
CO_2	Hydrocortisone acetate+DMFA	Crystal patrticle	About 5 μm About 100 μm	Schmitt et al. 1995 [66]
CO_2	Acetates (Ba, Cu, Y, Sm, Nd) + DMSO	Spherical amorphous particles	< 1 μm About 10 μm	Reverchon at al. 1997,1998 [67,68,9]

Table II *continues*

Supercritical Fluid	Compounds Solute	Particle types	Particle size	References
CO_2	Ascorbic acid, Paracetamol, Chloramphenicol + Ethanol	Needle like crysyals Deformed prismatic crystals	< 2 μm	Weber at al. 1998 [4]
CO_2	Paradroxybenzoid acid+ Methanol, PLGA + Acetone, PLA + Dimethylchloridero methane	Agglomerated Amorphous polymer	< 10 μm	Sze et al. 1998 [36]
CO_2 (SEDS)	α-Lactose monohydraye+ Water + Methanol (Three coaxial nozzle)	Particles	4-5 μm	Palakodaty et al. 1998 [69]
CO_2 (Batch and continuous GAS)	Para-hydroxybenzoid acid + Methanol	Uniform flat platelets Agglomerated spherically shaped particles	0.1-1.0 μm	Thiering et al. 1998 [30]
CO_2 (SEDS)	Lysozyme or Trypsin + Water + Ethanol (Three coaxial nozzle)	Spherical particles Agglomerated irregular shaped particles	Mean diameter 0.8 μm 0.5-6 μm	Sloan et al. 1998 [70]
CO_2 (SEDS)	Salmeterol xinafoate + Methanol or Acetone	Micronised particles Polymorphs I and II	Microns	Hanna et al. 1998 [71]
CO_2 (ASAS)	Naproxen + Poly-L-Lactic acid (L-PLA)	Particles	Microns	Chou et al. 1997 [72]

Application of the continuous GAS, ASES and SAS has allowed a successful precipitation of a range of compounds including pigments [43] and polystyrene in the form of microspheres, fibres and balloons [73,51], the production of pharmaceuticals such as the precipitation of biodegradable polymers [10], polymer-pharmaceutical composites [1,72], and a range of proteins including insulin [56] and lysozyme [74]. The pharmaceutical material applications of the SEDS techniques include sodium cromoglycate, salmeterol xinafoate, lysozyme and trypsin [55,70,71]. Biodegradable polymers and water soluble compound applications are such as α-lactose [60] and monohydrate [33].

1.2.5 PRINCIPLES TO CHOOSE A PROCESS FOR PARTICLE DESIGN

Jung and Perrut [5] have presented a survey of published knowledge to optimize the route to the desired particles using supercritical fluids techniques. To choose a process for particle design, it is necessary to know advantages and drawbacks of each technique and to have a principal knowledge of the phase behaviour of the system. Technological features of the various supercritical particle formation processes are summarized and compared In Table III [24].

The first thing to consider is the solubility of the recrystallizing material and the solvent/recrystallizing material matrix in the supercritical fluid. The choice between different methods will then be made considering the desired particle size, shape and structure, processing cost and production scale .

RESS application could be considered at first. Advantages of RESS techniques are, that submicronic and micronic particle can be formed and no organic solvent used. Drawbacks are high fluid consumption, especially there is a low solubility of compounds in supercritical CO_2.

If the recrystallizing material and matrix solubility is too low to lead to a profitable process, then anti-solvent processes are to be considered. In those techniques it is possible to control particle size, shape and structure on very wide range from nano particles to micro particles. The drawbacks of anti solvent techniques could be high processing cost, medium to large volume of pressurized equipment and difficulty to operate in high pressure at large scale. Since an organic solvent is used, difficult fluid/solvent separation and fluid recycling are drawbacks of antisolvent techniques [5].

Table III *Technological features of RESS, GAS/SAS/PCA and PGSS process [24].*

	RESS	GAS/SAS/PCA	PGSS
Establishing gas-containing solution	Discontinuous	Semicontinuous	Continuous
Gas demand	High	Medium	Low
Pressure	High	Low to medium	Low to medium
Solvent	None	Yes	None
Volume of pressurized equipment	Large	Medium to large	Small
Separation gas/solid	Difficult	Easy	Easy
Separation gas/solvent	Not required	Difficult	Not required

The PGSS processes should be preferred for large particles and lower value materials. Advantages of PGSS processes are low fluid consumption, low to medium pressure and small volume of pressurized equipment. The drawbacks of PGSS are the impossibility to produce submicronic particles and to monitor particle size.

1.3. BEHAVIOR OF SUPERCRITICAL FLUID

To fully comprehend the unique solvent characteristics of a supercritical fluid (SCF), it is necessary to understand the behaviour of pure SCF solvents and SCF-solute mixtures.

1.3.1. PURE COMPONENTS

An understanding of the term supercritical fluid may be obtained by examining the phase diagram for carbon dioxide presented in Fig. 6, showing the relationship of the supercritical fluid region to the solid, liquid and vapor states [75].

The curves represent conditions where two phases coexist, and at the triple point the three phases coexist. Crossing a solid curve by changing the pressure and/or the temperature results in a phase change. A substance is referred to as a supercritical fluid when its pressure is an above the critical pressure (P_c), and its temperature above the critical temperature (T_c), of the substance. In this area, lowering the pressure or the temperature will bring the substance into the vapor or the liquid region, respectively, without any phase change occurring.

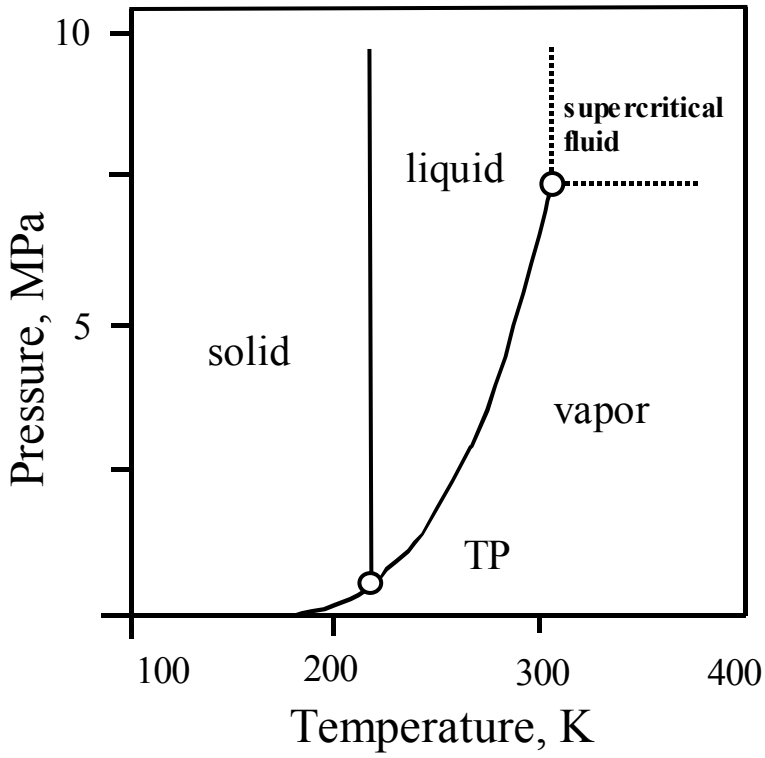

Fig. 6. *Phase diagram for carbon dioxide* [75]. *The triple point is designated as TP and the critical point as CP.*

When a substance is subjected to pressures and temperatures above its critical point, a highly compressed gas known as a supercritical fluid results with densities similar to normal liquid densities. It is convenient to define the pressure-volume-temperature (PVT) region of interesting solvent properties for any fluid in terms of reduced density diagram. Fig. 7 shows the reduced pressure-density diagram of carbon dioxide [76]. The supercritical regime is that which lies above a reduced pressure of 1.0, and above the reduced temperature isotherm of 1.0. The region of condensed phase below reduced temperature of 1.0, but above the value of about 0.95 may be defined as near-critical liquid (NCL). There is, of course, a continuity of properties between these regions, and the selection of appropriate temperatures and pressures within these regimes for any given extraction is often made empirically.

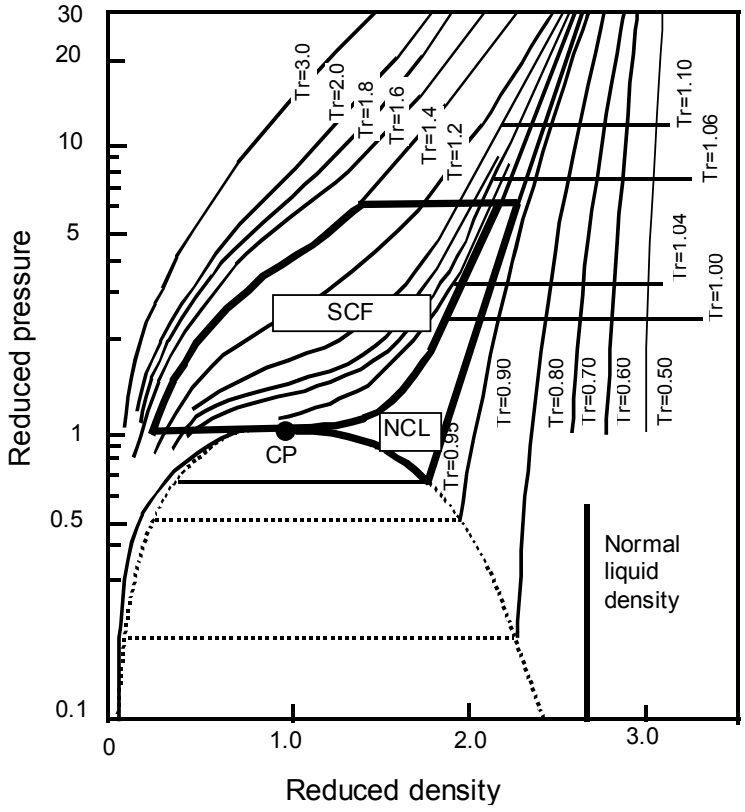

Fig. 7. *Reduced pressure-density diagram of carbon dioxide [76]. Supercritical fluid (SCF) and near-critical liquid (NCL) regions as indicated. The critical point is designated as CP.*

A commonly accepted opinion is that the solvent power of a supercritical fluid is mainly related to its density in the critical point region [89]. A high density generally implies a strong solvating capacity. The unique property of a supercritical fluid is, that the solvating power of a supercritical fluid can be tuned by changing either temperature or pressure.

As illustrated, the fluid is highly compressible in the near-critical region where small changes in the temperature or pressure result large changes in density, while the changes become more moderate in the supercritical region far from the critical point. At high values of reduced temperature, the fluid density may be reduced to a point where solvent properties are no longer favourable. At reduced pressures above the values of 5 or 6, the process economics may suffer because of high-pressure conditions involved. Finally, at low reduced temperatures, such as liquid CO_2 below ambient temperature, solvent properties may be adversely influenced by decreasing temperature.

Even though the density of a supercritical fluid increases with pressure and becomes liquid-like, the viscosity and diffusivity remain between liquid-like and

gas-like values [89]. Comparison of selected physicochemical properties of liquids, gases and supercritical fluids is seen in Fig. 8.

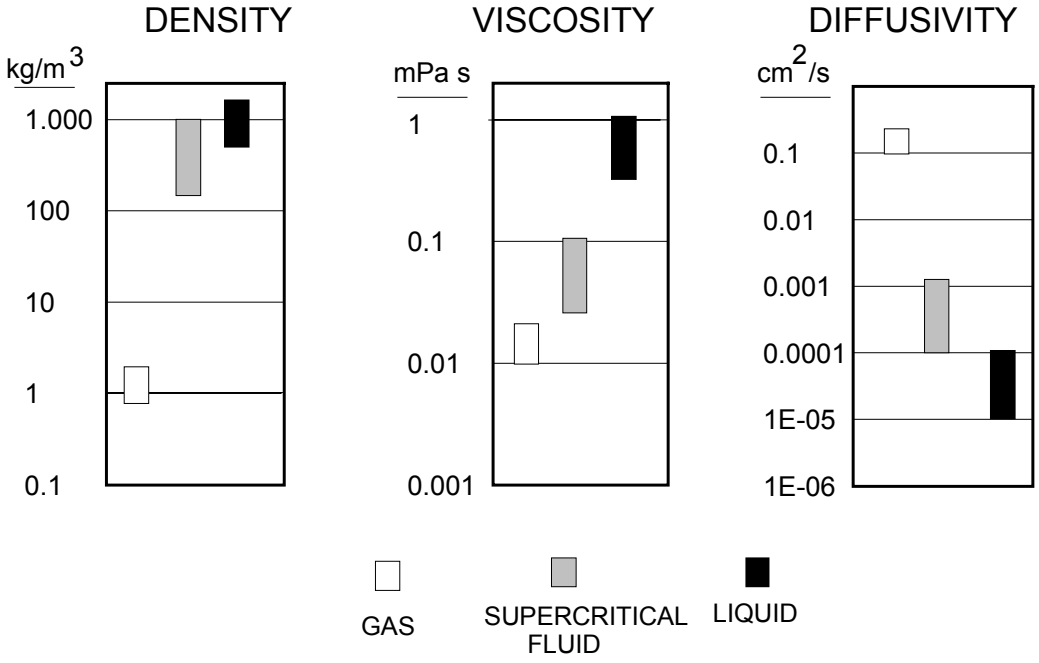

Fig. 8. *Selected physicochemical properties of liquids, gases and supercritical fluids [89].*

Additionally, supercritical fluids exhibit almost zero surface tension, which allows facile penetration into microporous materials. As a result of advantageous combination of physicochemical properties, the extraction process can often be carried out more efficiently with supercritical than with organic liquid solvent.

Table IV lists the critical temperatures, pressure, and densities for a number of gases and liquids, potential for used as the supercritical fluid in a supercritical fluid process [88,89].

Table IV *Critical properties temperature, pressure and density of selected solvents [88,89].*

SOLVENT	T_c (K)	P_c (MPa)	ρ_c (g/cm^3)
Ammonia	405.7	11.28	0.24
Benzene	562.2	4.89	0.30
n-Butane	425.2	3.80	0.23
Carbon dioxide	304.3	7.38	0.47
Chlorotrifluoromethane	302.0	3.95	0.58
Dichlorodifluoromethane	384.9	3.99	0.56
Ethane	305.6	4.89	0.20
Ethanol	516.6	6.38	0.28
Ethylene	282.5	5.04	0.22
Krypton	482.3	5.50	0.92
Isopropanol	508.5	4.76	0.27
Methanol	513.7	7.99	0.27
Nitrous oxide	309.7	7.23	0.46
n-Propane	367.0	4.26	0.22
Propylene	365.1	4.62	0.23
Toluene	591.8	4.11	0.29
Water	647.6	22.1	0.34
Xenon	562.9	5.84	1.11

Some trends are found by a thorough investigation [85]:

- Small and light molecules tend to have lower critical temperatures and higher critical densities than large and high molecular weight molecules.
- The critical pressures of most of the components are between 3 and 6 MPa.
- The presence of hydrogen bonds or polarity of the molecules tends to increase the critical temperature or pressure of the compound.

Although a variety of the components can be utilized in supercritical fluid processing, common substances such as light hydrocarbons, water and carbon dioxide have received the greatest attention. The critical temperatures of non-polar gases, such as carbon dioxide or ethane, are below 325 K, whereas for polar compounds, such as methanol or water, the critical temperature is well above 475 K. Generally in extraction practice, it is usually desirable, that the critical temperature is below 375 K. Therefore, the commonly used supercritical fluids are low molecular weight gases, such as carbon dioxide, ethane and propane [77]. Ethylene and ethane are good solvents for solid hydrocarbons because of the natural affinity between similar molecules. By the introduction of functional groups (except alkyl groups) in the parent compound, the solubility decreases. Polar compounds such as trifluoromethane are good solvents for all solids except nonpolar hydrocarbons. Solubilities of polar but non-associated compounds are high in such solvents. Carbon dioxide is a fairly good solvent. An electron-

releasing substituent makes it a good solvent and an electron withdrawing substituent reduces its dissolution power.

Suitable chemicals for use as supercritical fluids in the particle formation are carbon dioxide, nitrous oxide, sulphur hexafluoride, pentane, propane, xenon, ethylene, chlorotrifluoromethane, ethane and trifluoromethane [78,90]. The current antisolvent is carbon dioxide but also chlorodifluoromethane, dichlorodifluoromethane and ethane are used.

One might notice that the properties of the rare gases, krypton and xenon, are favourable (See Table IV), but these are seldom employed because they are very expensive. Particularly prefer is carbon dioxide. Carbon dioxide is the most commonly used solvent in industrial practice due to several reasons. Compared with organic liquid media [79]:

- CO_2 is a nontoxic, nonflammable, readily available and cheap solvent.
- It leaves no solvent residues in production.

Compared with all liquid phase media :

- The high and large scale of diffusivity, low viscosity, and low surface tension of CO_2 is expected to speed up mass-transfer controlled process.
- The solvent power of CO_2 depends strongly on temperature and pressure. Thus the material can precipitate from the CO_2 by mere pressure reduction. This separation then becomes a gas-liquid or gas-solid separation, and fractionation of large amounts of dilute liquid solutions in the downstream phase can be avoided.
- CO_2 separation from the mixture is energy efficient. If the CO_2 must be evaporated from the mixture, the heat of vaporization of CO_2 is only a small fraction of the energy needed to evaporate organic solvent or water.
- Product fractionation and purification are possible directly from the mixture without any solvent changes. This can be done in a train of separator vessels arranged in descending pressure/temperature order or in countercurrent contactors.
- Purified products can be crystallized directly from the CO_2 by letting the fluid expand into lower pressure through a pressure reduction. Ultra-small particles or particles with tailor-made size and size distribution can rapidly produced in this way.
- CO_2 creates a nonoxidizing atmosphere for substrates and products throughout the process.
- The whole process can be operated at relatively low temperatures (305-333 K), which protects thermally unstable compounds.

The density of carbon dioxide as a function of pressure and temperature is shown in Fig. 9 The density of CO_2 was calculated by a method of Angus et al. [75]. The critical temperature is 304.2 K, the critical pressure 7.38 MPa and the critical density 468 kg/m^3. The density of supercritical CO_2 depends especially on

temperature and pressure near the critical point. In Fig. 9 the change of phases under the critical point is shown with a broken line.

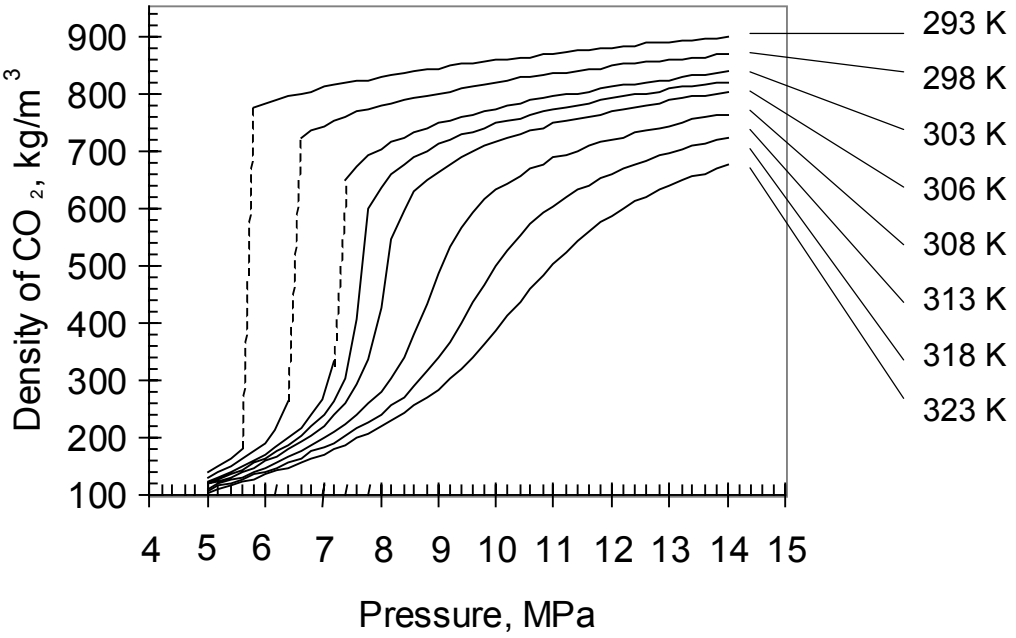

Fig. 9. *Density of carbon dioxide as a function of pressure and temperature [75].*

In Fig. 10 the density ρ, the viscosity μ and the product $D_{11}\rho$ (where D_{11} is self-diffusion coefficient) of pure carbon dioxide are plotted against pressure up to 500 bar and at 313 K [80]. The viscosity and $D_{11}\rho$ remain essentially constant up to about 8.0 MPa. As the pressure rises further, an increase of viscosity and a decrease of $D_{11}\rho$ are found. At 40 MPa the ratio of μ(40 MPa)/μ(0.1 MPa) is about 7 and D_{11}(40 MPa)/D_{11}(0.1 MPa) is about $4*10^{-4}$. Thus properties of fluid can profit from relatively low viscosities in the gaseous phase as well as from diffusion coefficients that are considerably higher than the usual values for liquids ($D_{11} < 10^{-5}$ cm^2 s^{-1}).

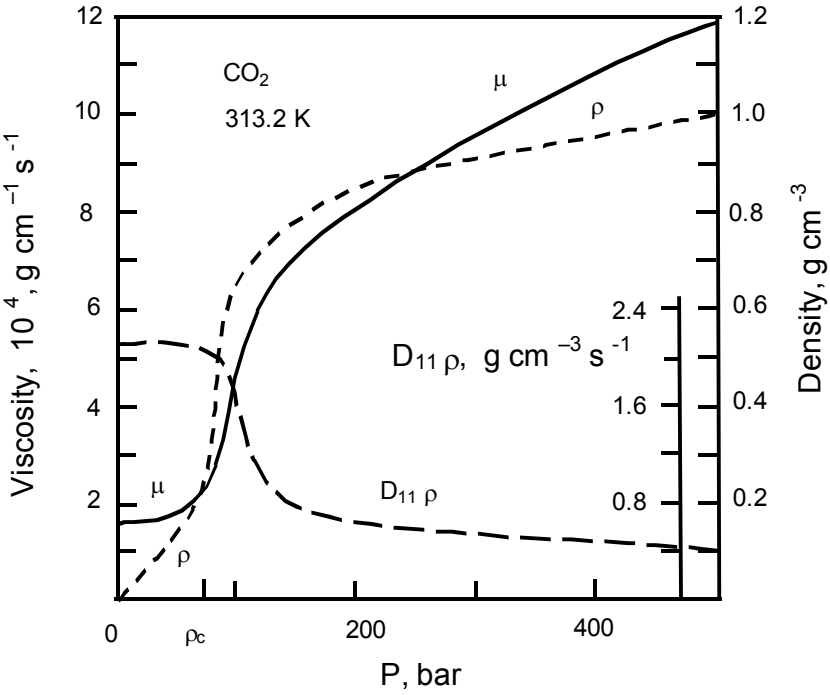

Fig. 10. *Density ρ, viscosity μ and the product $D_{11}\rho$ (where D_{11} is self-diffusion coefficient) for pure CO_2 as a function of pressure at 313 K [80].*

Supercritical carbon dioxide is a lipophilic solvent since the solubility parameter and the dielectric constant are small compared with a number of polar hydrocarbon solvent. It can be seen from Fig. 11 that the dielectric constant (DC, ε-1) values rise steeply with density between 7.0 MPa and 20 MPa and reach values similar to those for liquids. The both parameters increase only slightly above about 30 MPa. This provides further explanation for the fact that several supercritical gases exhibit considerable solvent power above a certain pressure and can therefore be used in place of the usual solvents [81].

Pressurized carbon dioxide dissolves a large number of different types of substances in the lower pressure range [81]. The solubility is dependent of the individual groups of substances, e.g. the aromatic hydrocarbons, phenols, aromatic carboxylic acids, pyrones, and lipids. It is immediately evident that solubility falls sharply in the pressure up to 40 MPa as the number of C-atoms increases and particularly following the introduction of polar functional groups. One can see here the possibilities for fractionating extraction of complex samples in a pressure gradient.

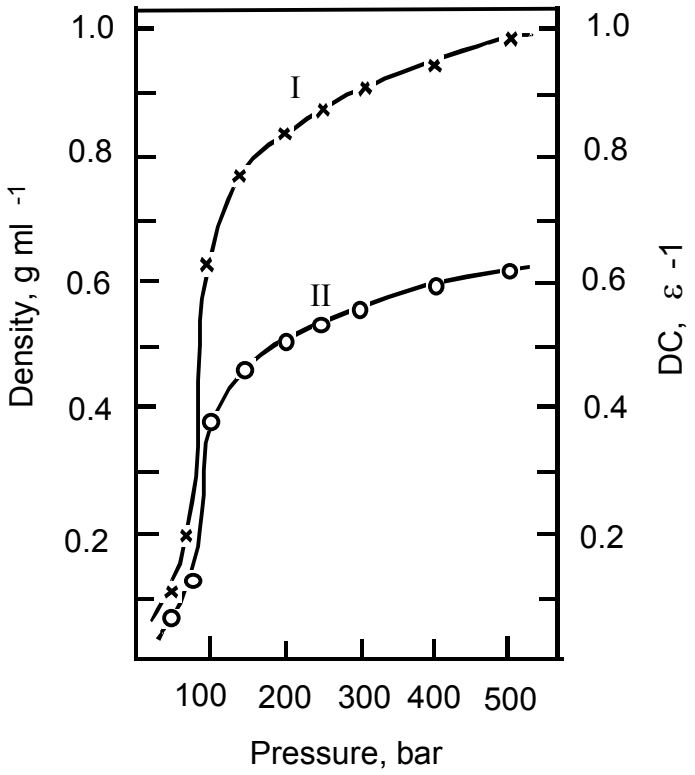

Fig. 11. *Dependence of the dielectric constant (right side) and the density (left side) of carbon dioxide at 313 K on pressure [81].*

Stahl et al. [81] have evaluated the dissolving power of supercritical carbon dioxide:

- Hydrocarbons and other typically lipophilic organic compounds of relatively low polarity, e.g. esters, ethers, lactones and epoxides, are dissoluble in the lower pressure range, i.e. 7-10 MPa.
- The introduction of strongly polar functional groups (e.g. -OH, -COOH) decreases solubility. In the range of benzene derivatives, substances with three phenolic hydroxyls are still soluble, as are compounds with one carboxyl and two hydroxyl groups. Substances in this range that decreases solubility are those with one carboxyl and three or more hydroxyl groups.
- More strongly polar substances, e.g. sugars and amino acids, are not soluble in the range up to 40 MPa.
- Fractionation occurs in the pressure gradient when there are greater differences in the commencement of boiling or sublimation, i.e. in the volatility, and/or marked differences in the polarity of the substances (dielectric constant value). The fractionation effects are most marked in the range where there is a sharp rise in the density and dielectric constant of fluid carbon dioxide.

The solubility of polar, non-volatile solutes in supercritical carbon dioxide can be enhanced by adding small amounts of polar co-solvents, called entrainers, in the carbon dioxide. Water and short-chain alcohol's are efficient and usually the most acceptable co-solvents. An excellent review of solid solubilities in supercritical carbon dioxide is offered by Bartle et al. [82].

Short-chain hydrocarbons and alcohols, examples acetone, ethanol, 1-propanol, 2-propanol and 1-butanol, are completely miscible in supercritical carbon dioxide at relatively moderate pressures [83,84]. All above mentioned alcohol-CO_2 mixtures as above become supercritical one phase systems at pressure greater than about 8 MPa at 313 K and about 10 MPa at 333 K. The solubility of alcohol at fixed pressure increases with temperature, and decreases with its carbon number. The solubility of 2-propanol (secondary alcohol) is greater than that of 1-propanol (a primary alcohol) and very similar to that of ethanol for each temperature [83].

1.3.2. BINARY MIXTURES

Most of the supercritical fluid processing such as extraction, fractionation, chromatography, recrystallization etc. involves multi-component systems, but the essential features of the phase equilibrium behaviour for such systems can be shown by considering only binary systems [85]. The phase rule specifies a maximum of three independent variables for a binary system, that is the systems will be completely described in a phase diagram with the variables pressure, temperature and composition. Fig. 12 show the phase diagram of such systems, where one equilibrium phase is represented by a volume, two phases in equilibrium are represented by a surface, three phases in equilibrium are represented by a line, and eventually four phases in equilibrium are represented by a point (quadruple point).

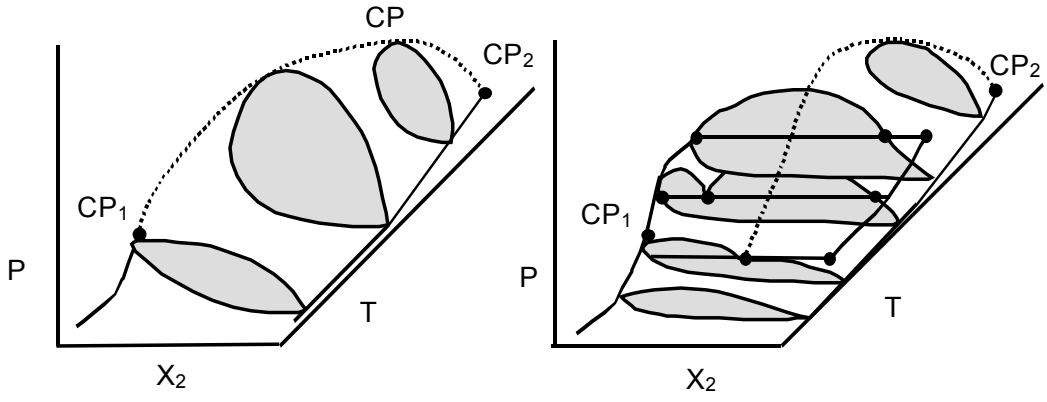

Fig. 12. *Pressure-temperature-composition (P-T-x) diagram of type I (left side) and type IV (right side) binary mixture [85]. The pure component 1 critical point is designated as CP_1, component 2 as CP_2 and the mixtures critical point as CP.*

Van Konynenburk and Scott [86] state the existence of six fundamentally different *P-T-x* diagrams for binary systems, which in principle classify the system by the differences between the two components. Classifications are usually based on P-*T* projections of mixture critical curves and three phase equilibrium lines. Using this categorization the systems depicted in Fig. 12 relate to the type I and type IV phase behaviour categories, respectively. The appearance and explanation of the various P-*T-x* diagrams and *P-T* projection are given in numerous publications, e. g. Street [87], McHugh and Krukonis [88] and Schneider [89].

In GAS recrystallization process (Gas Antisolvent Process) the solution of solid in an organic solvent is pressurized with a near critical gas leading to precipitation of the solid. The main problem in this process is to find for a given solid the appropriate combination of the solvent and the gaseous antisolvent. The gas (antisolvent) must be totally miscible with the solvent in the desired temperature and pressure range, that is, the binary mixture should belong to the so-called Type I of fluid-phase behaviour according to Van Konynenburg and Scott [86,90].

In RESS processes (Rapid Expansion of Supercritical Solution Process) binary systems are often involved [91]. Fig. 13 shows the P-*T* behaviour of highly asymmetric binary mixture, that is, a mixture containing two substances with large differences in molecular size, structure, and intermolecular interactions. This is the situation, for example, in a system with a light supercritical fluid (such as CO_2, ethylene, or ethane) and a heavy hydrocarbon (either an aliphate one, such as C-20, or an aromatic one, such as naphthalene or biphenyl).

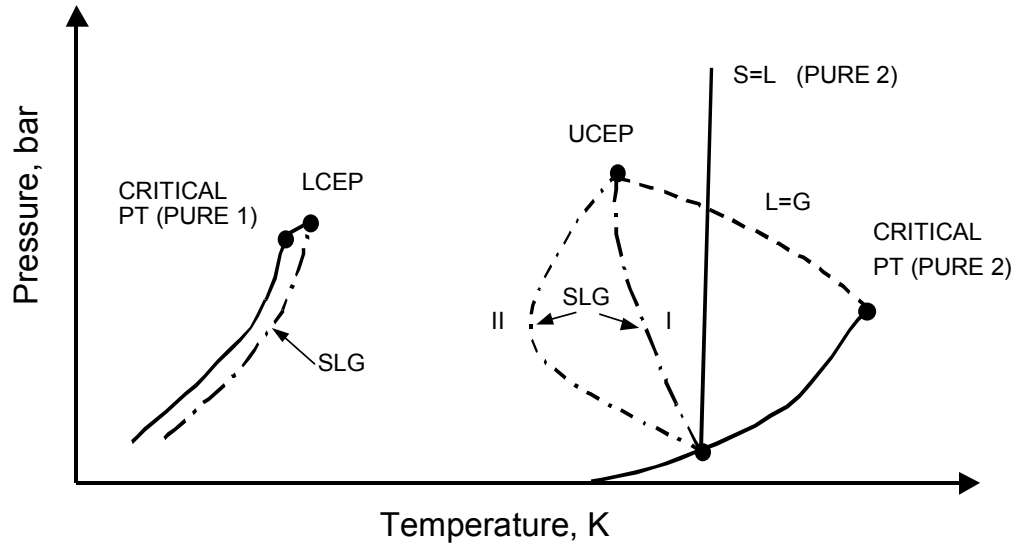

Fig. 13. P-*T behaviour of highly asymmetrical binary system [91]. The upper critical end point is designated as UCEP, the lower critical end point as LCEP, solid phase as S, liquid phase as L and vapor phase as V.

Two main features involved are;

1) the triple-point temperature of the heavy component is much higher than the critical temperature of the light one
2) the solubility of the light component in the liquid phase is quite limited.

Accordingly, the solid-liquid-vapour (S-L-V) equilibrium takes place also at elevated pressures, and the S-L-V curve intersects the gas-liquid critical curve in two points: the lower critical end point (LCEP) and the upper critical end point (UCEP). At these two points, liquid and gas phases merge into a single fluid phase in the presence of excess solid. At temperatures between T_{LCEP} and T_{UCEP} a S-V equilibrium is observed. At the isotherm containing a vapor-liquid critical point must exhibit here a zero slope on a *p-x* diagram, the solubility of the heavy component in gas phase increases very rapidly with pressure near the LCEP and the UCEP [91].

The LCEP is usually close to the critical point of the light component: T_{LCEP} is in general quite low. Therefore, the solubility of the heavy component in the light one is limited. On the contrary, the temperature of the UCEP is much higher, leading to high solubility of the heavy component in the supercritical fluid.

Two kinds of behaviour may occur. Class I system (curve I in Fig. 13) the P-*T* trace of S-L-V equilibrium presents a decreasing temperature at increasing pressure. At temperature below T_{UCEP}, only solid-fluid equilibrium occurs. At temperature between T_{UCEP} and the melting temperature of the heavy component, there is a range of pressure in which either V-L or S-V equilibrium can be observed, depending on the global composition of the mixture. A peculiar behaviour is observed at T_{UCEP}. As UCEP is a vapor-liquid critical point in the presence of excess solid, the corresponding P-*x* isotherm presents an inflection point at $P=P_{UCEP}$.

Class II system (curve II in Fig. 13) the *P-T* trace a minimum appears when the pressure is increased. At temperature below the minimum in the S-L-V line (in Fig. 13) a S-V equilibrium exists for each pressure. At temperatures between the minimum and T_{UCEP}, an isotherm intersects the S-L-V line in two points. Between the corresponding two values of pressure, either L-V or L-S equilibrium is observed. At T_{UCEP} and pressure below P_{UCEP} a vapor-liquid equilibrium occurs, but at P_{UCEP} two phases merge into one fluid phase, together with the appearance of a solid phase. A S-V equilibrium is again observed by increasing pressure. At $T > T_{UCEP}$, the behaviour is similar to Class I systems. Depending on the general composition, either L-V or S-V equilibrium can be encountered [91].

1.3.3. TERNARY MIXTURES

As ternary mixtures, which are mostly related to continuous GAS processes, the SAS (Supercritical Antisolvent Recrystallization Process) and the SEDS (Solutions Enhanced Dispersion by Supercritical Fluids) process, a thermodynamic study of the system solute-solvent-antisolvent is extremely useful

to address the feasibility of the process and to exploit the effects of temperature and pressure [91]. The antisolvent (dense gas) is miscible with the solvent, and its solubility increases with temperature, but it is immiscible with the solute. Once a certain pressure is reached, the solution becomes supersaturated and the solute precipitates. An understanding of the behaviour of the ternary mixture may be obtained by examining the ternary diagram of CO_2-toluene-naphthalene in Fig. 14.

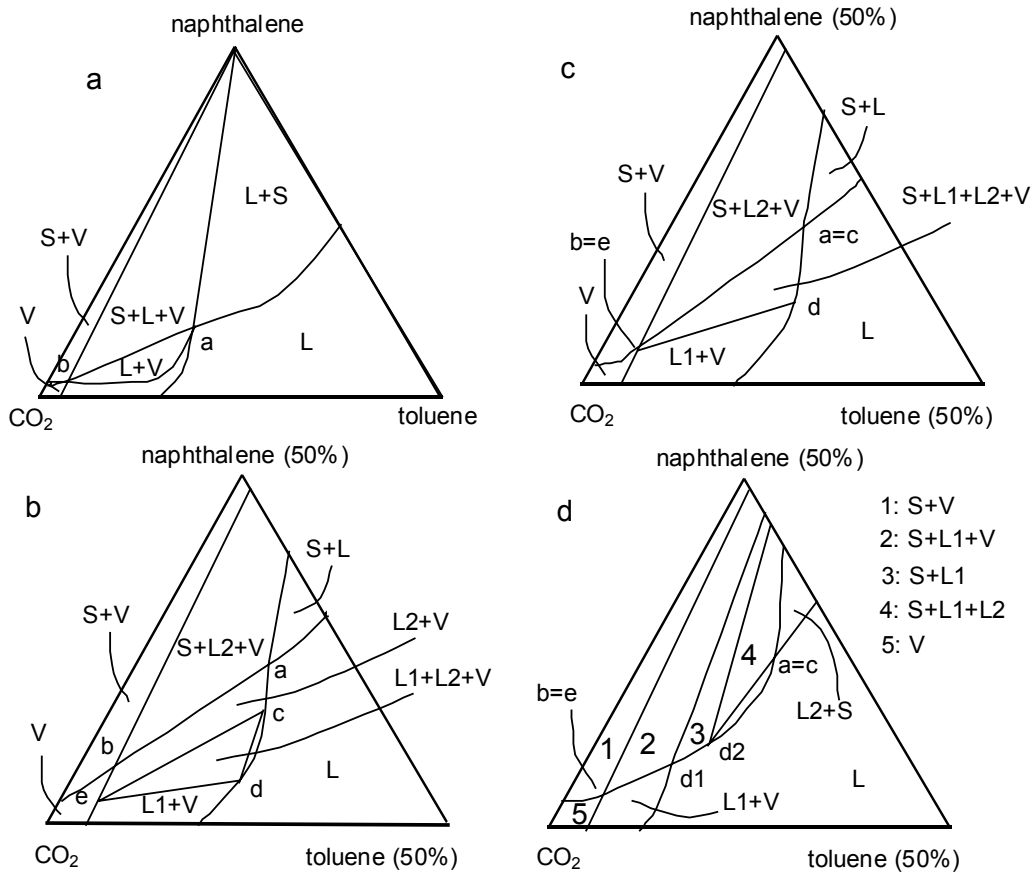

Fig 14. *Ternary diagrams for the system CO_2-toluene-naphthalene: (a) typical S-L-V equilibrium at T and P assigned; (b) S-L1-V and L1-L2-V equilibrium occurring at a temperature between 315 and 325 K and pressure between 8.2 and 9.8 MPa; (c) S-L1-L2-V equilibrium occurring at a temperature between 315 and 320 K and pressure between 8.2 and 9.1 MPa; (d) S-L1-V and S-L1-L2 equilibrium occurring at a temperature between 315 and 320 K and pressure above that of S-L1-L2-V equilibrium at each temperature [91].*

In Fig. 14a equilibrium without liquid-liquid immiscibility is presented. Point *a* corresponds to the composition of the liquid phase in equilibrium with vapor and solid and is determined once pressure *P* and temperature *T* are set. If *P* is raised at constant *T*, point *a* goes toward pure CO_2. At a temperature between about 315 and 325 K (Fig. 14b), raising pressure lets a second liquid phase to appear:

Depending on the overall composition, either L1-L2-V or S-L2-V equilibrium may occur. If pressure is raised above L1-L2-V critical point, two different behaviours are evidenced:

1) At a temperature between about 320 and 325 K the second liquid phase appears at a L1-L2 critical point (*c*=*d*); at increasing pressure, *d* goes toward *e* until the two phases *d* and *e* merge at a liquid-vapor critical point, and the triangle *c*-*d*-*e* degenerates.
2) At a temperature between about 315 and 230 K the second liquid phase appears at a liquid-liquid critical point, as in the first case. By an increase in pressure, the two pairs of point's *a*-*c* and *b*-*e* approach and merge: a four-phase equilibrium S-L1-L2-V is obtained (Fig. 14c). By another increase in pressure, the S-L1-L2-V area split into two triangles having a common vertex (Fig. 14d: the splitting occurs in point *d* of Fig. 14c, from which *d1* and *d2* originate).

1.4. VOLUMETRIC EXPANSION

In a batch process the volumetric liquid expansion is a function of temperature, pressure and type of solvent and anti-solvent gas [48]. In Fig. 15 the volume expansion of DMSO in supercritical CO_2 is shown at various temperatures [3,90,56]. The experimental data are from Yeo et al. [56] and Kordikowski et al. [90] and the volume expansion is calculated using a modified Peng-Robinson EOS [92]. The expansion curves move towards lower pressures when temperature increases; i.e., the same volumetric expansion can be obtained at lower pressure.

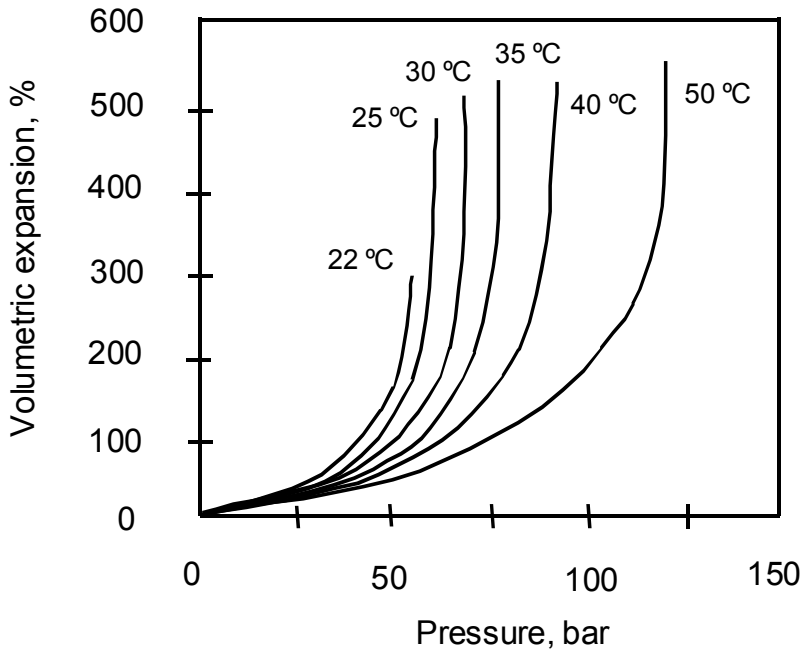

Fig. 15. *The volume expansion of DMSO in supercritical CO_2 at various temperatures [3,90,56].*

The volumetric expansion of liquid depends on the antisolvent. Kordikowski et al. [90] have studied the behaviour of several general binary liquid systems with carbon dioxide, ethane and ethene. The investigation of gas-solvent systems revealed differences in liquid density behaviour and liquid volume expansion. The result show large differences in the volume expansion, depending on the binary system investigated. Highly polar solvents like acetonitrile and DMF cause liquid-liquid immiscibility with ethane and probably also with ethene. Including DMSO, with dipole moment of almost 4 Debye, these solvents are miscible with carbon dioxide. Carbon dioxide does not have a dipole moment but it has a relatively large quadrupole moment, causing a small polarity for carbon dioxide. The extent of miscibility is reflected in the volume expansion of the liquid phase. With the occurrence of a liquid-liquid immiscibility, no further expansion takes place. In Fig. 16 is shown the volume expansion of aprotic solvents as function of the mole fraction of ethane, ethene and carbon dioxide in solvent.

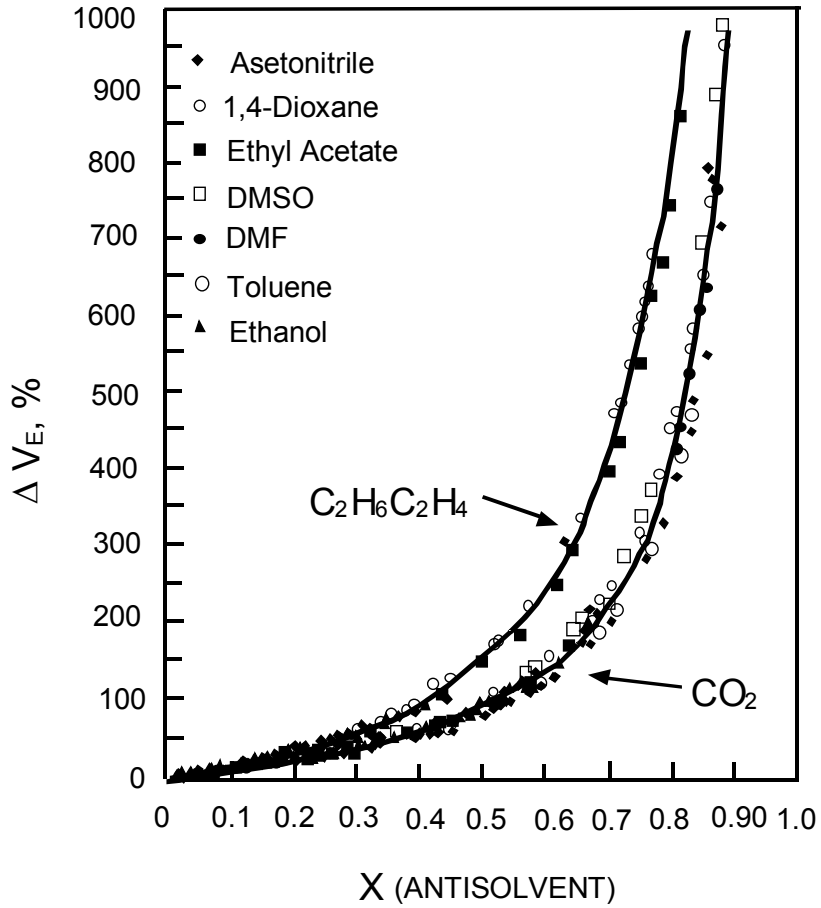

Fig. 16. *The volume expansion of aprotic solvents as function of the mole fraction of ethane, ethene and carbon dioxide in solvent [90]. The temperature range is from 295 to 313 K and pressure range from 0.5 to 7.8 MPa.*

However, the plot of expansion vs. mole fraction instead of pressure as show in Fig. 16 reveals a striking similarity between the various systems. Not only that various solvents coincide, but also for all temperatures the expansion curves are

indistinguishable. The curves for ethane and ethene coincide due to their physico-chemical similarity but are different compared to the carbon dioxide curve. The expansion of the solvent is responsible for the crystallization, and recognizing that at given mole fraction all expansion values for a given antisolvent are equal, the solubility of solid in the solvent is the limiting factor for a successful crystallization.

1.5. PRINCIPLES OF RECRYSTALLIZATION

The equilibrium in an assembly of dissolved molecules, which can combine to form a critical nucleus beyond which size favourable fluctuations will cause the nuclei to grow has been described by Gibbs [93] and Adamson [94]. Gibbs presented the conditions of critical nuclei formation based upon free energy considerations. The formation of an embryo, i. e., an assembly of molecules of a size smaller than the critical nucleus, requires that an interface between two phases form. Thus, the free energy of the system will have to increase initially until an embryo reaches some critical diameter. Once the embryo is of sufficient size, there are two competing modes of lowering the particle free energy:

- nucleus can grow indefinitely
- nucleus can shrink and disappear

Critical nuclei will grow at the expense of subcritical embryos so that the final particle size will be dependent upon initial critical nuclei concentration. The nucleation rate is very strongly influenced by the supersaturation ratio [2]. Crystallization is not occurring as soon as the solution gets saturated. Instead, the solution becomes metastable i.e. supersaturated solution in which the spontaneous deposition of the solid phase in the absence of crystallizing material will not occur, which means that the existing crystals will grow, but nucleation of new crystals into crystal free solution is not happening significantly. As the supersaturation level is increased, the nucleation rate becomes dominant and new crystals are formed. Operation at low supersaturations tends to favor growth of large crystals, whereas high supersaturation close to metastable limit favors formation of many small nuclei, which means formation of small crystals. The methods of generating supersaturation are [95]

- *Cooling/heating*
  The supersaturation level is increased by decreasing the temperature (if the solubility is decreased with decreased temperature). For some chemicals, which solubility is creased with increasing temperature, heating can be used to generate the supersaturation. The supersaturation level is dependent on solubility.
- *Solvent evaporation*
  The concentration of solution can be increased by evaporating the solvent, which will increase generation of supersaturation.
- *Change of pressure*
  The decreased pressure will decrease the boiling temperature and the solubility of the solution (compare cooling/heating).

- *Flash or evaporative cooling*
  The solvent is evaporated and therefore liquid cool off and supersature reached. The evaporation can be done under vacuum, the boiling point temperature due to flashing of solution is decreased and the concentration of the solution increased.
- *Salting out*
  Addition of another salt which dissolves in the solution and reduces the solubility of the desired product.
- *Drowning out*
  Addition of another solvent, which is miscible with main solvent, then the desired product is less soluble in the mixture.
- *Chemical reaction or reactive crystallization*
  Addition of two or more components, which will react in the solution to form a desired product, which crystallizes out.

In a GAS process the supersaturation is achieved by drowning out and solvent evaporation and in a RESS process with a change of pressurized. In an anti-solvent recrystallization process the particle size and particle size distribution is determined by interaction between [2]:

- nucleation rate
- growth rate of crystals
- rate of creation of supersaturation

All the three factors are influenced by the manner of antisolvent concentration and its rate of concentration change in solute. In batch GAS process those are influenced by the manner of addition of the antisolvent to crystallizer. Fig. 17 presents the qualitative picture of simultaneous events that occur when an anti-solvent is added into a batch GAS process [2].

In Fig. 17 three zones are presented;

1) In zone I no growth of particles will occur and any particles, that are present, will dissolve.
2) In zone II some nucleation can occur and particles that are present can grow by the diffusion mechanisms.
3) In zone III represents very high supersaturation levels, and in this regime catastrophic nucleation can occur.

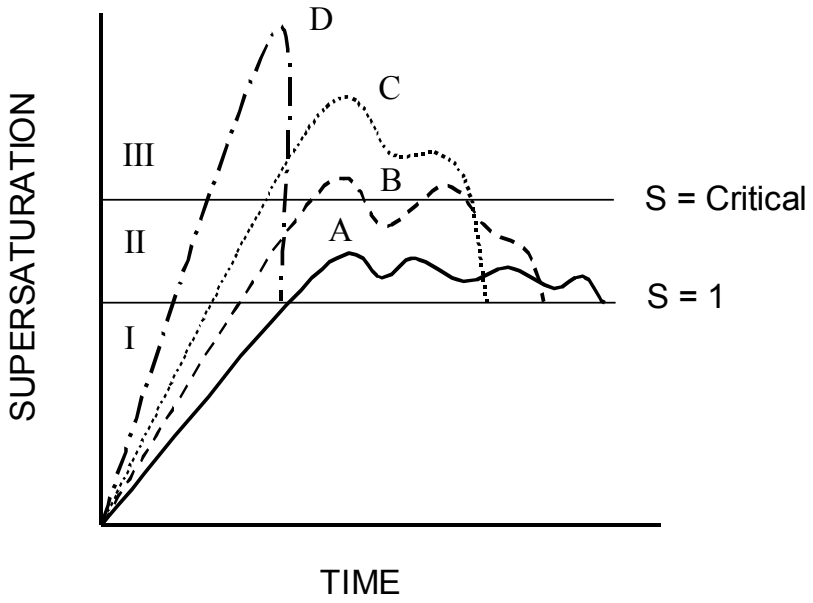

Fig. 17. *Variation of supersaturation with rate of addition of anti-solvent [2]. The three zones shown; Zone I) supersaturation S is less than 1, i.e. for actual solute concentrations less than saturation; Zone II) supersaturation is less than the critical value; Zone III) very high supersaturation level.*

The four paths, A, B, C and D represent different rates of addition of antisolvent. They depict the generation of supersaturation by anti-solvent addition and the simultaneous consumption of supersaturation by nucleation and growth. On path A the rate of addition is so low that the rate of nucleation and the diffusional growth of those nuclei formed maintain the supersaturation below the critical value until the concentration of solute in solution eventually falls to saturation (S=1). Curve B represents a higher rate of addition, high enough to exceed the critical supersaturation level. The solution is rather quickly depleted of solute by higher rate of nucleation and the higher overall growth rate. The addition via Curve C is a variant of Curve B, a still higher rate of anti-solvent addition. The addition depicted by Curve D is so high that almost all the solute in solution is consumed by formation of nuclei, and the solute in solution is depleted almost solely by that mechanism [2].

Above is described the batch GAS process, but in continuous GAS, where the solvent is sprayed continuously through the nozzle into anti-solvent, the mechanism of nucleation is similar to batch process. In continuous GAS process the variation of supersaturation is near line D and C in Fig. 17. The mass transfer of liquid solvent to anti-solvent phase and anti-solvent to liquid phase is confined to the supersaturation rate. The increasing of concentration of anti-solvent in solution is actuated by the volumetric expansion of solution. Nucleation and growth events are depicted differently on a solution expansion time.

The threshold pressure (TPH), where visible nucleation is occurred, is a function of solution concentration, the higher the concentration, the lower the pressure required to initiate nucleation. Nucleation and growth events are depicted

differently on solution expansion-time plot for anti-solvent addition in Fig. 18. If the subsequent expansion is essentially nil as show by the Curve A expansion path, relatively few nuclei are formed as related earlier. Those nuclei can grow to be large because relatively large amount of solute remains in solution after some nuclei are formed. Curves B and C depict the faster rates of addition of gas antisolvent, both rates of addition will result in a wide distribution. Curve D represents an extremely high rate of expansion by rapid gas injection and pressure rise, essentially monodisperse and very small particles will result.

Anti-solvent gases, which are soluble in liquids can be admixed almost instantaneously, i.e., complete expansion can be made to occur literally within a few seconds. Thereby extremely high supersaturation levels and nucleation rates can be attained by continuous GAS recrystallization processes resulting in the formation of extremely small particles not readily achievable by other processes.

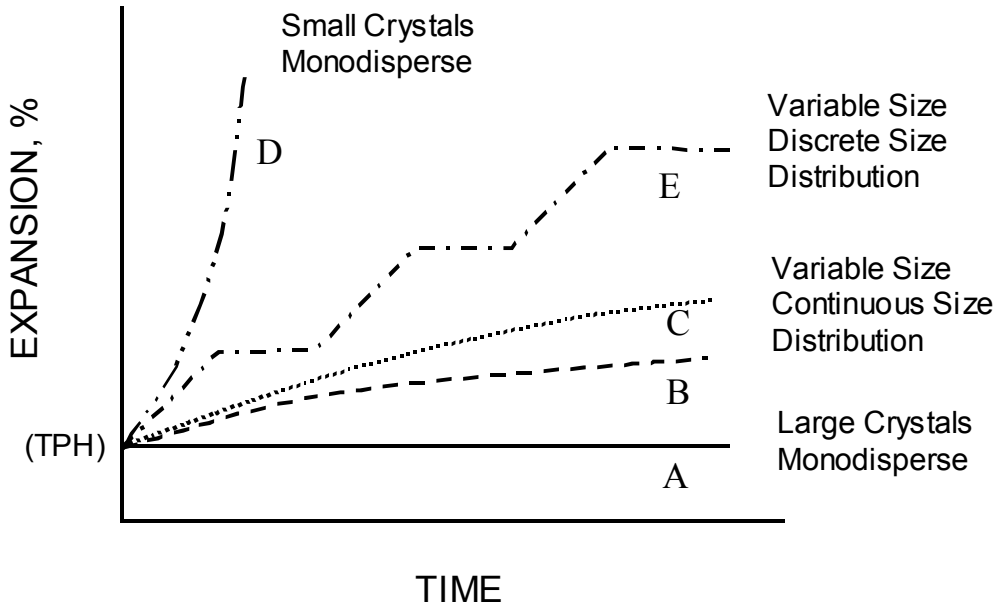

Fig. 18. *The expansion paths for anti-solvent addition in batch GAS process. The starting point on the vertical axis is that amount of expansion, which results in the onset of visible nucleation (the threshold pressure; THP) [2].*

The precipitation of the solute is ascribed to the volumetric expansion of the liquid phase due to increasing amount of dissolved antisolvent in the liquid phase with increasing pressure. The appropriate combination of antisolvent-solvent was chosen in such a way that at the lowest pressure possible, the majority of the dissolved solute be forced to crystallize. In order to select the proper operational temperature, the nature of the solute, its melting temperature, the temperature at which thermal decomposition may occur, the solubility of the solute in the anti-solvent-free solvent as a function of temperature have to be considered [146]. For operational temperatures lower than the critical temperature of the antisolvent, the operational pressure, that corresponds to the final concentration (approximately zero) of the solute in the liquid phase, is close to the vapor pressure of each pure

antisolvent at the given temperature. In Fig. 19 for instance the solubility of naphthalene in toluene is shown as a function of the pressure of various antisolvents [146]. The Peng-Robinson equation of state was used to describe the solubility in ternary near-critical antisolvent-liquid-solid systems.

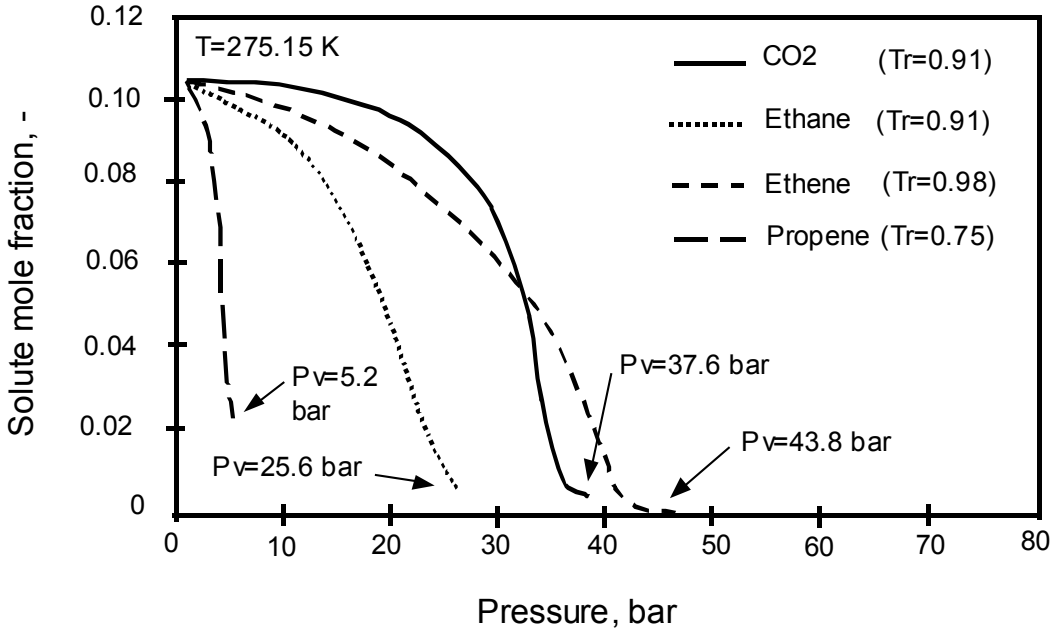

Fig. 19. *Solubility of naphthalene in toluene as a function of the pressure of various antisolvents. T_r is the reduced temperature of the antisolvent and P_v the saturated vapor pressure of the antisolvent at the chosen temperature of 276.2 K [146].*

On the other hand, if the temperatures are higher than critical temperature, the pressure required to crystallize the same amount of solute from the solution is substantially higher. In such a case, an antisolvent with a higher critical temperature and a saturated vapor pressure as low as possible should be selected.

It is difficult to form crystals of the larger molecules by using a supercritical antisolvent SAS process[96]. During the SAS operation, the mixing process of the solvent and antisolvent generates high turbulence within the solution, which affects both the nucleation and growth of the resulting particles. These disturbed conditions, which exist during the particle formation process, interrupt the regular arrangement of molecules. Indeed, the crystallization of proteins and polymers requires conditions during the supersaturation and particle growth stages. Therefore, in SAS operation, the precipitated macromolecular compounds are more likely to exist in the amorphous state rather than the crystalline state, unless the molecule itself has an exceptionally high level of crystalline structure, which might be induced by a molecular backbone of exceptional rigidity. Under carefully controlled experimental conditions, such as an extremely low contact speed between the solvent and antisolvent, the supercritical antisolvent technique can provide a suitable environment for the nucleation and growth of crystallizable material [96,49].

The crystal's internal structure and its external characteristics determine the physical behavior of the material. For example the absorption rate of a pharmaceutical depends on the crystal structure of the drug. Amorphous materials are known to dissolve more rapidly than crystalline substances [97]. The slow injection of antisolvent in to solute with batch gas antisolvent technique produces somewhat different particles in terms of morphology and size compared with continuous SAS operation, which involves extremely rapid contact between solvent and antisolvent [49,56]. Yeo et al. [49] have studied both batch and continuous modes of supercritical antisolvent operation. Carbon dioxide was contacted with 0.03-0.12 wt % polymer in dimethyl sulfoxide (DMSO) and N,N-dimethylformamide solutions. In these systems, the particles are produced in either the amorphous or spherulitic state. Slow expansion of the solution produces polycrystalline spherulites in the 1-10 μm diameter range, and the degree of crystallinity was affected by turbulence caused by carbon dioxide injection.

Yeo et al. [96] used the supercritical antisolvent (SAS) process to produce crystals of $BaCl_2$ and NH_4Cl from solutions of DMSO. Crystallization was performed by introducing carbon dioxide into DMSO solutions at different injection rates. Variations in crystal properties such as particle size, crystal habit, and internal space lattice were observed in the SAS process crystals. The average particle size of the crystals decreased with increasing CO_2 injection rate for both compounds. As the injection rate increased, the crystal habit of $BaCl_2$ was modified from an equant to an acicular habit, and that of NH_4Cl changed from an equant to a tabular habit. X-ray diffraction showed the transition of the space lattice of $BaCl_2$ from the orthorhombic to hexagonal crystal system.

Jaarmo et al. [55] have studied sodium cromoglycate particle tailoring in methanol with supercritical CO_2 by using continuous gas antisolvent technique. Both crystalline and completely amorphous particles were obtained. The starting material and the produced amorphous particles were of same polymorph class. The amorphous particles were spherical and the size varied around one micrometer.

1.6. LIQUID-GAS INTERFACIAL TENSION

When droplets are produced in an atomizer, droplet size and distribution depend on interfacial tension. Interfacial properties have a fundamental influence on dense gas/liquid separation processes, with the interfacial tension being an important quantity associated with mass transfer [98]. In spraying technique the interfacial tension is changed during the droplets flying time in dense gas. When small droplets of liquid are falling through a gas, surface tension tends to make the droplets nearly spherical, and the coefficients for mass transfer to the droplet surface are often quite close for solid spheres. The interfacial tension of the liquid phase decreased by dissolution of gas at the interface [99]. In near and subcritical fluid all these factors are dependent on temperature and pressure.

Interfacial tension between liquid and CO_2 has been presented by some authors [98,100,101,102]. Generally, the interfacial tension of the liquid phase decreased by dissolution of gas at the interface. The increase the pressure of gas phase increased the gas concentration of the liquid phase. The density of the liquid phase decreases with increasing pressure whereas the density of the gas phase increases. Due the dissolution of gas the interfacial tension decreases. The decreasing of interfacial tension depends on the gas. In Fig. 20 shows the interfacial tension of some liquids as a function of CO_2 pressure [100,101,103].

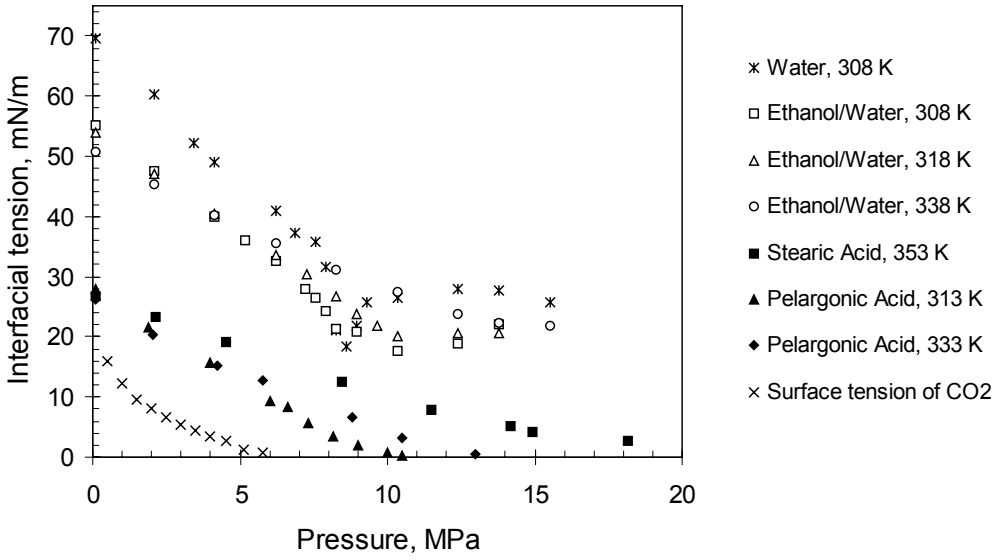

Fig. 20. *Interfacial tension of liquids in CO_2 as a function of CO_2 pressure. The interfacial tension data of water-CO_2 and ethanol-water-CO_2 systems were from Chun et al. [103] data of stearic acid and pelargonic acid from Schiemann et al. [100] and surface tension of CO_2 from Jasper [101]. In the water-ethanol mixtures was 0.184 mole fraction ethanol.*

Schiemann et al. [100] have studied interfacial tension of pelargonic acid and stearic acid as non-volatile component in dense carbon dioxide temperatures ranging from 313 K to 393 K and pressures up to 25 MPa. The interfacial tension was found to be mainly a function of the gas content of the coexisting liquid phase. With increasing pressure of CO_2, the interfacial tension first strongly decreased and then at small values approached zero asymptotically in high values of pressure.

Chun and Wilkinson [103] have studied interfacial tensions of water-alcohol-CO_2 mixtures on the pressure up to 190 bar, temperatures ranging from 278 K to 343 K and concentration of alcohols in water up to 30 vol-%. Interfacial tension decreased with both temperature and pressure of CO_2 but was largely independent of pressure at high pressure (liquid or supercritical CO_2). With increasing pressure of CO_2, the interfacial tension first strongly decreased and then at small values approached constant value asymptotically. The interfacial tension decreases with

decreased ethanol mole fraction in water. The internal tension decreased acutely as the CO_2 rich phase approached the dew point and then increased as the bubble point was passed. For example in Fig. 20 the interfacial tension of water decreases markedly at temperature 308 K and pressure 8.5 MPa. This effect increased with decreasing temperature and disappeared at high temperature. For example for water over the temperature 318 K the effect of acutely decreasing interfacial tension does not anymore exist.

The effect of temperature for interfacial tension is twofold. ”Crossover” pressure is the pressure below which interfacial tension decreases with temperature and above which it increases. In Fig. 20 ethanol-water systems the crossover pressure is about 8.5 MPa [103].

The value of surface tension between liquid and CO_2 at high pressure is dependent on the initial liquid surface tension at atmospheric pressure. In organic liquid (example in Fig. 20 pelargonic acid and stearic acid), the value of interfacial tension near 0.1 MPa is near 28 mN m^{-1} and at pressure over 10 MPa value is about 2 mN m^{-1}. Table V shows the surface tension of various liquids in contact with air or vapour at 0.10 MPa pressure [104]. A typical value of interfacial tension in organic liquids in air or vapour system is in the range of 20 mN m^{-1} to 30 mN m^{-1}. The interfacial tension decreases slightly with increasing temperature.

Table V *Surface tension of various liquids in contact with air or vapour in 0.10 MPa pressure [104]. The surface tension of liquid carbon dioxide is defined at liquid-vapour equilibrium state.*

		Surface tension (mN/m)	
Substance	Contact in	at 273 K	293 K
Water	Air	75.6	72.8
Acetone	Air or vapour	26.2	23.7
Ethyl alcohol	Air or vapour	24.1	22.8
Chloroform	Air		27.1
Dichloromethane	Air		26.5
Toluene	Vapour		28.5
Carbon dioxide (5.7 MPa)	Vapour		1.2

The interfacial tensions of some organic liquid-CO2 systems are in the range of 0.1-7 mN m^{-1}. Moser et al. [102] have done interfacial tension measurements between α-tocopherol and carbon dioxide at a density value range of 450 to 900 kg m^{-3} and at a pressure of up to 37 MPa. Interfacial tension is at operation conditions in the value range of 4.5 to 1.3 mN m^{-1}. Fig. 21 is shows interfacial tension of some liquids as a function of CO_2 density [100,102].

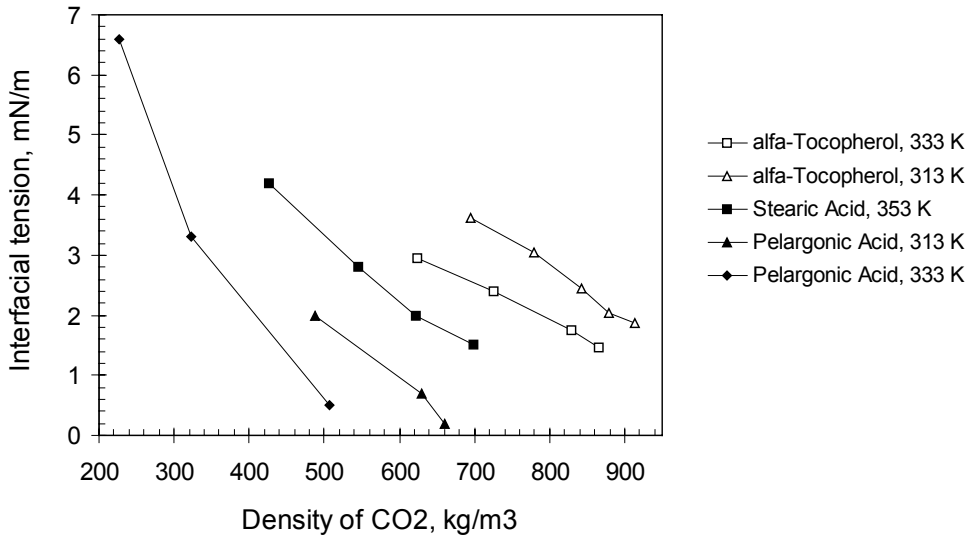

Fig. 21. *Interfacial tension of liquids in CO_2 as a function of CO_2 density. The interfacial tension data of α-Tocopherol -CO_2 systems were from Moser et al.* [102] *and other data from Schiemann et al.* [100].

1.7. MASS TRANSFER

1.7.1. MASS TRANSFER COEFFICIENT

The mechanism of mass transfer changes at different stages of the evaporation process. The first stage is the shrinking balloon stage, where the rate of evaporation is balanced by the transfer of liquid from the center to the surface of the droplet [105]. In the SAS process the solution is generally dilute and the equilibrium compositions of the binary and ternary mixtures are not significantly different. Accordingly the solid present in the solution is not likely to affect the rates of mass transfer of CO_2 and solvent to and from the droplet respectively [106].

Mukhhopadhyay and Dalvi [154] have shown schematically (Fig. 22) how a single atomized droplet travels through the supercritical CO_2 continuum in a SAS process. In State 1 the droplet contains only solution and the surrounding environment is pure supercritical CO_2. The driving forces are in maximum at this condition. As the CO_2 dissolves into the droplet, the concentration in the droplet changes and so does the driving force for the CO_2 transfer. Because the dissolution of CO_2 is an exothermic process, the heat liberated enables simultaneous evaporation of solvent into the CO_2 environment (State 2). The temperature of the droplet instantaneously increases and subsequently decreases by 1 to 3 K at the immiscible conditions for a lower CO_2 rate irrespective of initial temperature. At the miscible conditions, it remains almost steady for the higher CO_2 flow rate, though there is an instantaneous rise in the stable temperature at the lower flow rate. The higher CO_2 and solution flow rates and a lower

volumetric flow ratio at the miscible condition are desirable to have a steady temperature profile of the droplet with time. The droplet may swell (State 3) or shrink (State 4) depending upon the diffusion or back diffusion of CO_2 respectively during its flight through the CO_2 continuum. The droplet tends to shrink in the vicinity of the mixture critical point, whereas it swells at all conditions away from the mixture critical point irrespective of the nature of the thermodynamic state.

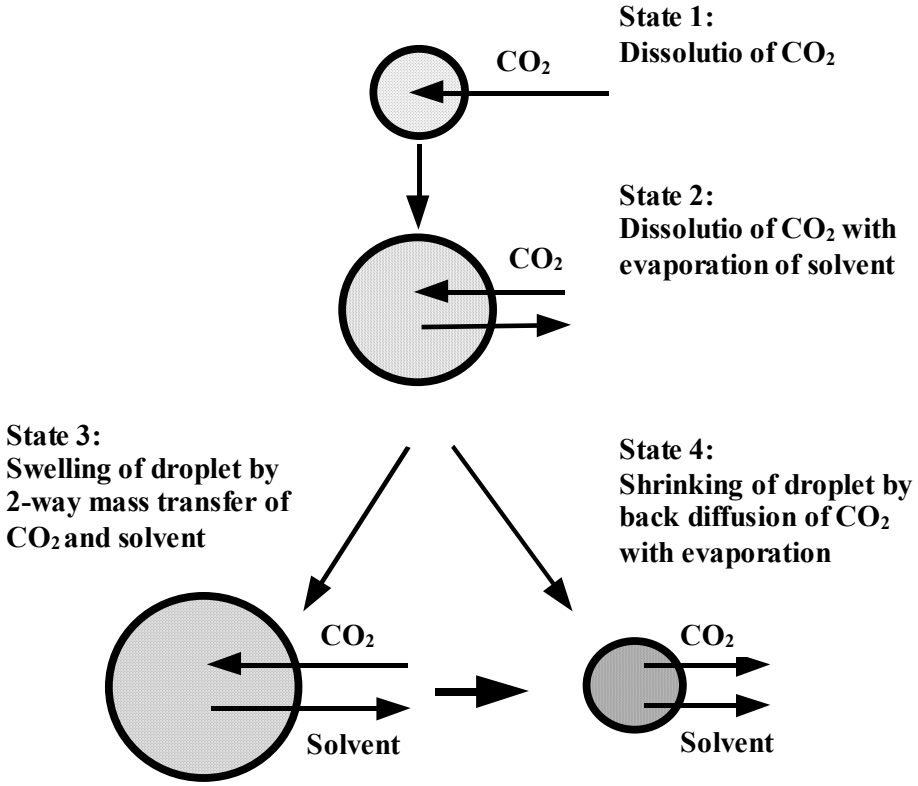

Fig. 22. Schematics of single atomized solution droplet travelling through the supercritical CO_2 continuum of SAS process [154].

In the supercritical fluid-solid systems the mass transfer coefficient was found to be in the same range as in gas-solid and liquid-solid systems. Table VI shows the range of mass transfer coefficients for gases, liquids and supercritical fluids on packed-bed operations [107].

Table VI *The ranges of mass transfer coefficients for gases, liquids and fluids on packed-bed operations [107].*

System	Range of mass transfer coefficient (cm s^{-1}) [a]
Liquid-Solid	$1.51*10^{-5}$ - $5.35*10^{-4}$
Gas-Solid	$1.51*10^{-3}$ - $5.35*10^{-2}$
Supercritical fluid-Solid	$5.52*10^{-4}$ - $2.03*10^{-3}$

[a] Reynolds number is in the range from 2.0 to 20

The mass transfer is a function of continuous phase density, viscosity, diffusivity, porosity of solid, droplet or particle diameter and solvent flow rate. The influence of the variables is expressed using dimensionless numbers. It is common to use the Sherwood, Schmidt, Reynolds and the Grashof numbers. The dimensionless numbers are given by

$$Sh = \frac{k_G d_d}{D} \tag{1}$$

$$Sc = \frac{\mu_G}{\rho_G D} \tag{2}$$

$$Re_d = \frac{d_d U_G \rho_G}{\mu_G} \tag{3}$$

$$Gr = \frac{d_d^3 g \Delta\rho}{\mu^2} \tag{4}$$

where *Sh* is Sherwood number, *Sc* is Schmidt number, *Re* is Reynods number, *Gr* is Grashof number, k_G is gas side mass transfer coefficient (m s^{-1}), d_d is droplet (or particle) diameter d_p (m), U_G is gas flow rate (m s^{-1}), ρ_G is gas density (kg m^3), μ_G is gas viscosity (Pa s), *D* is binary diffusion coefficient of liquid in gas phase (m^2 s^{-1}) and $\Delta\rho$ is density difference at the solid surface as compared to the bulk (kg m^{-3}). The Schmidt number for supercritical fluids is around 10 (between from 3 to 16) and lie between those for gases and for liquids. The Grashof number is used especially systems where the natural convection is important [107,112,113]. Some papers discuss mass transfer in supercritical fluid-liquid systems [11,98,108,109,110,111,118] and SCF-solid systems [111,112,113,114,115,116]. Generally the mass transfer mechanism in dense gas is presented by Bertucco and Vetter [117]. Table VII shows some mass-transfer coefficient correlations for supercritical fluid-solid and supercritical fluid-liquid systems.

Table VII *Mass transfer coefficient correlations for supercritical fluid-solid and supercritical fluid-liquid systems.*

Systems	Equation	Reference
Supercritical fluid-Solid		
Packed bed	$\frac{Sh}{(ScGr)^{1/4}} = 1.692\left[\frac{\mathrm{Re}}{Gr^{1/2}}\right]^{0.356}$ $2<Re<70$, $2<Sc<11$, $78<Gr<3.25*10^7$ Average deviation 15%	Lim et al. [116]
Packed bed	$\frac{Sh}{(ScGr)^{1/4}} = 1.451\left[\frac{\mathrm{Re}}{Gr^{1/2}}\right]^{0.525}$ $0.05\leq Re\leq 1.0$, $6.5\leq Sc\leq 18$ $0.6\leq Gr\leq 300$ Mean deviation 13%	Ferreira et al. [111]
Packed bed	$Sh = 0.839\,\mathrm{Re}^{0.667}\,Sc^{1/2}$ $Sh = 2 + 1.1\,\mathrm{Re}^{0.6}\,Sc^{1/3}$ $2<Re<55$, $4<Sc<16$	Catchpole et al. [113]
Supercritical fluid-Liquid		
Sieve tray/	$k_G = 0.698\left(\frac{D}{d_d}\right)\left(\frac{\rho_G U_G d_d}{\mu_G}\right)^{0.5}\left(\frac{\mu_G}{\rho_G D}\right)^{0.42}\left(1-\phi_d\right)$ [a]	
Spray	Average deviation < 25%	Seibert et al. [109]
Spray	$Sh = 2.0 + Sc^{1/3}\,\mathrm{Re}_d^{1/2}$	Eggers et al. [11]
SAS	$Sh = 2 + 0.0187\,\mathrm{Re}^{0.779}\,Sc^{0.564}\,(dg^{0.333}D_G^{-0.667})^{0.116}$	Lora et al. [151], Mukhopadhyay and Dalvi [154]

[a] ϕ_d is dispersed phase holdup, fraction of void volume occupied by the dispersed phase.

Lim et al. [116] have studied gas-solid mass transfer and liquid-solid CO_2-naphthalene system at pressures from 1 MPa to 20 MPa and at a temperature of 308 K in a packed bed extractor. They found out that both natural and forced convection are important under these conditions and that mass transfer rates at near-critical conditions are higher than at lower or higher pressure. Reynolds

number was between 2 and 70, Schmidt number between 2 and 11 and Grashof number between 78 and $3.24*10^7$. At 308 K, the gas-solid mass transfer coefficient increases dramatically near the critical point, has its maximum value near 10 MPa, and then decreases gradually as pressure increases. The system consisted of a cylindrical extraction vessel, which is 104 ml in volume, 14.8 cm in length and 3.45 cm in diameter.

Debenedetti and Reid [115] have studied diffusion and mass transfer of solids in supercritical fluids. They showed, that significant rate enhancements due to natural convection would result in supercritical extraction processes whenever the controlling resistance to mass transfer is in the supercritical phase. This is a consequence of the unusually low kinematics viscosities of fluids in the near supercritical region, which in turn arises as a result of the different behavior of density and viscosity when moving from the dilute gas to the dense fluid region.

Seibert et al. [109] have presented fundamental mass transfer models applicable to spray columns and compared them with actual experimental data. The hydrodynamic and overall mass transfer characteristic in the high pressure CO_2 spray extraction was observed to behave similarly to those of conventional liquid-liquid extraction with conventional droplet formation and movement. They used to extract isopropanol or ethanol from water at pressure of 8.1 to 15 MPa and temperatures of 293 to 318 K using high pressure extraction column (without fixed bed) with internal diameter of 2.54 cm and 9.88 cm and a contacting height of 1.68 m. It was noted that the fundamental mass transfer models assume that the dispersed phase may be represented as spherical droplets with a mean droplet size.

Ferreira et al. [111] have studied the mass transfer coefficient correlations for supercritical fluid extraction of black pepper essential oil using a fixed bed extractor at temperature of 302 K to 323 K and at pressure of 15 MPa to 300 MPa. The mass transfer coefficients varied from $2.5*10^{-5}$ to $30*10^{-5}$ m s^{-1}. The Sherwood number varied from 0.3 to 16. They have used five general mass transfer correlation equations. The mean deviation for the literature correlation varies from 33 % to 224 %. The mean deviation of expressions between the calculated and experimental mass transfer was 13 %. They evaluated the combined effect of natural and forced convection. Both the natural as well as the forced convection were important in the range of operating conditions.

Jaeger et al. [98,108] have shown that interfacial tension properties essentially influence fluid-liquid separation processes. Generally, interfacial tension decreased with increasing pressure due to increased adsorption of the compressed fluid at the interface. In the case of considerable mutual solubility, interfacial tension further decreased with time as mass transfer into the bulk phase proceeded.

Laitinen and Kaunisto [118] studied the extraction of 1-butanol from aqueous solutions using supercritical carbon dioxide at 10 MPa and 313 K as a solvent. Experimental studies were performed using a 35 mm diameter mechanically agitated supercritical fluid extraction column. The values of the overall mass

transfer coefficient were in the range 0.0019-0.034 s^{-1}. Mechanical agitation had no effect on the column efficiency at the selected extraction conditions.

Lora et al. [151] have modeled thermodynamic, hydrodynamics, and mass transfer phenomena in order to simulate a semicontinuous antisolvent recrystallization process. They have used by Hughmark [119] mass transfer coefficient in the continuous phase. They have shown, that in a CO_2-toluene-naphthalene-phenanthrene system the dissolution of the antisolvent in the liquid phase is usually faster than the evaporation of the solvent. Mukhhopadhyay and Dalvi [154] have studied the droplet dynamics for single droplet of CO_2-acetone solution falling in a CO_2 stream. A model based on the SAS mechanism of simultaneous mass and heat transfer has been simulated to study the effects of the thermodynamic states and the individual flow rates of CO_2 and solution. They have also used by Hughmark mass transfer coefficient in the continuous phase as Lora et al. [151].

The Table VIII shows some mass transfer coefficient correlations used for the liquid phase in *SAS technique.*

Table VIII *Mass transfer coefficient correlations for liquid phase in SAS technique.*

Systems	Equation		Reference
SAS	$k_L = \frac{2\rho D_{12}}{d_p}$		Lora et al. [151]
SAS	$k_L = \sqrt{\frac{4D_{12}}{\pi\ t_c}} = \sqrt{\frac{4D_{12}U}{\pi\ d_p}}$	a)	Mukhopadhyay and Dalvi [154]

a) *D_{12} is the diffusion coefficient of the antisolvent in the liquid phase and t_c is the contact time between the two phases.*

Lora et al. [151] calculated the mass transfer coefficient in the liquid phase by using Hughmark [119] mass transfer coefficients in the continuous phase equation. As a first step assumption, convective motions and circulation within small droplets can be neglected, so that mass transfer in the droplet is driven only by molecular diffusion. Then Reynods number is equal or greater than zero. Mukhopadhyay and Dalvi [154] calculated the liquid phase mass transfer coefficient by the penetration theory [120]. They were calculated k_L with the expression in Table VIII, where t_c is the contact time between the two phases and it is taken as the time required for the droplet to travel the distance equal to its diameter.

1.7.2. DIFFUSION COEFFICIENT

In supercritical fluid systems diffusion coefficients *D* are slightly larger than those in liquids and much lower than in low pressure gas mixtures. The binary diffusion

coefficient for solute in a supercritical gases is around 10^{-8} m^2 s^{-1}. The typical binary diffusion coefficient in liquid system is in the range $0.5*10^{-9}$ to $2*10^{-9}$ m^2 s^{-1} and for those vapours in air at 298 K $5*10^{-6}$ to $20*10^{-6}$ m^2 s^{-1} [121,122].

Many authors have studied binary diffusion coefficients in supercritical carbon dioxide [123,124,125,126,127,128,129,130,131]. Generally it was found that the Wilke-Chang equations give the best-fit [123,128,129,131]. The Wilke-Chang equation for binary diffusion coefficient is [132]

$$D_{21} = 7.4 \cdot 10^{-15} \frac{T(\phi M_1)^{0.5}}{\mu_1 v_2^{0.6}} \tag{5}$$

where the subscripts 1 and 2 refer to the solvent and solute respectively, M_1 is the solvent's molecular weight (g mol^{-1}), T is temperature (K), μ_1 is the pure solvent's viscosity (Pa s^{-1}), v_2 is the solute's solid molar volume (cm^3 mol^{-1}) and ϕ is the association factor for the solvent. For example the association factor for unassociated solvent is 1.0, methanol 1.9, ethanol 1.5 and water 2.6 [133].

Entrainers can have an influence on diffusion coefficients in supercritical solvent mixtures. Shenai et al. [127] have studied diffusion of benzoic acid, phenanthrene and acridine in acetone and supercritical CO_2 mixtures. The addition of methanol (5 mole percent methanol) at a temperature range of 308 K to 328 K and pressure range 17.0 MPa to 27.2 MPa reduces the observed diffusivities in all cases. The decreasing of diffusivities is dependent on the solute. The diffusivities of benzoic acid decrease in the range of 23% to 35% and the diffusivities of benzoic acid decrease in the range of 6% to 11% in those operation conditions.

As the CO_2 diffuses into the droplet and the solvent evaporates, the composition of the ultra-fine droplet changes drastically which in turn changes the diffusivity of CO_2 in the solution droplet. The variation of liquid phase diffusivity with change of composition can be estimated in SAS mass transfer modeling [134,149,151,154] by using the Vignes approach [135]:

$$D_{12} = (D_{12}^0)^{1-x_1} (D_{21}^0)^{x_1} \tag{6}$$

where D_{12}^0 is diffusion of CO_2 in an organic solvent, D_{21}^0 is diffusion of pure organic solvent in supercritical CO_2 and x_1 *is the liquid phase mole fraction of* CO_2.

2. AIMS OF THE RESEARCH

The objective of this study is to consider the development and feasibility of supercritical antisolvent (SAS) particle production process. The specific aims were to:

1. Study the applicability of the variable volume view cell (VVV -cell) to find appropriate combinations of the solvent and the gaseous antisolvent for a given solid.
2. Describe models for the SAS technique and examine which controls particle sizes in the near critical and supercritical regions; the mass transfer or jet break up and hydrodynamics or both.
3. Study applicability of the two special supercritical precipitation techniques to production of particles in the following applications; amorphous pharmaceutical particle production with supercritical antisolvent precipitation (SAS) and selective extraction/crystallization of cholesterol from supercritical CO_2.
4. Develop a calculation tool for estimating the capital and manufacturing costs and to study the cost structure of large scale SAS processes.

3. PHASE SEPARATION STUDIES IN A STATIC VARIABLE VOLUME VIEW-CELL

The main problem in a gas antisolvent process is to find the appropriate combinations of the solvent and the gaseous antisolvent for a given solid. The gas (antisolvent) must be totally miscible with the solvent in the desired temperature and pressure range. The liquid solvent has to dissolve quite well the solid materials. However, the limiting factor for successful crystallization process is the solubility of solid material in the solvent. The solubility of solid material is a function of density. The expansion of the solvent is responsible for the crystallization. The volumetric expansion of the liquid carrier mainly controls the morphology of particles produced by GAS precipitation. Most common organic solvents vary widely in molecular structure and polarity. Consequently, it is not possible to predict a priori whether a certain solvent is miscible with the antisolvent. The commonly used liquid solvents in supercritical carbon dioxide are dimethyl sulfoxide (DMSO), N,N-dimethyl formamide (DMF), toluene, acetonitrile, acetone, methanol, ethanol and dichloromethane (See Table II).

In this work feasible combinations of the solvent and the antisolvent were studied for four different pharmaceutical compounds by using static variable volume view cell (VVV-cell) method. The VVV-cell is principally used for solubility measurement of compounds [136]. In this work, however the VVV-cell was used for finding the appropriate combinations of operating conditions for particle formation.

3.1. VARIABLE VOLUME VIEW CELL

The static variable volume view cell is equipped with a sapphire window, which allows visual observation of high-pressure phase behaviour. A schematic diagram of the variable volume view cell is shown in Fig. 23 [77,118]. The main component of system is a variable volume view cell, which allows the visual determination of the phases present at equilibrium. The maximum operating temperature of the system is approximately 390 K and the maximum operating pressure is 50 MPa. The piston inside the cell is driven by a Isco 260 D high pressure syringe pump. The maximum internal volume of the cell with the piston inside is 30.4 ml. The cell content is mixed with a magnetic stirrer. The cell is inside an air bath, and the temperature is maintained constant within ±0.5 K by a controller. The temperature in the cell is measured by a calibrated J-type thermocouple. The pressure is measured by Philips P21 pressure sensor and registered by digital Philips Digital 380 indicator. The maximum estimated error for pressure measurements is ±0.05 MPa. The data are collected by Notebook Pro 8.01 data acquisition program and process was controlled by Labtech software. The Olympus borescope and light source, Hitachi VK-C220E camera, monitor and tape-recorder are used to make the visualization easier [137].

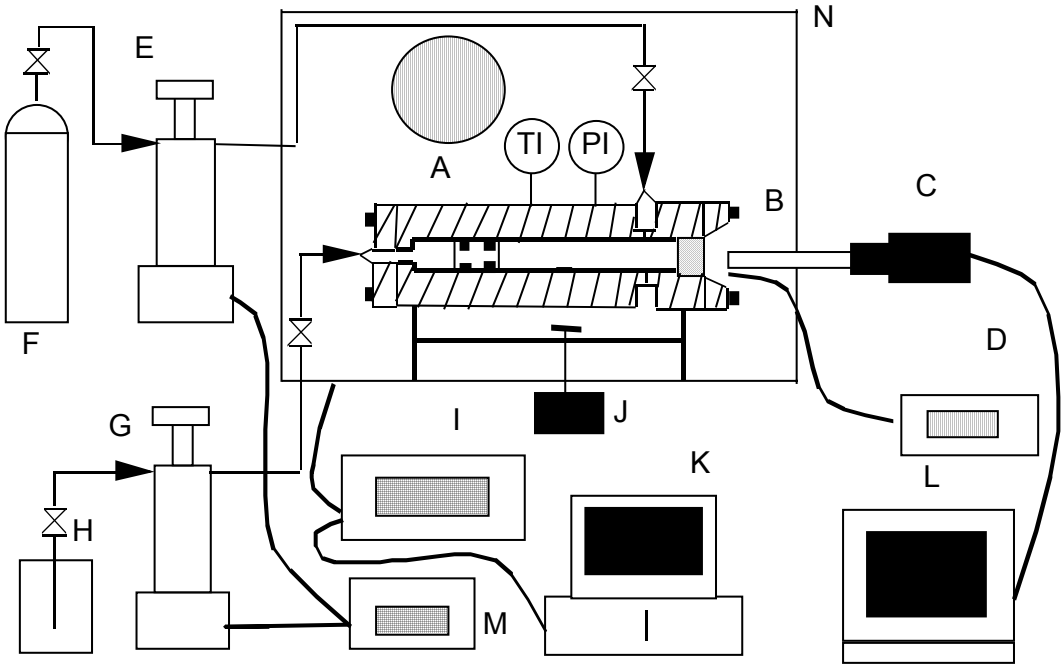

Fig. 23. *A variable volume view cell apparatus used in solubility measurements* [77,118]*; A) variable volume view cell; B) Boroscope; C) camera; D) light source; E) carbon dioxide pump; F) carbon dioxide container; G) hydraulic oil pump; H) oil container; I) data acquisition and control unit; J) magnetic stirrer; K) computer; L) monitor; M) pump control unit; N) air bath*

Figure 24 presents the principle of the variable volume view cell procedure for finding the appropriate combinations of the solvent and the gaseous antisolvent for a given solid. The formation of particles was carried out by first charging a desired amount (1-4 ml) of pharmaceutical material and liquid solvent solute to bottom of the cell after which the cell was warm up desired temperature. The cell was slowly pressurized by pumping in CO_2. At the same time the volumetric expansion of the solute takes place due to the dissolution of the CO_2 antisolvent into the solute phase. A CO_2 pump control unit was used to calculated the amount of CO_2 pumped to the cell. The pump unit showed, how much the volume of the pump cylinder changed during the pressure vessel loading while the piston was adjusted to maintain constant pressure.

The pressurization was completed when a solid phase appeared in solvent/CO_2 solute or one phase was achieved (i.e. when solvent and pharmaceutical material dissolved in CO_2). In 'one phase without particle formation' case, the pressure in the closed cell was slowly increased/decreased at different temperatures by moving the piston inside the cell until the particle formation was reached.

If one phase was reached without particle formation and the change of temperature and pressure in one phase did not produce particles, then the combination of pharmaceutical material, solvent and anti-solvent for particle

formation was not possible. At the end of the experiment the pure CO_2 was pumped through the vessel to rinse the particles from in the solvent.

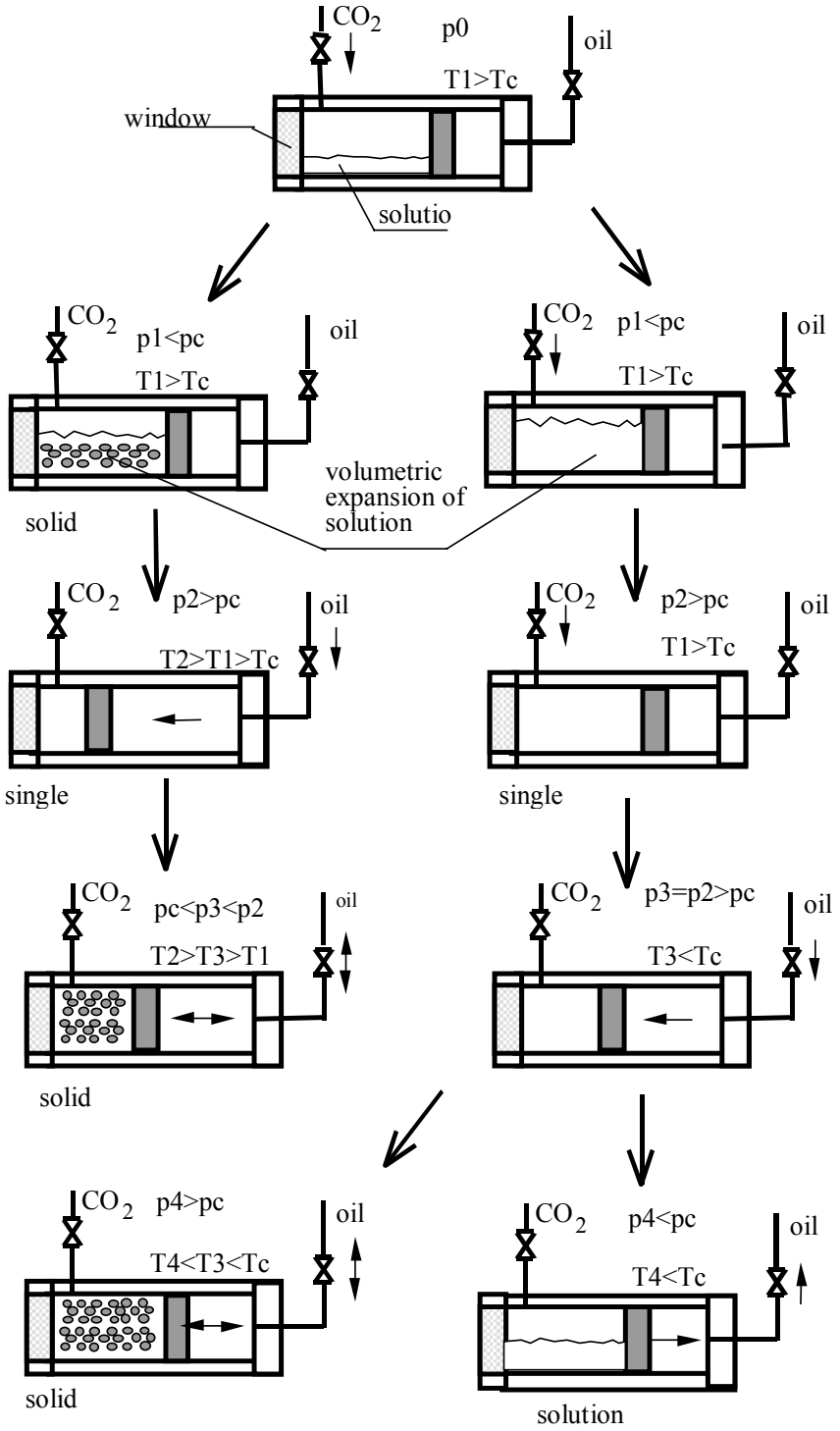

Fig. 24. *Application of variable volume view cell (VVV -cell) for finding the appropriate combinations of the solvent and the gaseous antisolvent for a given solid. P_c is solution critical pressure and T_c critical temperature.*

3.2. RESULTS OF PHASE SEPARATION STUDIES

In this work four different pharmaceuticals compounds were examined; nalmefene HCl, oxybutynine HCl, clonidine base and clonidine HCl. The material basic data are shown in Table IX and the structural formulas are shown in Appendix I.

Table IX *The four pharmaceuticals compounds; molecular weight (M), melting point (T_{mp}) and solubility profile.*

Compound	M (g/mol)	T_{mp} (K)	Solubility profile
Nalmefene HCl	376	476-479	Freely soluble: water, methanol Soluble: ethanol Slightly soluble: acetonitrile Very slightly soluble: chloroform
Oxybutynine HCl	394	402-403	Soluble: water, methanol, ethanol DMF Insoluble: Toluene
Clonidine base	230	403	Soluble at 293–302 K: water, methanol, ethanol, acetone Insoluble at 293–302 K: isopropanol, Toluene
Clonidine HCl	267	578	Partly soluble: methanol Not soluble at 10 wt%: water, Ethanol, isopropanol, acetone, toluene

Observations of phase separation studies in a static variable volume view -cell:

Nalmefene HCl:
Solvent EtOH and concentration in fluid is 7.8 wt%, nalmefene concentration in EtOH is 1.2 wt% and in fluid 0.098 wt%: Nalmefene HCL separated from ethanol solution, forming a cloudy layer on ethanol surface as soon as CO_2-pressure had reached 85 bars at 45 °C. The precipitate fell to the bottom of the cell and the amount increased until pressure had reached 100 bars, where the liquid phase had disappeared. After stabilizing for 50 minutes, 5-10 mm long and 10-40 μm diameter needles had formed in the cell. The needles retained their form after the cell was flushed with CO_2 and depressurized.

Based on the behaviour in the view cell nalmefene HCl appears to be a good candidate for particle production with CO_2-antisolvent techniques.

Oxybutynine HCl:
Solvent *EtOH* and concentration in fluid 7.0 and 4.2 wt%, oxybutynine concentration in EtOH 0.62 wt% and in fluid 0.026 wt% and 0.044 wt%:

Oxybutynine hydrochloride did not precipitate from the EtOH solution over CO_2 pressure range 0 - 270 bars at 21 - 45 °C. The conditions include both one-phase (fluid) and two-phase (liquid / fluid) regions. The solubility of oxybutynine HCL in the ethanol-containing CO_2 is higher than what was tested in these experiments.

Solubility to *pure CO_2* and EtOH containing CO_2 at 0.49 and 0.1 wt% concentrations: Oxybutynine HCl did not dissolve to pure CO_2 at 0.1 wt% concentration at 80 C and up to 350 bars. It is not a suitable candidate for RESS-processing. Oxybutynine HCl dissolves well in EtOH-containing CO_2. It did not clearly precipitate from the liquid in the two-phase area (< 80 bars, 40 °C) nor in the one-phase area (80-350 bar, 40 C).

Solvent *acetone* and concentration in fluid 1.0 wt%, oxybutynine concentration in acetone 8.8 wt%, and in fluid 0.1 wt%: Oxybutynine HCl dissolves 8.8 wt% in acetone at 40 °C. It did not precipitate from either the liquid or fluid phases at 75 - 170 bars and 32 - 40 °C. At room temperature and 70 bar a few small particles separated, indicating that the solubility of oxybutynine HCl is close to 0.1 wt% in the fluid under tested conditions.

Solvent chloroform and concentration in fluid 6.4 wt%, oxybutynine concentration in chloroform 0.96 wt% and 2.8 wt% and in fluid 0.065 wt% and 0.195 wt%: Oxybutynine HCl precipitates from chloroform forming distinct crystals at 31 °C when the concentration is 0.19 wt% in fluid. At 40 °C there is no precipitation regardless of pressure. At 0.065 wt% concentration a few small particles appeared in the fluid phase at 67 - 95 bars and 32 - 34 °C.

Clonidine base:
Solvent *EtOH* and concentration in fluid 4.1 wt%, clonidine base concentration in EtOH 1.54 wt% and in fluid 0.063 wt%: Clonidine base did not precipitate from the EtOH solution over CO_2 pressure range 0 - 85 bars at 40 °C. It did not quickly precipitate either in the one-phase region, after ethanol had completely dissolved in CO_2 at 100 - 150 bar, 35 - 42 °C. After about 24 hours under CO_2-pressure (87 bar, 23 °C) the liquid phase contained platelets, which dissolved in the residual ethanol during pressure release and could not be recovered.

Solvent DMSO and concentration in fluid 5.4 wt%, clonidine base concentration in DMSO 1.2 wt% and in fluid 0.066 wt%: Clonidine base did not precipitate from DMSO at these concentrations at 41 °C under pressure up to 104 bar.

Solvent isopropanol and concentration in fluid 4.0 wt%, clonidine base concentration in isopropanol 1.6 wt% and in fluid 0.068 wt%: Clonidine base can be precipitated/crystallized from 1.6 wt% isopropanol with CO_2. It dissolves 1.1 wt% in isopropanol at 40 °C. Clonidine base separates from the liquid phase quickly at 77 bars and 40 °C.

Clonidine base appears to be a good candidate for particle production with CO_2-antisolvent techniques based on the behaviour in the view cell.

Clonidine HCl:
Clonidine HCl precipitated from EtOH solution when CO_2 pressure reached 100 bars at 40 °C forming needle-like crystals. The liquid started to become turbid at 70 bars. The crystals were retained in the fluid phase at 260 bars and 35 °C and also in EtOH phase at 70 bars and 35 °C. After depressurization the crystals formed bundles of 3-5 mm diameter. Single crystals were 50 - 300 μm long and 10-15 μm thick.

Based on the results from view-cell experiments clonidine HCl appears to be a suitable candidate for particle formation with CO_2 antisolvent technique.

3.3. DISCUSSION OF VVV-CELL APPLICABILITY FOR PHASE SEPARATION STUDIES

In this work four different pharmaceuticals compounds were examined; nalmefene HCl, oxybutynine HCl, clonidine base and clonidine HCl. Based on the results from view-cell experiments nalmefene HCl, clonidine HCl and clonidine base appears to be a suitable candidate for particle formation with CO_2 antisolvent technique. For example in an appropriate combination of the solvent and the CO_2 antisolvent; nalmefen HCl precipitates from EtOH, clonidine base from isopropanol and clonidine HCl from EtOH.

Oxybutynine HCl did not precipitate from the EtOH, chloroform and acetone solution in the studied conditions. Because only a few experiments were carried out with oxybutynine HCl/CO_2/solvent –systems, it cannot be concluded that oxybutymine HCl cannot be precipitated by supercritical antisolvent techniques. A factorial experimental design could be used as a tool to study the effects of different factors.

A static variable volume view cell is a useful and fast way to find out for a given solid the appropriate combinations of the solvent and the gaseous antisolvent. Often pharmaceutical materials are expensive and hardly available in large amounts, which makes impossible the phase separations studies in a laboratory or production scale SAS equipment. In VVV-cell experiments it is possible to use little amount of materials to examine fast a material in many recrystallization temperatures, pressures and concentrations. It is not possible to conclude from the VVV-cell experiments, what are the properties of particles produced by a SAS technique, such as particle size, size distribution, crystal habit and morphology, because the formation dynamics and residence times are different.

4. EFFECT OF INTIAL DROP SIZE AND MASS TRANFER ON PARTICLE SIZE

It is necessary to understand the mechanism, which controls particle sizes in the near critical and supercritical regions. The objective of this works is to develop a model for the SAS technique and examine, which phenomena control particle size in the near critical and supercritical regions. The proposed mean particle size control mechanisms are the mass transfer, jet breakup and hydrodynamics [10,147,51]. The mathematical model developed includes a model of initial droplet size at the exit of nozzle, model of ternary fluid phase equilibrium inside the droplet and a model of mass transfer between a drying droplet and the drying medium as a function of time. The model was tested with experimental results from spraying poly(L-lactid acid) (in this work; L-PLA) in dichloromethane into carbon dioxide. The values of experiments and the calculated particle sizes were compared.

The spray extraction/precipitation has attracted considerable interest as a viable process for manufacturing materials of a variety of geometries. Benefits are gained in rapid solidification, increased solidification, non-equilibrium phases and small sized precipitates. The RESS technique has been modeled by many authors and is well understood [138,139,140,141,142,143,144,145]. Different gas antisolvent techniques have also been well investigated [1,2,5,7,8,10,33,35,91,146,147,70] and modeled [8,11,90,91,147,148,149,45]. Recently mathematical models for the mass transfer between a droplet of organic solvent and a compressed antisolvent has been proposed by Werling and Debenedetti [147,149], Elvassore et al. [148,150], Lora et al. [151], Kikic et al. [152], Shekunov et al. [153] and Mukhopadhyay et al. [154].

4.1. THE MODELS ON GENERAL

In the SAS technique mass transfer occurs between the dispersed drops and the surrounding gas phase. In order to describe the mass transfer, the drop size distribution as well as the fluid dynamics of the dispersed liquid must be known. In this work a simple mathematical model of SAS particle technique is created. The mathematical model includes two parts: In the first model the effect of initial drop size on final particle size is considered [155,156]. In the second model the mass transfer effect on droplet properties and final particle size in continuous GAS systems is discussed [155,157]. The effect of liquid density and solubility of the heavy component on the particle formation are not discussed in this thesis.

The drop size in the two-fluid atomization depends closely on turbulent breakup, the gas to liquid ratio, system dimension, and on the physical properties of liquid and gas (liquid density, viscosity, gas density and interfacial tension between gas and liquid). The physical properties of supercritical fluid, for example the density and viscosity, depend especially on the temperature and pressure near the critical point [75,158]. Although the mass flow rate is constant, change in temperature and pressure near the critical point affects on the velocity of dense gas in the

nozzle. The interfacial tension of liquid-supercritical fluid system depends also on temperature and pressure [11,102]. Therefore, a change in operation conditions of temperature and pressure of the liquid-supercritical fluid also changes the drop size more than in liquid-gas systems.

The SAS particle processes are usually operating at constant temperature and pressure. The initial droplets size and distribution is difficult to measure experimentally and therefore estimated in this work. In the first model [156] the Sauter mean drop size is calculated from various correlations and the largest-sized droplets are estimated. The effect of temperature on liquid viscosity [158] and the effect on temperature and pressure on gas density and viscosity [75,159] are calculated. The liquid-gas interfacial tension is estimated from literature [100,104,102]. The effect of temperature, pressure, gas density, interfacial tension, gas velocity and nozzle diameter on initial mean droplet size is calculated. In the model it is assumed, that from one initial droplet one agglomerated microparticle is formed. The calculated and experimentally measured mean particle sizes are compared in different temperatures, pressures, densities of gas, relative velocities of CO_2 and liquid in the nozzle, Reynolds and Weber numbers. The programming of the first model was done with Fortran 77 language and the model was linked to Excel worksheet by a function procedure.

The second model [157] calculates the mass transfer effects on droplets properties. In the model a time history is calculated for each droplet size. During the flight the liquid evaporates from the droplet and at the same time CO_2 diffuses into the droplet. These processes are modeled in the same way as in spray drying. As the concentration of CO_2 in the droplet increases the antisolvent action takes place at constant temperature and pressure. The solvent is distributed evenly inside droplets. When the supersaturation is high enough the nucleation rate becomes significant and the polymer starts to condensate into particles. Thus the supersaturation increases because of the antisolvent action and decreases because of the condensation. These processes are determined mainly by

- diffusion of CO_2 into the droplet
- evaporation of liquid from the droplet
- condensation of polymer into solid phase particles

The particles in the droplet are described with an aerosol equation, which describes the evolution of particle size distribution with time. A lognormal distribution of droplets and particles sizes is used in the model [160]. An experimental distribution of particle sizes is measured from a SEM photograph and from this estimate the parameters of lognormal distribution are calculated. The lognormal size distribution is divided into five discrete classes. The distribution is described as a set of particle size classes. As the particles grow they jump from one class into another. The viscosity and interfacial tension of liquid and carbon dioxide are estimated. The diffusion coefficient is obtained from the Wilke Chang equation and the liquid and CO_2 side mass transfer coefficients are calculated. The tertiary solubilities of the components are calculated with the Peng-Robinson equation by calculating the fugacities of coexisting phases. The

critical parameters of polymer within Peng-Robinson EOS are estimated as well as the binary interaction parameters. The calculation program was programmed with Pascal and MathCad 7.

4.1.1. EQUATION OF STATE

The supercritical fluid phase can be considered as a compressed gas or an expanded liquid phase [161]. Relationship between the fugacity and the solubility of the solid can be found at given temperature and pressure [91]. In this work the systems involve three components 1) supercritical antisolvent CO_2, 2) organic solvent DCM, 3) heavy solute poly(L-lactid acid)) and their three phases (S solid, L liquid and G gas). It is assumed that the solid phase is pure. The equilibrium equations for each component in the liquid phase and in the gas phase are [91]

$$x_1^L \varphi_1^L P = y_1^G \varphi_1^G P \quad (7)$$

$$x_2^L \varphi_2^L P = y_2^G \varphi_2^G P \quad (8)$$

$$x_3^L \varphi_3^L P = y_3^G \varphi_3^G P \quad (9)$$

where x_i^L x is the mole fraction of the component i in the liquid phase, y_i^L is the mole fraction of the component i in the gas phase, φ_i^L is the fugacity coefficient of the component i in the liquid phase, φ_i^G is the fugacity coefficient of the component i in the gas phase and P is the system absolute pressure. The equilibrium equation for the solute between the liquid and the solid phase is

$$f_{30}^S = x_3^L \varphi_3^L P \quad (10)$$

where f_{30}^S is the fugacity of the solute in the solid and liquid phase. The solid was modelled as pure solid phase, even though it was noted that solid material was also dissolving carbon dioxide. This assumption is probably not strictly valid, but this was made for simplicity [137]. The fugacity of the solid component is

$$f_{30}^S(T,P) = \varphi_3^{Sat}(T) P_3^{Sat}(T) \exp\left(\int_{P_3^{Sat}}^{P} \left(\frac{v_3^{SO}}{RT} \right) dP \right) \quad (11)$$

where $P_i^{Sat}(T)$ is the saturation pressure of the pure solid at the system temperature, v_3^{OS} is the molar volume of the pure solid (mol kg^{-1}), R is the universal gas constant (8.314 J mol^{-1} K^{-1}), P is the system absolute pressure (Pa) and T is the system absolute temperature (K). Because of the relatively small value of the saturation pressure of the solid, the solid component saturation fugacity coefficient φ_3^{Sat} can be set equal to 1. Also the molar volume of the solid can be considered to be constant over the pressure range. After these

simplifications Eqs. (10) and (11) are set equal. Then the solubility of solid material in liquid phase is obtained

$$x_3^L = \frac{P_3^{Sat}(T)\exp\left[\frac{(P+P_3^{Sat})v_3^{OS}}{RT}\right]}{\varphi_3^L P} \tag{12}$$

The Peng-Robinson equation of state [92] was used to calculate the fugacity coefficient φ_3^L of the solid in the liquid phase. The Peng-Robinson equilibrium equation has been commonly used in solubility calculations for solid materials [91,137] and for CO_2–dichloromethane (DCM) binary system phase equilibrium [136]. In this work the method by McHugh and Krukonis [88] was used for calculating the phase equilibrium. The Peng-Robinson binary vapour-liquid equilibrium equation is

$$P = \frac{RT}{v-b} - \frac{a}{v(v+b)+b(v-b)} \tag{13}$$

where v is the molar (liquid or vapor phase) volume (mol m^{-3}). The *a* and *b* are the characteristic parameters of compound. For pure components

$$b = 0.07780(RT_{ci}/P_{ci}) \tag{14}$$
$$a = a_i(T_c)\alpha_i(T_R) \tag{15}$$
$$a_i(T_c) = 0.45724(RT_{ci}/P_{ci}) \tag{16}$$
$$\alpha_i^{1/2}(T_R) = 1 + m_i(1 - T_{R_i}^{1/2}) \tag{17}$$
$$m_i = 0.37464 + 1.54226\omega_i - 0.26992\omega_i^2 \tag{18}$$

where T_c and P_c are the critical temperature (K) and pressure (Pa), T_R is the reduced temperature ($T_R = T/T_c$), and ω_i is the acentric factor for component *i*. In this work physical properties of CO_2 and dichloromethane are from Yaws et al. [162]. L-PLA data are from manufacturer Boehringer Ingelheim. The acentric factor, critical pressure and critical temperature of the polymer were estimated and these reproduced the observed solubility's data from Tom and Debenedetti [179] The polymer density 1270 kg m^{-3} was measured experimentally. The attractive and repulsive parameters required by the Peng-Robinson EOS for fluid mixture were calculated from the pure component values using mixing rules with two binary interaction parameters.

$$a = \sum_i^n \sum_j^n x_i x_j a_{ij} \tag{19}$$
$$a_{ij} = (a_i a_j)^{0.5}(1 - k_{ij}) \tag{20}$$
$$b = \sum_i^n \sum_j^n x_i x_j b_{ij} \tag{21}$$

$$b_{ij} = \frac{b_i + b_j}{2}(1 - \eta_{ij}) \tag{22}$$

where k_{ij} is a mixture parameter describing the intermolecular interaction between the molecules and η_{ij} stands for the effect of the different size and structure of components.

For binary systems (1, supercritical antisolvent, 2 organic solvent), only one adjustable parameters k_{12} is needed in the modeling of solubility data. In ternary systems involving three components (1, supercritical antisolvent, 2 organic solvent, 3 heavy solute) the evaluation of the fugacity coefficient requires an additional interaction parameter, k_{23}, to account for solvent-solute interactions in the fluid phase. In this work the interaction parameters for antisolvent – solute interactions, k_{13}, k_{13}, are determined from binary solubility data [179]. The calculation of interaction parameters has been presented elsewhere [91,161]. These parameters were fitted to the experimental data using the previously presented method [137,163] by minimizing the following function with the Simplex search method

$$SF = \sum_{n01}^{NEP} \left(\frac{x_3^{cal} - x_3^{ep}}{x_3^{ep}} \right)^2 \tag{23}$$

where superscript *cal* refers to the value predicted by the model and *ep* the experimentally obtained point. NEP is the number of experiments.

For the regular solutions in general the vapor-liquid equilibrium constant K_i is

$$K_i = \frac{y_i}{x_i} = \frac{\varphi_i^G}{\varphi_i^L} \tag{24}$$

where x is the mole fraction in liquid phase, y is the mole fraction in gas phase and φ is the fugacity coefficient. Superscript L denotes liquid phase and G gas phase.

4.1.2. VOLUMETRIC EXPANSION OF LIQUID IN CO_2

A key role in the precipitation process is played by the volumetric expansion of the liquid solvent due to the fast dissolution of the supercritical antisolvent inside the liquid phase [3]. Volumetric expansion of organic liquid has been studied by several authors [6,9,90,164,38,42,56]. Reverchon et al. [9] have studied supercritical antisolvent precipitation of nanoparticles of superconductor precursors. Volumetric expansion of the liquid carrier mainly controls the morphology of particles produced by supercritical antisolvent precipitation (GAS). In a batch process the volumetric liquid expansion is a function of temperature, the pressure and the type of solvent and anti-solvent gas. In a batch GAS process the volumetric expansion profile depends on the profile of pressure

and mixing efficiency. In the SAS system the liquid is sprayed into a supercritical antisolvent and the liquid droplets and supercritical phases are contacted with an excess of supercritical fluid. Therefore the mass transfer of supercritical antisolvent to liquid phase is more effective than in batch GAS process. However, the volumetric expansion of droplets is faster in SAS system than in conventional batch antisolvent precipitation. The measure of liquid solvent solubility is given by the volumetric expansion of the liquid phase in the presence of the antisolvent. Mathematically, the relative volume expansion $\Delta V_E\%$ is defined [15] as:

$$\Delta V_E\% = 100 * (V(P,T) - V_0)/V_0 \qquad (25)$$

where V(P,T) is the volume of the liquid phase loaded with the antisolvent at pressure P and temperature T. V_0 is the volume of the pure liquid phase at atmospheric pressure conditions. The density of the liquid phase was obtained by Peng-Robinson EOS and from this data the volume expansion of liquid phase was calculated.

4.1.3. VISCOSITY OF COMPRESSED CO_2 AND LIQUID

Sovová and Procházka [165] compared various carbon dioxide viscosity equations with published experimental data covering gas, liquid and supercritical regions. The viscosity models of Vesovic et al. [166] and of Altunin and Sakhabetdinov [159] where recommended as most reliable for predicting the viscosity of dense carbon dioxide. Altunin and Sakhabetdinov correlated the dilute carbon dioxide viscosity in the temperature range 220 K ≤ T ≤ 1300 K:

$$\mu_{0,CO_2} = T_R^{0.5} (27.2246461 - 16.6346068/T_R + 4.66920556/ T_R) \qquad (26)$$

where μ_{0,CO_2} is the low–pressure viscosity of carbon dioxide (μPa s), T_R is reduced temperature ($T_R = T/T_c$). Altunin and Sakhabetdinov [159] proposed an empirical equation for the viscosity ratio as a function of reduced temperature and density:

$$\mu_{CO_2} = \mu_{0,CO_2} \exp \sum_{i=1}^{4} \sum_{j=0}^{1} a_{ij} \rho_R^i / T_R^j \qquad (27)$$

where μ_{CO_2} dynamic viscosity (μPa s). The low–pressure viscosity μ_{0,CO_2} is calculated from Eq. (25). Coefficients: a_{10} = 0.248 566 120, a_{11} = 0.004 894 942, a_{20} = -0.373 300 660, a_{21} = 1.227 534 88, a_{30} = +00.363 854 523, a_{31} = -0.774 229 021, a_{40} = -0.063 907 075 5 and a_{41} = 0.142 507 049. The correlation has been derived for the temperature range 220 K ≤ T ≤ 1300 and pressure up to 1200 bar, and it is effective for both the gas and liquid phases. Fig. 25 shows the calculated viscosity of pressured carbon dioxide by the model of Altunin and Sakhabetdinov.

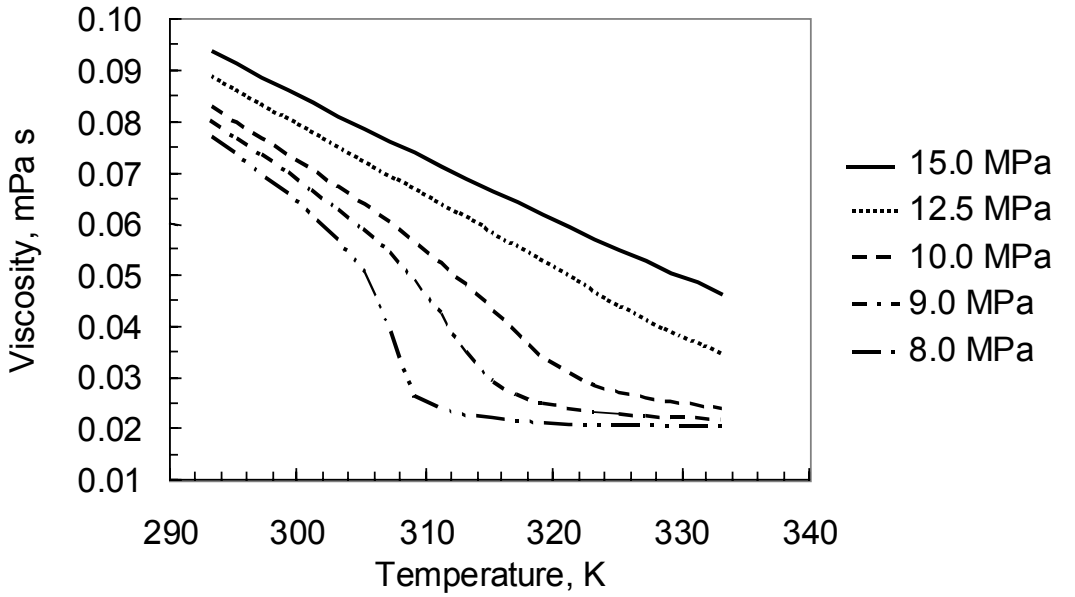

Fig. 25. *The calculated viscosity of pressured carbon dioxide by the model of Altunin and Sakhabetdinov [159].*

The viscosity of liquid affects on turbulent rupture in two-fluid atomizers [167]. To calculate the viscosity of an organic liquid the following equation (28) was used [158].

$$\log_{10}(\mu_L) = A\,(1/T - 1/B) \qquad (28)$$

where μ_L is liquid viscosity (mPa s), T is temperature (K) and A and B are constants. For the dichloromethanes used in this work, the value of A is 359.55 and B is 225.13.

4.1.4. MEAN DROP SIZE

The effect of initial droplet size on particle size in the supercritical antisolvent precipitation (SAS) technique is shown elsewhere [155]. Because the initial droplet size and distribution is difficult to measure experimentally, it is estimated from equations in the literature [168,169,170]. The effectivity of a spray dryer system is determined by droplets size produced in the nozzle and by the manner in which the gaseous medium mixes with the drops. In this context an atomizer is defined as a device which causes liquid to disintegrate into droplets of a specified size range, and which controls their spatial distribution [170,171].

The general category of two-fluid atomizers includes such diverse applications as venture atomizers and reactor fluent quenches systems in addition to two-fluid spray nozzles. Several breakup mechanisms may be applied depending on the manner in which the two fluids meet. The main mechanism to produce droplets is

high level turbulent rupture. The drop size in the two-fluid atomization depends closely on turbulent breakup, the ratio of gas to liquid, the physical properties of the liquid and gas and system dimensions. Further differences from hydraulic nozzles are the stronger increase in drop size with increasing surface tension and decreasing gas density. The basic breakup mechanisms, however, is unaffected by these variables [167].

The correlation of droplets size shows a dependence on the ratio of gas to liquid and systems dimensions. The relationships equations are valid only for specific systems dimensions and experiments conditions. However, the form of the main droplet size equations in the literature [168,169,170] shall be the same in gas-liquid spray atomizers as in supercritical fluid-liquid systems, but the values of the equations constants shall be different. For example the mass transfer into or out of liquid jet can significantly affect jet stability and breakup length [172,173]. Steinmeyer [167] has reformulated Hinze's relationship [174] of drop size in two-fluid atomization:

$$d_{32} = 0.29\ (\sigma/\rho_G)^{0.6}\ (\ 1/U_{GL})^{1.2}\ (1 + L/G)^{0.4}\ (d_{nozzle})^{0.4} \qquad (29)$$

where σ is interfacial tension (N m^{-1}), ρ_G is gas density (kg m^{-3}), U_{GL} is velocity (U_G - U_L) between gas velocity U_G and liquid velocity U_L (m s^{-1}) at the exit of the tube, L/G in mass ratio of liquid flow to gas flow, d_{nozzle} is diameter of the gas discharge (m) and d_{32} is Sauter mean diameter (m). d_{32} has the same ratio of surface-to-volume as the total drop population. The Sauter mean diameter is defined later by Eq. (36). El-Shanawany and Lefebvre [168] give a relationship of drop size for a prefilming atomizer:

$$d_{32} = 0.0711\ (\sigma/\rho_G)^{0.6}\ (\ 1/U_{GL})^{1.2}\ (1 + L/G)\ (d_{nozzle})^{0.4}\ (\rho_L/\rho_G) + 0.015\ [(\mu_L)^2/(\sigma\ \rho_L)]^{0.5}\ (d_{nozzle})^{0.5}\ (1 + L/G) \qquad (30)$$

where ρ_L is liquid density (kg m^{-3}), μ_L is liquid viscosity (Pa s). Eq. (30) is based on a wide range of data and generally follows the changes of the variables on which it based: velocity, L/G, d_{nozzle} and liquid viscosity. In regions of high gas density, the numerical results from Eq. (29) are close to the first term in Eq. (30). Jasuja [169] has a similar correlation of drop size correlation for air-blast atomization of liquid under high-pressure conditions:

$$d_{32} = 0.17\ (\sigma/\rho_G)^{0.45}\ (\ 1/U_{GL})^{0.9}\ (1 + L/G)^{0.5}\ (d_{nozzle})^{0.55} + 0.015\ [(\mu_L)^2/(\sigma\ \rho_L)]^{0.5}\ (d_{nozzle})^{0.5}\ (1 + L/G) \qquad (31)$$

The last term of Eqs. (30) and (31) is called viscosity term. Eq. (31) does not fit the effect of changing velocity as well as Eqs. (29) and (30). Steinmeyer [170] gives a relation of drop size for pipeline contactor:

$$d_{32} = 0.79\ (\sigma/\rho_G)^{0.6}\ (\ 1/U_{GL})^{1.2}\ (d_{pipe})^{0.4} \qquad (32)$$

where d_{pipe} is diameter of pipe (m). The Eqs. (29), (30), (31) and (32) are dimensionally consistent; any set of consistent units on the right-hand side yields the droplet size in units of length on the left-hand side. The largest-sized droplet in the population d_{dmax} is typically 3 to 4 times d_{32} in turbulent break-up processes [160]. d_{dmax} is estimated from d_{32} by

$$d_{dmax} = d_{32}/0.3 \tag{33}$$

The four above mentioned equations for initial droplet size calculation in SAS formation are discussed by Rantakylä [155]. Jasuja's equation was selected for further studies by Rantakylä et al. [156].

4.1.5. DROPLET AND PARTICLE SIZE DISTRIBUTION

A lognormal distribution of particle sizes is used in the model. An experimental distribution of particle sizes is measured from a SEM photograph. From this estimates for the parameters of lognormal distribution are calculated. The lognormal size distribution is divided into five intervals. The calculated particle size distribution and the results from experimental measurement of particle size distribution are compared. In the literature lognormal distribution is used for defining droplet and particle size distributions [160,175]. In this work the Sauter mean diameter d_{32} is used for characterizing the drop size. d_{32} has the same ratio of surface-to-volume as the total droplet population. The mean of the logarithm of the diameter (of droplets or particles) d is

$$\overline{\ln d} = \frac{\sum_i n_i \cdot \ln d_i}{\sum_i n_i} \tag{34}$$

where $\overline{\ln d}$ is the mean of the logarithm of diameter, $\ln d_i$ is the logarithm of diameter in size interval i and n_i is number of particles or droplets in size interval i. The standard deviation $\sigma_{\ln d}$ for the logarithm of the diameter is

$$\sigma_{\ln d} = \sqrt{\frac{\sum_i n_i \cdot (\ln d_i - \overline{\ln d})^2}{\sum_i n_i}} \tag{35}$$

The Sauter mean d_{32} can be calculated as follows:

$$d_{32} = \frac{\sum_i n_i d_i^3}{\sum_i n_i d_i^2} \tag{36}$$

In calculations this lognormal distribution of diameter d is comparable to

$$f(d) \propto e^{-0.5\cdot\left(\frac{\ln d - \overline{\ln d}}{\sigma_{\ln d}}\right)^2} \tag{37}$$

To get the particle rates of different bars we normalize with a coefficient A such that

$$m_j^{'} = A \cdot m_j \tag{38}$$

where $m_j^{'}$ is number of droplets for volume feed V and size d_j, m_j is number of droplets of size d_j and A is normalization coefficient. The overall volume V of droplets in a given time interval is set equal to

$$V = \sum_j m_j^{'} \cdot \frac{\pi\, d_j^{\,3}}{6} \tag{39}$$

4.1.6. MASS TRANSFER

The effect of mass transfer on droplet properties in the supercritical antisolvent precipitation (SAS) technique is presented by Rantakylä et al. [157]. Generally the droplet drying occurs in two stages. Mass transfer changes during different stages of the evaporation process. The first stage is the shrinking balloon stage, where the rate of evaporation is balanced with the transfer of liquid from the center to the surface of the droplet [105]. However, the rapid expansion of the solute due the solvent diffusion to the droplet concurrently grows the volume of droplet. In the second stage the transport of solution from the inner parts of droplet to its outer surface becomes the rate-limiting step. A solid layer forms at the outer surface of the droplet. From this point forward, due the partial surface solidification, the diameter of the droplet remains essentially constant.

In the continuous GAS technique, where the initial velocity of drops at the exit of the nozzle is high, both natural and forced convection exists in mass transfer from liquid drops to fluid. In this work two mass transfer equations are used for calculating the mass transfer coefficient between fluid-liquid systems. Eggers et al. [11] have studied the extraction of coffee oil by spraying of oils into supercritical CO_2. They have used a modification of the Frössling equation to calculate mass transfer coefficient of liquid to supercritical fluid

$$Sh = 2.0 + Sc^{1/3}\,\mathrm{Re}_d^{1/2} \tag{40}$$

In the above equation Sh is dimensionless is Sherwood number, Sc is Schmidt number and Re_d is Reynolds number. The equations for these were show earlier Eqs. (1), (2) and (3). Here it is assumed that liquid droplets are like shrinking particles and Reynolds numbers are below 1000. McCabe et al. [99] have given the following equation for calculating mass transfer to droplets

$$Sh = 1.13\, Sc^{1/2}\, \mathrm{Re}_d^{1/2} \tag{41}$$

The dimensionless Sherwood number and Schmidt number *Sc* include the binary diffusion coefficient of liquid in gas phase *D* (m^2 s^{-1}). The binary diffusion coefficient D_{21} of solute (liquid DCM) in a solvent (supercritical fluid CO_2) was estimated through Wilke-Chang equation [123], which was shown earlier as Eq. (5). Also the diffusion coefficient of the heavy solute (L-PLA) molecule in liquid D_{32} and the diffusion coefficient of the heavy solute molecule in liquid solvent D_{12} are calculated by Wilke-Chang equation.

The liquid is mass transferred concurrently from droplets to gas phase, the gas is mass transferred from continuous phase to liquid droplets. With droplets the resistance to mass transfer may be significant in both phases. The diffusion inside a stagnant droplet is an unsteady-state process, but for convenience in combining coefficients an effective internal mass transfer coefficient k_L [99] can be used in equation

$$k_L = \frac{10 D_{12}}{d_d} \tag{42}$$

where k_L is effective internal mass transfer coefficient in liquid phase, D_{12} is the diffusion coefficient of CO_2 molecule in liquid phase (m^2 s^{-1}) and d_d is droplet diameter (m).

The overall mass transfer coefficient K_L in liquid phase and the overall mass transfer coefficient K_G in gas phase are calculated [176] with following equations

$$\frac{1}{K_L} = \frac{1}{k_L} + \frac{1}{m k_G} \tag{43}$$

$$\frac{1}{K_G} = \frac{1}{k_G} + \frac{m}{k_L} \tag{44}$$

where K_L is the overall mass transfer coefficient in liquid phase (m s^{-1}), K_G is the overall mass transfer coefficient in gas phase (m s^{-1}) and *m* the slope of equilibrium curve. The individual terms in equations (43) and (44) correspond to mass-transfer resistance's. The gas phase is controlling the mass transfer, if less than about 10 % of the overall resistance resides in the liquid phase. Then the overall mass transfer coefficient in gas phase K_G is equal to k_G ($K_G \rightarrow k_G$). In this situation the gas is highly dissolved in liquid phase. Similarly, the liquid phase is controlling mass transfer if more than 90 % of the overall resistance resides in liquid phase. Then the overall mass transfer coefficient in liquid phase K_L is equal to k_L ($K_L \rightarrow k_L$). In this situation the gas is poorly dissolved in liquid phase [177]. When the slope of equilibrium curve *m* value is 1.0, the overall mass transfer coefficients K_L and K_G are equal.

The mass transfer rate between liquid phase and gas phase is calculated with equation

$$N_i = K_x A_d \Delta C_i \tag{45}$$

where N_i mass transfer rate of component i (kg s^{-1}), K_x is overall mass transfer coefficient (m s^{-1}), A_d is droplets surface area (m^2) and ΔC_I is concentration gradient of component i near gas-liquid interface (kg m^{-3}).

4.1.7. VELOCITY OF DROPLETS

The mass transfer between a droplet and the ambient antisolvent depends on the velocity of the droplet inside the precipitation vessel. The change in the velocity of the droplet is accounted for by using a momentum balance for the drops. In the mathematical model of particle formation at spray atomization it has been assumed that

- the concentration of droplets in atomization fluid is sufficiently dilute, so that droplet-droplet interactions may be safely neglected
- droplets are spherical and their size remains unchanged during flight, so that the correlation for the drag coefficient of solid sphere applies

The net forces acting on the droplet consist of the downward gravity force, the upward friction and buoyant forces [105]. The resulting net force is balanced with the acceleration of the droplet resulting in [105]

$$\frac{dU_d}{dt} = g\frac{\rho_d - \rho_G}{\rho_d U_d} - \frac{3}{2}\frac{C_{drag}\rho_G}{d_d \rho_d U_d}(U_G - U_d)^2 \tag{46}$$

where U_d is the droplet velocity (m s^{-1}), t is flying time (s), g is gravity acceleration (9.81 m s^{-2}), ρ_d is droplets density (kg m^{-3}), ρ_G is density of ambient gas (kg m^{-3}), C_{drag} is the friction factor and U_G is ambient gas velocity (m s^{-1}). The friction factor C_{drag} is also know as the drag coefficient, which is a function of Reynolds number for the drops, is calculated using approximation by Liu et al. [178]. The velocity of droplet inside the nozzle is the same as the velocity of CO_2. Initial velocity of drop inside the precipitation vessel is same as the velocity of drop inside the nozzle. It is supposed that the stream of CO_2 broadens after the nozzle inside the vessel and the velocity of CO_2 approaches zero. In this work the solute velocity inside the nozzle is in the range of 0.7 m s^{-1} to 2.7 m s^{-1}, when the Re_d is from 280 to 900. In the calculation the mean droplet size was 30 μm.

4.2. EXPERIMENTAL

The objective of experimental part is to measure the solubility of polymer in dichloromethane-CO_2 solute to determine the parameters of Peng-Robinson EOS

and to produce particles for comparison of the calculated and experimentally measurement particles distributions. The particle formation model is tested with experimental results from spraying L-PLA in dichloromethane into carbon dioxide. The stability of L-PLA in dichloromethane-CO_2 solute is defined by obtaining the molecular weight after the particle formation in SAS particle production**.**

4.2.1. MATERIALS

Carbon dioxide was obtained from AGA at a purity of 99.7 % (H_2O < 200 ppm). HPLC grade dichloromethane (DCM) was obtained from Rathburn. Poly(L-lactid acid) was obtained from Boehringer Ingelheim (Mw 5500, Mw/Mn 5.3, L-104, lot. no. 33007). HPLC grade tetrahydrofuran (THF) was obtained from Rathburn. Polystyrene standard for molecular weight determinations was obtained from Aldrich.

4.2.2. SEMI-CONTINUOUS GAS APPARATUS

A schematic diagram of the semi-continuous laboratory-scale SAS apparatus is shown in Fig. 26.

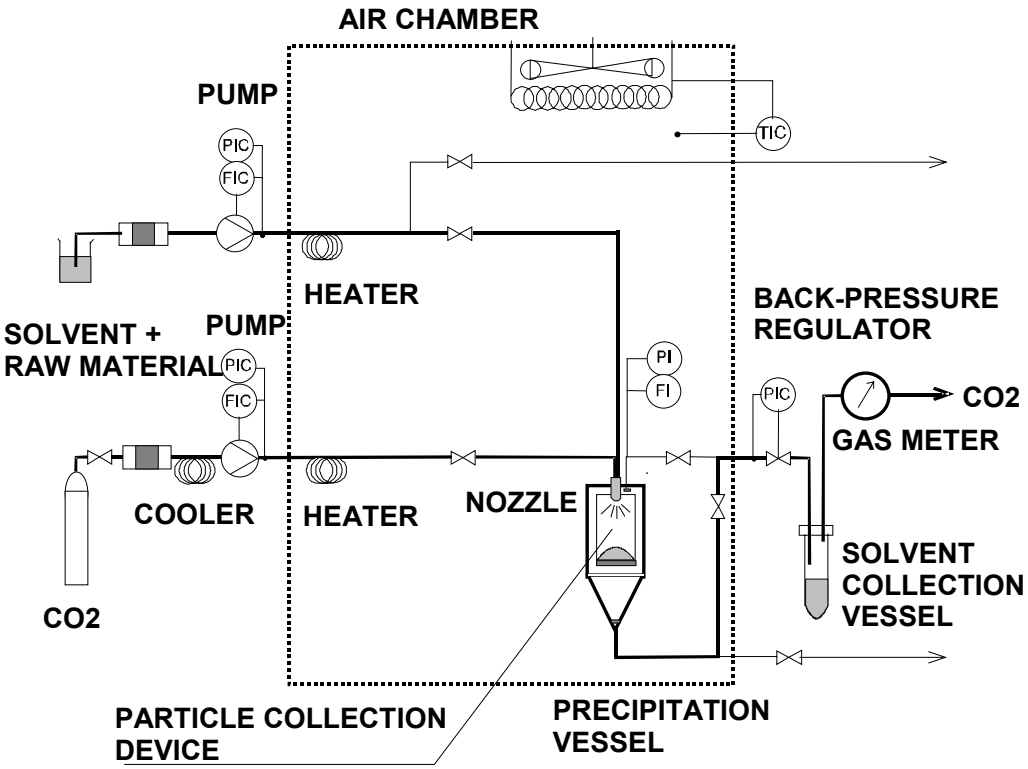

Fig. 26. *The semi-continuous laboratory-scale SAS experimental apparatus.*

The volume of the particle collection device is 100 ml. At the bottom of the collection device there is a polytetrafluoroethylene membrane. This particle collection vessel is inside of a larger 200 ml pressure vessel. The assembly was placed in a thermo-stated air chamber. The solution and CO_2 was pumped with piston pump. The pressure inside the vessel was held constant with a vibrating back- pressure regulator. The nozzle was made by VTT machine shop and constructed of coaxial tubes of stainless steel. A more detailed description of the equipment, nozzle and experimental methods has been given by Rantakylä et al. [156].

4.2.3. MEASURE OF POLYMER SOLUBILITY

The solubility of L-PLA in modified CO_2 was measured using a Variable Volume View Cell (VVVC). Solubility was also obtained from the mass balance of the precipitation experiments. A schematic diagram of the variable volume view cell is shown in Fig. 23 [77,118]. The solubility of the polymer is calculated from masses of the solid, liquid solvent and carbon dioxide. The solubility was also calculated with the Peng-Robinson equation of state [92].

4.2.4. ANALYSIS

A rough measurement of particle mean size and size distribution was done with light microscope (GWP Olympus BH-2). The sizes of about 120 particles from each experiment were measured to obtain the distribution. The particle fine structure was observed with High Resolution Scanning Electron Microscopy (SEM) (LEO DSM 982 Gemini).

Molecular weight and purity of L-PLA was measured by Gel Permeation Chromatography (GPC). The apparatus; HP-1050 series with HP 1047A RI- and HP-1050 diode array detector, software HP ChemStation and PL Caliber GPC, column: Waters Styragel HR 4E, inside diameter 7.8 mm and length 300 mm. The method of analysis: eluent tetrahydrofuran (THF), flow rate of eluent 0.5 ml/min, temperature 40 °C, injection volume 20 µl, concentration of injection 10 mg/ml, the standard was polystyrene (Boehringer Ingelheim), the molecular weights of standards were 800, 3680, 13 100 and 47 960 g mol^{-1}.

4.3. EXPERIMENTAL RESULTS

The L-PLA was stable in the GAS process. The molecular weight of L-PLA did not change during the particle formation. The molecular weight of L-PLA before and after particle the formation was determined with gel permeation chromatography.

The solubility of L-PLA in DCM/CO_2 -mixture was determined in this thesis. The results are presented in Table X. The solubility data of Tom and Debenedetti

[179] for L-PLA in pure supercritical CO_2 are given in the same table too. The molecular weight of L-PLA was 5500 g/mol, which is same as is our work. It can be seen that the solubility of L-PLA in DCM modified CO_2 was negligible (0.01-0.03 wt% in the operating conditions).

Table X *The solubility of L-PLA in pure supercritical CO_2 [179] and in DCM/CO_2 -mixture measured in this work. The molecular weight of L-PLA is 5500 g/mol.*

L-PLA /CO_2 (Tom et al. [179])			L-PLA /DCM/CO_2 (this work)			
Pressure MPa)	Temperature (K)	Solubility (wt%)	Pressure (MPa)	Temperature (K)	DCM (wt%)	Solubility (wt%)
20.0	318	0.0128	8.5	302	3.3	0.0090
25.0	318	0.0200	10.5	303	2.9	0.0085
30.0	318	0.0427	10.0	308	3.0	0.0130
20.0	338	0.0280	11.0	313	5.0	0.0123
25.0	338	0.0477	13.0	323	4.9	0.0336
30.0	338	0.0738	14.0	313	5.1	0.0190
			17.0	333	4.8	0.0297

The solubility of L-PLA in dichloromethane at atmospheric pressure was determined in this work in vitro. The L-PLA/DCM solute was heated until complete miscibility of the polymer and the solvent was reached. The temperature was slowly reduced until a second phase appeared. The measured solubility of L-PLA in dichloromethane is shown in Table XI.

Table XI *The measured solubility of L-PLA in DCM . The molecular weight of L-PLA is 5500 g/mol.*

Temperature (K)	Solubility (wt%)	Solubility (mol/mol DCM)
296	66	0.010
318	91	0.014
331	109	0.017

The Peng-Robinson EOS interaction parameters k_{ij} are shown in Table XII. The interaction parameters of k_{ij} are calculated from experimental data of solubility. The subindex 1 is for CO_2, 2 is for DCM and 3 is for L-PLA. The parameters for the effect of the different size and structure of unlike components η_{ij} are set to zero.

Table XII *The interaction parameters k_{ij}. The subindex 1 denotes CO_2, 2* DCM *and 3 L-PLA. The parameters for the effect of the different size and structure of unlike components η_{ij} are set to zero.*

	i		
j	1	2	3
1	0.000	0.100	0.103
2	1.000	0.000	0.200
3	0.103	0.200	0.000

The experimental conditions and results of L-PLA mean particle size in the continuous GAS technique are shown in Table XIII.

Table XIII *The experimental conditions of L-PLA particle formation by SAS techniques.*

	Experiment							
	1	2	3	4	5	6	7	8
Pressure (MPa)	14.0	17.0	11.0	13.0	10.0	10.5	8.5	8.5
Temperature (K)	313	333	313	323	308	303	302	302
CO2 flow in coaxial nozzle	inner	inner	outer	outer	outer	outer	outer	outer
Mass flow (CO2 g/min)	13.0	13.8	13.0	13.6	13.4	13.6	12.6	11.6
Density (CO2 kg/m3)	764	666	685	638	714	783	741	741
Viscosity (CO2 mPa s)	0.0661	0.0530	0.0548	0.0494	0.0585	0.0690	0.0624	0.0624
Mass flow (DKM g/min)	0.66	0.66	0.66	0.66	0.40	0.40	0.40	0.40
Viscosity (DKM mPa s)	0.356	0.304	0.356	0.328	0.371	0.388	0.392	0.392
Polymer/DKM (wt-%)	1.52	1.52	1.52	2.28	2.28	1.52	1.52	1.52
Velocity at exit of nozzle (m/s)	0.74	0.90	0.82	0.92	0.81	0.75	0.74	2.71
Nozzle diameter (mm)	0.70	0.70	0.70	0.70	0.70	0.70	0.70	0.35
Concentration of polymer in liquid (wt-%)	1.52	1.52	1.52	2.27	2.27	1.52	1.52	1.52
Mean particle diameter (μm) experimental value	8.1	25.7	10.9	13.7	10.7	3.5	3.9	3.3

Fig. 27 shows SEM photographs of L-PLA particles. Operating conditions were: 8.5 MPa, 302 K, concentration of L-PLA in dichloromethane 20 mg/ml, mass flow rate of CO_2 12 g min^{-1} and flow rate of dichloromethane solution 0.30 ml min^{-1}. The inner diameter of nozzle was 0.35 mm.

The overall outlook of particles is shown in the Fig. 27 a). It can be seen from Fig. 27 b) that the particles (3-10 μm) are composed of agglomerated microparticles (1-2 μm). These particles (3-10 μm) are sintered with other particles to form even larger agglomerates (10-30 μm). In this work the term 'particle' and the size measurements and calculations refer to the agglomerated particles (3-10 μm). It is assumed that one agglomerated particle is developing in each droplet. These are several possible reasons for the formation of larger agglomerates (10-30 μm): Presumably the drying droplets have collided with other drying particles on the wall of the particle collection vessel. Second explanation for agglomerated particles is that the flying time of droplets is too short for the drops to dry before the end of the particle collection device. Third explanation for macro-

agglomerated particles will be that CO_2 - DCM solution has melted the particles during the experiment of particle formation. The formed particles are at the bottom of collection device on membrane and the CO_2-DCM-polymer solute is flowing between the particles.

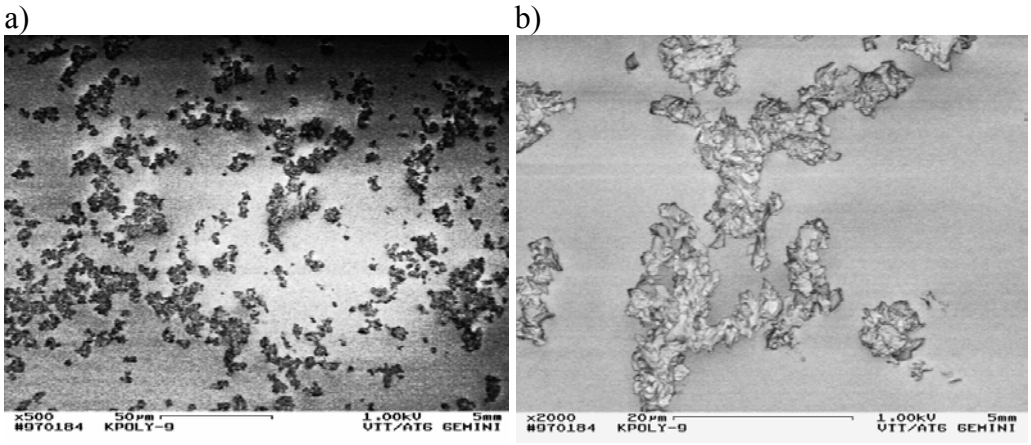

Fig. 27. *SEM photographs of L-PLA particles from continuous GAS precipitation using CO_2. The SEM pictures a) and b) are from the same experiment. The scale of pictures is a) 500*, b) 2000*.*

4.4. EFFECT OF INITIAL DROPLET SIZE ON PARTICLE SIZE

4.4.1. CALCULATION OF INITIAL DROPLET SIZE

The initial droplet size and distribution are difficult to measure experimentally. Therefore they are estimated in this work. The Sauter mean drop size is calculated by four different equations from literature Eqs. (29-32) [168,169,170]. The density of supercritical fluid depends especially on the temperature and the pressure near the critical point. A change of operation conditions in temperature and pressure will change the drop size more in a liquid-supercritical fluid system than in a liquid-gas system. The effect of temperature, pressure, solute velocity in the nozzle and nozzle diameter on droplet diameter are shown by Rantakylä [155]. The present study showed that changing process parameters (temperature, density, pressure, interfacial tension between liquid and gas and velocity of gas) have a small calculated effect on initial droplet size in SAS process.

4.4.2. COMPARISON OF EXPERIMENTAL AND CALCULATED INITIAL DROPLET SIZES

The initial droplet size and distribution in supercritical fluid is difficult to measure, because of the high pressure, small diameter and high velocity of droplets. The He-Ne laser Doppler [180] and three-dimensional argon ion laser

Doppler anemometer [181] measurements of particle size and velocity of gas and particles in gas-atomized spray systems have been used in literature. However, the online measurement systems are complicated and impossible in this work. Therefore calculated values from photographs are used instead. It can be postulated from SEM photographs (Fig. 27) that one agglomerated particle is formed from one droplet. It is assumed in this thesis that each initial droplet gives birth to one agglomerated microparticle and the distribution is lognormal (see chapter 4.5.1). The Scanning Electron Microscopy (SEM) picture from the agglomerated microparticles gives the diameter of particles and the size distribution. The final particle size and distributions can be calculated from the equations of droplets [168,169,170] and mass balance.

The experimental results of the mean particle diameter and the calculated final mean particle sizes from the droplet size correlations of Steinmeyer and Hinze Eq. (29), El-Shanawany and Lefebvre Eq. (30), Jasuja Eq. (31) and Steinmeyer Eq. (32) are shown in Table XIV. Jasuja's Eq. (31) and Steinmeyer and Hinze Eq. (29) gave the best correlations with the experimental droplet size results. It can be seen, that in the supercritical media, in the temperature range 308-323 K and pressure range 10-14 MPa, the mean agglomerated particle size in the experiments was about 8-14 μm. The smallest agglomerated mean particle sizes were produced in liquid media (experiment numbers 6, 7 and 8). In that case the mean agglomerated particle size was less than 4 μm. In liquid media the velocity of CO_2 did not affect the obtained particle size (experiments 7 and 8).

Table XIV *Comparison of experimental and calculated final mean particle diameters from droplet size correlations by Steinmeyer and Hinze Eq. (29), El-Shanawany and Lefebvre's Eq. (30), Jasuja's Eq. (31) and Steinmeyer's Eq. (32). The particle diameters are determined from SEM pictures.*

	Experiment							
	1	2	3	4	5	6	7	8
Pressure (MPa)	14.0	17.0	11.0	13.0	10.0	10.5	8.5	8.5
Temperature (K)	313	333	313	323	308	303	302	302
Mass flow (CO2 g/min)	13.0	13.8	13.0	13.6	13.4	13.6	12.6	11.6
Density (CO2 kg/m3)	764	666	685	638	714	783	741	741
Viscosity (CO2 mPa s)	0.0661	0.0530	0.0548	0.0494	0.0585	0.0690	0.0624	0.0624
Mass flow (DCM g/min)	0.66	0.66	0.66	0.66	0.40	0.40	0.40	0.40
Viscosity (DCM mPa s)	0.356	0.304	0.356	0.328	0.371	0.388	0.392	0.392
Velocity (m/s)	0.74	0.90	0.82	0.92	0.81	0.75	0.74	2.74
Interfacial tension (N/m)	0.010	0.010	0.010	0.010	0.010	0.010	0.010	0.010
Nozzle diameter (mm)	0.70	0.70	0.70	0.70	0.70	0.70	0.70	0.35
Concentration of polymer in liquid (wt-%)	1.52	1.52	1.52	2.27	2.27	1.52	1.52	1.52
Mean particle diameter (μm)								
experimental value	8.1	25.7	10.9	13.7	10.7	3.5	3.9	3.3
Eq. (29)	9.5	8.1	8.9	9.2	10.0	9.0	9.6	1.4
Eq. (30)	2.5	2.2	2.4	2.5	2.7	2.4	2.6	0.4
Eq. (31)	9.3	8.3	8.8	9.4	9.9	8.9	9.3	1.8
Eq. (32)	25.3	21.7	23.7	24.7	26.8	24.4	25.8	3.7

The temperature of 333 K and a pressure of 17 MPa (experiment 2) gave a mean particle size of about 26 μm. In this experiment the agglomerated particles are

strongly macro agglomerated because of the high temperature and pressure in the recrystallization vessel. Therefore the particle size was complicated to measure. At high temperature and pressure with CO_2-DCM solution the polymer was swelling during the experiment and it was agglomerating more than in the lower temperature and pressure.

4.4.3. EFFECT OF TEMPERATURE AND PRESSURE

Higher temperature and pressure increased the mean particle size. The results of experiments showed that with decreased temperature the mean particle size is decreasing.

Fig. 28. shows the experimental measurements of mean particle diameters (black bullets) and the calculated mean particle diameters from Jasuja's droplet size correlation Eq. (31) in the experimental conditions (white bullets). In Fig. 28 the lines show the calculated final particle sizes from Jasuja's droplet size correlation Eq. (31) at different temperatures (302-333 K) and pressures (8.0-15.0 MPa). The initial droplet size was calculated from Jasuja's droplet size correlation Eq. (31) and the final particle size from mass balance. The basic data were: CO_2 mass flow 13 g/min, interfacial tension 0.010 N/m, nozzle diameter 0.70 mm, DCM mass flow 0.66 g/min, solid density 1270 kg/m^3 and internal porosity 0.5.

In Fig. 28 the calculated results show that at near supercritical conditions the calculated mean particle sizes agree quite well with the empirical mean particle size measurements. The results of calculation show, that the effect of pressure and temperature is weak on the final particle size (same as initial droplet size) under the experimental conditions used. The experimental particle size, however, seem to have a strong correlation with the temperature. Therefore it can be concluded that the calculated initial droplet size did not correlate generally with the final particle size. Fig. 28 shows that the mean droplet size estimated broadly the final particle size, but did not correlate the influence of operation conditions such as pressure and temperature. The temperature seems to have a strong correlation on the final particle size. An explanation for this is that the assumption of one agglomerated particle developing from each droplet, is not adequate. The droplets are possibly colliding with each other and combining or some drops are breaking up. Another explanation would be, that inside a droplet several particles are born, which are later agglomerated. Therefore, the final particle size is possibly determined more by the mass transfer of CO_2 into the droplet and DCM out of the droplet than by the initial mean drop size and distribution. The change of temperature affects the density of CO_2 and therefore also the mass transfer between liquid and CO_2.

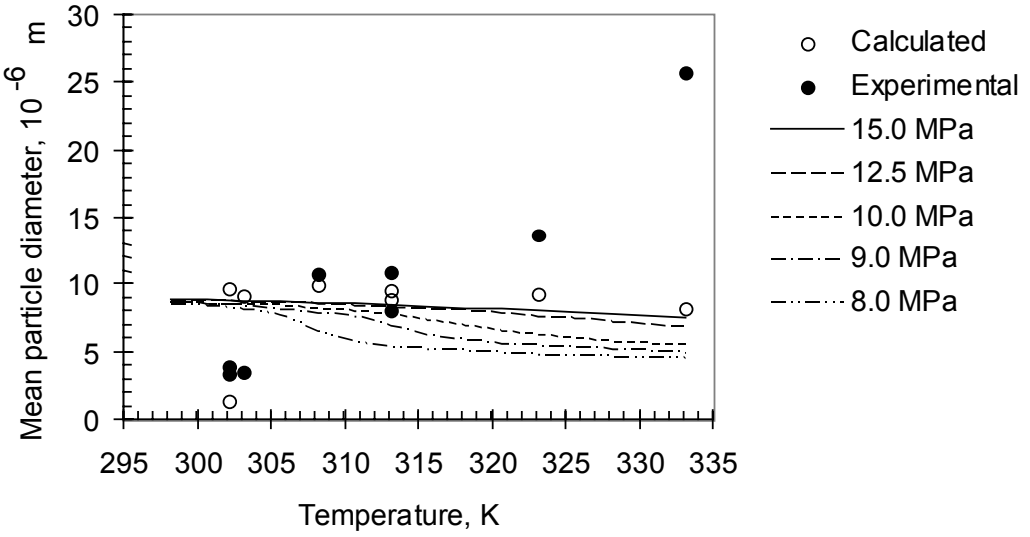

Fig. 28. *The effect of temperature and pressure on mean particle diameter (black bullets). The mean particle diameter has been calculated with Jasuja's [169] droplet size Eq. (31) (white bullets). The lines show the calculated final particle sizes from Jasuja's droplet size correlation Eq. (31) at different temperatures (302-333 K) and pressures (8.0-15.0 mPa). Basic data (lines): CO_2 mass flow 13 g/min, interfacial tension 0.010 N/m, nozzle diameter 0.70 mm, dichloromethane mass flow 0.66 g/min, solid density 1270 kg/m^3 and internal porosity 0.5.*

4.4.4. EFFECT OF DENSITY

The results of the experiments showed that with increasing density of CO_2 the mean particle size decreased quickly. The smallest particles are produced with liquid CO_2-systems (Table XIII, experiment 6, 7 and 8). Fig. 29 presents the experimentally measured mean particle diameters (black bullets) as a function of CO_2 density and calculated mean particle diameters from Jasuja's droplet size correlation Eq. (30) at the experimental conditions (white bullets).

At constant mass flow with increasing density of CO_2 the velocity of CO_2 decreased at the nozzle exit. Thus the effect of turbulent rupture decreased and larger droplets were produced with increasing density of CO_2 (see Eqs. 29-32). However, with increasing density of CO_2 the factor (σ/ρ_G) decreased (see Eqs. 29-32). Therefore the droplet size should decrease with the increasing density of CO_2 (and also particle size, if it is assumed that that one particle is formed from one droplet). The calculated results of the effect of CO_2 density on droplet diameter behave inversely to the particle size results of the experiments. This is shown also in Fig. 29 as the effect of the density of CO_2 on mean particle size (line) calculated from Jasuja's [169] droplet size correlation Eq. (31). The pressure in calculation was 11.0 MPa, temperature range from 298 K to 321 K, nozzle diameter 0.70 mm, interfacial tension 0.010 N m^{-1} and CO_2 mass flow 13 g min^{-1}.

The calculation showed that increasing the density of CO_2 increased weakly the mean particle size. The results of the experiment showed that the change in CO_2 density had a great effect on the measured particle size. Therefore the calculated initial droplet size did not correlate well with the final particle size.

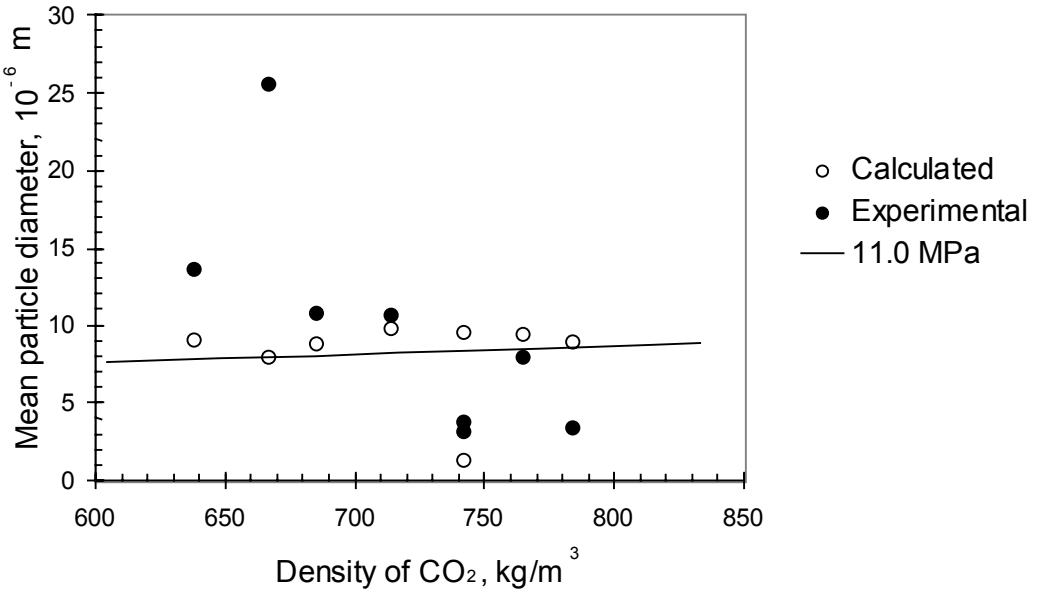

Fig. 29. *The effect of density of CO_2 on mean particle size in the experimental results (black bullets). The mean particle diameter is calculated (white bullets) from using Jasuja's [169] droplet size equation (31). Operating conditions (line): CO_2 mass flow 13 g/min, interfacial tension 0.010 N/m, nozzle diameter 0.70 mm, liquid dichloromethane and liquid mass flow 0.66 g/min, solid density 1270 kg/m^3 and internal porosity 0.5. The value of temperature is in the range 298 K to 238 K.*

A similar effect of CO_2 density on the final mean particle size as in this work has been shown by Dixon et al. [51]. They produced polystyrene particles by spraying a toluene solution into CO_2 through a 100 μm nozzle. They formed particles with diameters increasing from 0.1 μm to 20 μm as the CO_2 density decreased isothermally from 860 kg m^{-3} to 130 kg m^{-3}. The primary size of the micro particles was essentially constant at the density range between 860 kg m^{-3} and 400 kg m^{-3} at 308 K. At CO_2 densities greater than 700 kg m^{-3} and temperature below 303 K (subcritical condition) extremely small uniform micro spheres are formed.

4.4.5. EFFECT OF VELOCITY

The theoretical and the experimentally measured mean particle diameters as function of the velocity at the exit of the nozzle are shown elsewhere [155,156]. The results of the experiments show that the relative velocity does not correlate with the mean particle diameter. The hypothesis was that each initial droplet gives birth to one agglomerated particle. Then the initial droplet size and distribution

should correlate with the experimental results of final particle size (when the mass balance is known). Table XV shows the conditions in the tube, where the CO_2 and liquid are flowing, the velocity between gas and liquid inside the nozzle exit at the inner tube, and at the exit of the nozzle inside the particle collection device. Table XV shows also the values of Weber and nozzle Reynolds number and initial droplet sizes. The experimental values of Weber number were calculated from droplet size, which was calculated from the mass balance of experimentally measured particles size. The calculated Weber numbers are based on the Jasuja's droplet size correlation Eq. (31) in operation conditions. The initial droplet diameter was calculated from Jasuja's Eq. (31) and the experimental initial drop diameter was calculated from the mass balance of experimentally measured particles size.

Although the velocity is varying in the range 36 m s^{-1} to 0.4 m s^{-1} inside the nozzle at exit of the inner tube, the final particle size does not correlate well with the velocity. The velocity between spray and anti-solvent phase at the exit of the nozzle inside particle collection device is in the range of 0.74 to 2.74 m s^{-1}. With only a narrow range of velocities (0.74-0.92 m s^{-1}) a large mean particle size range from 4 μm to 26 μm was produced.

Table XV *The velocity of CO_2 and liquid at coaxial nozzle, Weber and nozzle Reynolds number. The Weber and nozzle Reynolds numbers are calculated from the Jasuja's Eq. (31) at the operating condition. The initial droplet size is calculated from measured particle size and from mass balance.*

	Experiment							
	1	2	3	4	5	6	7	8
CO2 flow in coaxial nozzle	inner	inner	outer	outer	outer	outer	outer	outer
CO2 velocity inside nozzle(m/s)	36	44	1.40	1.57	1.41	1.28	1.26	1.26
Liquid velocity inside nozzle(m/s)	0.037	0.037	1.1	1.1	0.64	0.64	0.64	0.64
Velocity at nozzle exit (m/s)	0.74	0.90	0.82	0.92	0.81	0.75	0.74	2.74
Density (CO2 kg/m3)	764	666	685	638	714	783	741	741
Viscosity (CO2 mPa s)	0.0661	0.0530	0.0548	0.0494	0.0585	0.0690	0.0624	0.0624
Nozzle diameter (mm)	0.70	0.70	0.70	0.70	0.70	0.70	0.70	0.35
Interfacial tension (N/m)	0.010	0.010	0.010	0.010	0.010	0.010	0.010	0.010
Mean particle diameter (μm)								
experimental value	8.1	25.7	10.9	13.7	10.7	3.5	3.9	3.3
Initial drop diameter (μm)								
Calculated experiment	23.4	74.3	31.5	34.6	27.0	10.1	11.3	9.5
Calculated Eq. (31)	26.8	23.9	25.6	23.7	25.1	25.8	27.0	5.3
Weber number (-)								
Experimental	0.97	3.99	1.46	1.88	1.28	0.45	0.45	6.14
Calculated	1.11	1.28	1.18	1.29	1.18	1.14	1.08	3.42
Reynolds number (nozzle) (-)	5965	7901	7199	8347	6947	5976	6127	12254

4.4.6. EFFECT OF REYNOLDS NUMBER

The contributing factor to drop breakup is the relative velocity between flowing liquid and CO_2 [51]. The dimensionless Reynolds number describes the inertial force to friction force ratio. The nozzles Reynolds number is given by

$$Re_n = \frac{d_{nozzle} U_{GL} \rho_G}{\mu_G} \tag{47}$$

where d_d is nozzle diameter (m), U_{GL} is velocity between gas and liquid (m s^{-1}), ρ_G is gas density (kg m^{-3}), μ_G is gas viscosity (Pa s). The data for Reynolds number calculation of nozzle is shown by Rantakylä et al. [156]. In the calculations we have used the velocity of the liquid at the exit of the nozzle. The mean particle diameter as a function of Reynolds number is shown in Fig. 30.

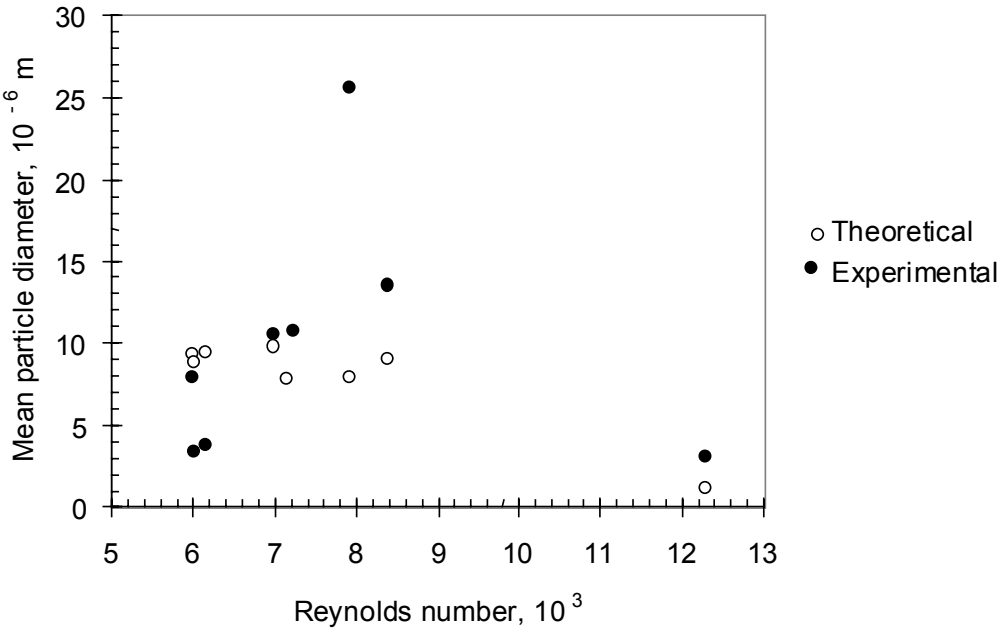

Fig. 30. *The theoretical and the experimentally measured mean particle diameters as a function of Reynolds number in the nozzle. The theoretical particle diameter is from Jasuja´s droplet size Eq. (31).*

The results of the experiments (black bullets) show that as the Reynolds number increases, the mean particle diameter also increases. The results of the calculations show (white bullets), however, that the estimated particle size is slightly decreasing with increasing Reynolds number. The effect of nozzle diameter is of minor importance on the particle sizes even when the relative velocity increases by 3.6 fold.

The smallest particles were produced at subcritical regions, where the Reynolds number was either very small (experiments 6-7) or very large (exp. 8). Since the Reynolds number describes the inertial force to friction force ratio, the droplet size should decrease with increasing Reynolds number. The hypothesis was that each initial droplet gives birth to one agglomerated micro particle. Then the final particle size should decrease slightly with increasing Reynolds number as it takes place in the subcritical experiments, but not in the supercritical. In addition, the

calculated particle sizes differ from the experimental ones. This verifies that the initial droplet size didn't correlate the final particle size especially in the supercritical conditions.

4.4.7. EFFECT OF WEBER NUMBER

The Weber number is used for describing the size of droplets formed in the spray process [182]. The Weber number relates the ratio of kinetic energy to surface energy. The Weber number is calculated from the equation

$$We = \frac{d_d U_{GL}^{\ 2} \rho_G}{\sigma} \tag{48}$$

where We is the dimensionless Weber number, d_d is drop diameter (m), U_{GL} is relative velocity between gas and liquid (m s^{-1}), ρ_G is gas density (kg m^{-3}) and σ is interfacial tension between liquid and gas (N m^{-1}). A large Weber number indicates that the deforming external forces are large compared to the reforming surface forces, thus leading to drop breakup into smaller drops [94].

Table XV tabulates the two Weber numbers. The experimental values of Weber number were calculated from droplet size, which was calculated from the mass balance of experimentally measured particles size. The calculated values of Weber number were calculated with the Jasuja's droplet size correlation Eq. (31) in operation condition. In Fig. 31 the mean drop diameter is shown as a function of Weber number. Fig. 31 shows also the effect of nozzle diameter, CO_2 mass flow, temperature, pressure and interfacial tension on Weber number and initial droplet diameter at typical operation conditions of the SAS technique. The conditions were: pressure between 8.5-17.0 MPa, temperature 298-338 K (then density of CO_2 between 220-809 kg/m^3), CO_2 mass flow 7.5-27.5 g/min, interfacial tension 0.0005-0.02 N/m, nozzle diameter 0.25-0.90 mm, dichloromethane mass flow 0.66 g/mind and density of L-PLA particle 1270 kg/m^3.

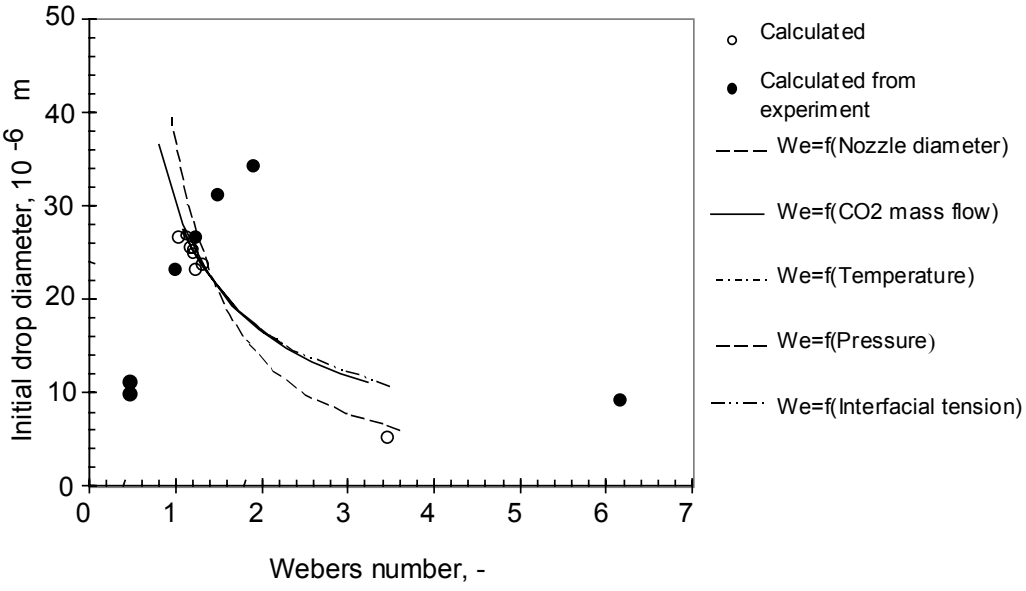

Fig. 31. *Initial droplet diameter as a function of Weber number. The diameters (white bullets) are calculated by Jasuja's droplet diameter correlation Eq. (31). Diameters from experimental (black bullets) are calculated from particle sizes and mass balance. Fig. 31 shows also Weber number of as function of nozzle diameter, CO_2 mass flow, temperature, pressure and interfacial tension on at typical operation conditions of SAS techniques. The conditions were: pressure between 8.5-17.0 MPa, temperature 298-338 K (then density of CO_2 between 220-809 kg/m^3), CO_2 mass flow 7.5-27.5 g/min, interfacial tension 0.0005-0.02 N/m, nozzle diameter 0.25-0.90 mm, dichloromethane mass flow 0.66 g/mind and density of L-PLA particle 1270 kg/m^3.*

The results of the experiments show that Weber number does not correlate with the mean drop size calculated by Eq. (30) as can be seen from Fig. 31. With increasing Weber number the initial droplet diameter increases contrary to the results of the calculations. An exception occurs when the relative velocity is high (Table XV experiment number 8). In experiment 8 CO_2 is in the liquid phase, as in the others experiments 6 and 7, where the initial drops diameter is the smallest.

4.4.8. DISCUSSION OF PARAMETERS AFFECTING THE PARTICLE SIZE

Several authors have studied how operating conditions affect the precipitation of poly(L-lactid acid) by using a dichloromethane/CO_2 system in an antisolvent process [7,10,156,183,184,185,186]. Generally, Thies and Müller [184], Mawson et al. [183] and Rantakylä et al. [156] reported a decrease in particle size, when the density of CO_2 was increased. Tu et al. [185] reported that although an increase in pressure resulted in a decrease in particle agglomeration, the average size of particle size was unaffected. Randolph et al. [10] produced a larger polymer particle size as the density of CO_2 was increased. They suggest that the

reduced diffusivity of the CO_2 was a more dominant factor influencing particle size.

In this work the calculations showed that changing process parameters temperature, density, pressure, interfacial tension between liquid and gas and velocity of gas have a small calculated effect on the initial droplet size. It was seen that the model of initial droplet size correlated broadly with the final particle size. The results of the experiments showed that the effect of variables in supercritical state (density of CO_2 and temperature) have a greater influence on the particle size than the model of droplets predicts. In subcritical state the trend follows better the droplet size correlation, even the calculated droplet size differ from the experimental particle size. It can be concluded that the smallest particles are observed in subcritical CO_2, where the value of liquid mass transfer coefficient k_L is highest. Therefore it is probable that the final particle size depends more on other variables than the initial mean droplet size and distribution. This is studied further in Chapter 4.5.

4.5. MASS TRANSFER

In the SAS technique mass transfer occurs between the dispersed droplets and the surrounding gas phase. One aim of using supercritical antisolvent technique is to improve mass transfer by generating fine drops with a high surface area and thereby to increase mass transfer between a drop and drying medium [11]. During the SAS operation, the mixing process of the solvent and antisolvent generates high turbulence within the solution, which affects both the nucleation and growth of the resulting particles. In order to describe the mass transfer, the drop size distribution, nucleation and particle growth during the drying of the drops as well as the fluid dynamics of the dispersed liquid must be known.

The droplet may swell or shrink depending upon the mass transfer of incoming of CO_2 to droplets and the mass transfer of solvent from droplets to fluid. Those both effect the degree and rate of supersaturation of recrystallizing materials in droplets. The objective of this work was to evaluate the simple model for the SAS technique and to examine how the operating variables (temperature and pressure) effect on liquid and gas side mass transfer coefficient and how mass transfer effects on the behaviour of solvent droplets at below and near supercritical conditions. The mathematical model includes a model of ternary fluid phase equilibrium inside the droplet and a model of mass transfer between the droplet and the drying medium as a function of time. The effect of mass transfer changes on droplet properties was calculated with the Peng-Robinson equation of state with experimental results from solubility of poly(L-lactid acid) in dichloromethane (DCM) into CO_2.

Earlier in this work and by Rantakylä et al. [156] it was shown that the model of initial droplet size predicted roughly the final particle size. The experimental results showed that all variables in supercritical state (density of CO_2 and temperature) have greater influence on the particle size than the model of droplets

predicts. In general the model of droplet size shows, that the change of temperature, pressure and mass flow at the typical values of the SAS technique has a minor effect on initial droplet size.

Other researchers have found the following results: Lengstfeld et al. [136] have explored the time scale of surface tension evolution in jets of miscible fluids injected into critical and near-critical solvents to determine whether the jets atomize into droplets or simply evolve as gaseous plumes. They have developed a method for predicting dynamic surface tension and combined this method with linear jet breakup equations to accurately predict jet breakup lengths in immiscible to highly miscible systems. They showed that because this distance is shorter than characteristic breakup lengths, distinct droplets never form. Rather, the jets spread in a fashion characteristic of gaseous jets, whose mixing is well described by the gaseous fluid mixing theory. They have presumed, that micro-particle formation results from gas phase nucleation and growth within the expanding plume, rather than nucleation within discrete liquid droplets.

Kröber and Teipel [188] have studied the effect of process parameters on tartaric acid processing with PCA method. They have found that the particle size is more or less independent on the nozzle diameter if similar nozzles are used. When changing the nozzle type from a Laval nozzle to a two-flow nozzle the mean particle size is reduced. Smaller droplets are formed with a two-flow nozzle and mass transfer is increased. In contrast to atomization process under atmospheric conditions the pressure drop across the nozzle does not affect the droplet size when the atomization takes place in compressed gases. Reverchon et al. [210] have studied pilot scale micronization of amoxicillin by SAS technique. They presented that the change of nozzle arrangement and diameter from the laboratory to the pilot scale does not affect significantly the particle size and distribution.

Goa et al. [187] studied preparation of fine particles of several kinds of pigments using a continuous GAS system. To obtain the finer particle products, a series of 5-500 μm nozzles were used to disperse the solution out from the recrystallizer. Larger pigment particles were formed at higher operation temperatures (temperature range from 298 K to 393 K) and larger nozzle diameter. Smaller pigment particles were formed at higher operation pressure (pressure range from 7 MPa to 26 MPa). The mean size diameter range of pigment was from 0.4 μm to 3.5 μm. Goa et al. [187] found experimentally that the size and structure of the nozzle plays an important role. Larger particles were formed when larger diameter nozzles were used. The explanation was that the final particle size is determined more by the mass transport of CO_2 into the droplet and organic solvent out of the droplet than by the initial mean drop size and distribution. They argued that by increasing the temperature in the recrystallizer, the collision movement of pigment molecules in the solution was accelerated and this in turn increased the chances of molecular nucleation and promotes the crystal growth process. Therefore, larger particles were formed at higher operation temperatures. When the operating pressure was increased, the CO_2 solubility in the solution increased, as the higher supersaturation concentration was attained. In this work the smallest particles were observed near the critical point of CO_2 or in subcritical conditions.

Near the critical point the mass transfer, high nucleation rates and short times for nuclei to grow caused formation of the smallest particles.

Werling and Debenedetti [147] presented a mathematical model to SAS technique for mass transfer between a droplet of organic solvent and a compressed antisolvent, which takes into account the two-way mass transfer both into the droplet and into the bulk antisolvent. The model includes the composition dependence of the diffusion coefficient, non-ideality of the liquid phase density due to addition of antisolvent, and the corresponding changes in the droplet radius. They presented that the supersaturation is not homogenous within the droplet for both miscible and immiscible conditions. They presented also that the initial interfacial flux is always into the droplet, causing droplet swelling. They show that at temperature range between 314-332 K and pressure between 7.6-8.6 MPa the mixture critical point droplet lifetime diverges. Away from the critical point, the lifetime of the droplets decreases as the pressure is increased, but shows a non-monotonic temperature dependence.

Lora et al. [151] presented a simulation of the semicontinuous supercritical antisolvent recrystallization process. The model included thermodynamics, hydrodynamics and mass transfer issues and it makes possible to calculate the composition and flow rate profiles of the vapour and liquid phases and the amount of the solid product along the precipitator. They have shown that in a CO_2-toluene-naphthalene-phenanthrene system, the dissolution of the antisolvent in the liquid phase is usually faster than the evaporation of the solvent. They presented also that the two solutes might behave in completely different ways at the same process conditions. Phenanthrene is easily precipitated by the antisolvent effect and the process is driven essentially by CO_2 dissolution in the liquid phase. For naphthalene the antisolvent effect needs to be coupled to evaporation, which occurs much more slowly and is a function of the flow rate ratio.

Randolph et al. [10] presented results similar to those in this work in their studies on sub-micrometer-sized biodegradable particles of poly(*L*-lactic acid) formed by using near critical and supercritical CO_2 as an antisolvent. Although two methods with very different mechanisms for forming droplets were used, similar particles sizes were observed as a function of carbon dioxide density. They suggest that mass transport, rather than jet breakup and hydrodynamics, controls particle sizes in the near-critical and supercritical regions.

4.5.1. DROPLET MEAN SIZE AND DISTRIBUTION

Because the mass transfer rate between liquid droplets and continuous CO_2 phase depends on the droplet size, the distribution of the droplet sizes exiting the nozzle needs to be studied. In this work it is assumed, that initial droplet size distribution is similar to final particle size distribution. The particle distribution has been conformed to a lognormal distribution. An experimental distribution of particle sizes is measured from SEM photograph and from this estimate the parameters of lognormal distribution are calculated. The calculated particle size distribution is

compared with the value of experiments to assess the models competency. Fig. 32 shows an example of the final particle size distribution obtained from one of the experiment (see Table XIII experiment 5).

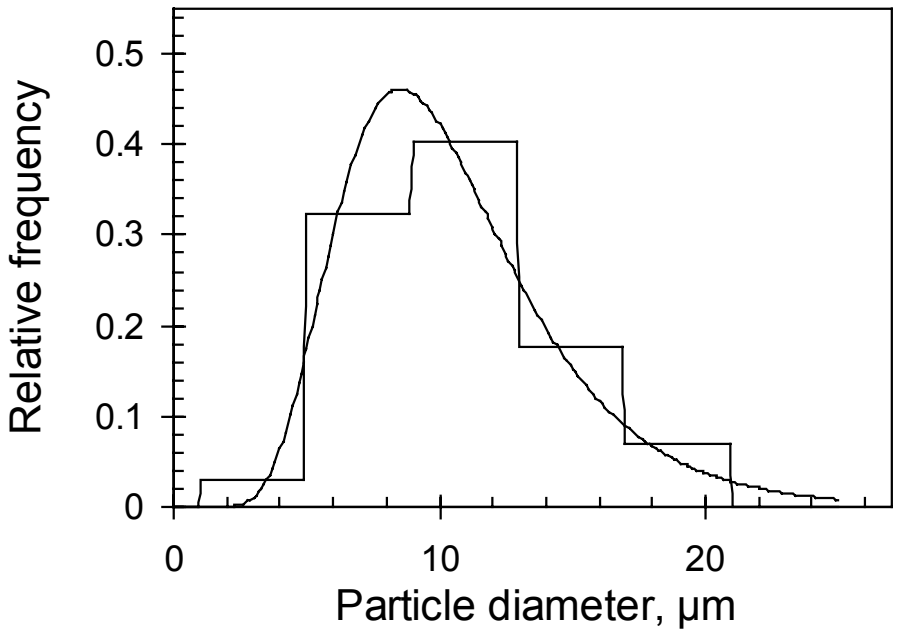

Fig. 32. *The final particle size distribution from experiments (bars) and the corresponding lognormal distribution (line).*

In this experiment the operating conditions were: 10 MPa, 308 K, concentration of L-PLA in methylene chloride 30 mg/ml, mass flow rate of CO_2 13 g/min and flow rate of methylene chloride solution 0.30 ml/min. The diameter of the nozzle was 0.70 mm. The flow rate of the mixture at the end of the nozzle was 0.8 m/s. The porosity of particles was assumed to be 0.5, density of solid 1270 kg/m^3 and liquid-fluid interfacial tension 0.010 N/m. The particle distribution conformed to the model of a lognorm distribution. The final mean particle size for particles d_{32} was found experimentally to be 10.7 µm. The calculation of droplet size from the lognormal distribution model gave 9.2 µm.

4.5.2. GAS SIDE MASS TRANSFER COEFFICIENT

The results of calculated gas side mass transfer coefficients in the SAS technique are presented by Rantakylä et al. [157]. Earlier in this work and elsewhere [155,156] we have shown that in the typical SAS technique experimental conditions the Reynolds number are in the range of 90-800 at the exit of the nozzle, when the initial droplet size is between 10-40 µm and the initial velocity of droplets inside the nozzle is in the range of 0.7 m s^{-1} to 2.7 m s-1. Then the Schmidt number is in the range of 3.1-5.0 and the calculated initial k_G at the exit of nozzle is in the range of $10*10^{-3}$ to $40*10^{-3}$ m s^{-1}.

The calculated Sherwood, Reynolds and Schmidt numbers and initial gas side mass transfer coefficient at the exit of the nozzle in experimental conditions are shown in Table XVI. The initial Sherwood number is calculated with Frössling Eq. (40) and Eq. (41). The value of the k_G is high in comparison to the average fluid-solid system, where k_G is in the range of $5.5*10^{-6}$ to $3.1*10^{-4}$ m s^{-1} [107,111]. This is due to the high velocity and the small diameter of the droplet by SAS technique. In a supercritical spray, a sieve tray or a packed extraction column the velocity between fluid and extraction material is generally in the range of 5 to $30*10^{-3}$ m s^{-1} and the diameter of the droplets or particles is about 1…5 *10 m^{-3} [107,109,111].

Table XVI *The calculated Sherwood, Reynolds and Schmidt numbers, diffusion and initial mass transfer coefficients at experimental conditions.*

	Experiment							
	1	2	3	4	5	6	7	8
Initial drop diameter (µm)	23.4	74.3	31.5	34.6	27.0	10.1	11.3	9.54
Schmidt number Eq. (2)	4.53	3.14	3.47	2.94	3.87	4.98	4.31	4.31
Reynolds number Eq. (3)	199	838	323	394	267	86.2	98.9	306
Sherwood number Eqs. (1)&(40)	16.0	27.5	18.4	19.1	17.4	11.5	11.7	19.1
Sherwood number Eqs. (1)&(41)	33.9	57.9	37.9	38.4	36.3	23.4	23.3	41.0
Initial diffusion coefficient								
D_{21} (10^{-9} m^2/s)	19.1	25.3	23.0	26.3	21.2	17.7	19.5	19.5
D_{12} (10^{-9} m^2/s)	5.30	6.08	4.96	5.32	4.79	4.77	4.56	4.46
D_{32} (10^{-9} m^2/s)	0.396	0.494	0.396	0.444	0.374	0.352	0.347	0.347
Initial gas side mass transfer coefficient								
k_G Eq. (40) (10^{-3} m/s)	13.1	9.40	13.4	14.5	13.7	20.2	20.2	39.2
k_G Eq.(41) (10^{-3} m/s)	27.7	19.7	27.7	29.3	28.5	41.0	40.2	84.2
Liquid phase mass transfer coefficient								
k_L Eq. (42) (10^{-3} m/s)	2.26	0.82	1.57	1.54	1.77	4.72	4.03	4.79

The droplet velocity affects external mass transfer rate and therefore the drying time of droplets. The gas compressibility along with a change in pressure may significantly influence the velocity of the droplets. Because the high density of CO_2 (usually in SAS technique between 600-900 kg m^{-3}), the velocity of the droplets first decreases quickly and then approaches a constant value asymptotically. In this model the velocity of the droplet decreases from 0.7 m s^{-1} - 2.7 m s^{-1} to in the range of 0.05 m s^{-1} to 0.1 m s^{-1} after 2 ms of flying time. Then the values of calculated k_G are decreased 5-15*10^{-3} m s^{-1}. The k_G was calculated from modified Frössling Eq. (39). In this calculation the Reynolds number is in the range of 15 to 40 and the Sherwood number is in the range of 2 to 10. Pressure influences weakly the velocity of droplets above the critical pressure of CO_2. However, the density of CO_2 changes slightly in a high pressures and low temperature.

The dependence of CO_2 side mass transfer coefficient k_G on temperature and pressure is shown in Fig. 33. The velocity of droplet is 0.050 m s^{-1} and the droplet diameter 30 μm.

Mass transfer coefficient k_G increased with temperature and decreased with increasing pressure. The effect of temperature and pressure on k_G is the same as the effect on D_{21}. Near to the supercritical values of CO_2 the change in k_G is pronounced. This is due to the increased temperature causing an increase in the diffusion coefficient and decreasing Schmidt number. The change of Reynolds number at the pressure range between 8.0 MPa and 15.0 MPa and temperature range between 298 K and 328 K is small.

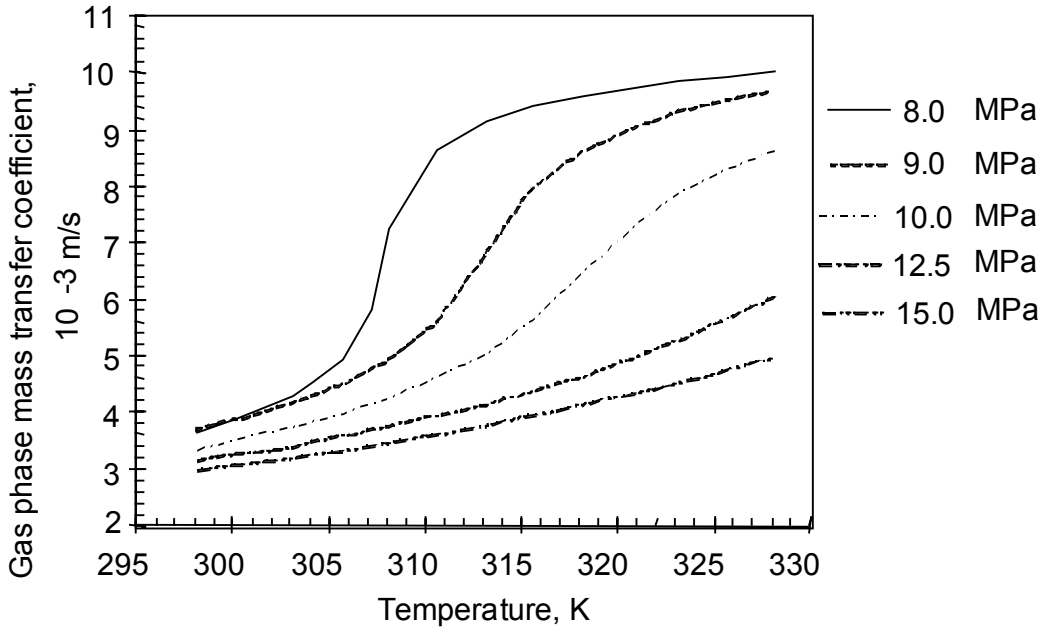

Fig. 33. *The calculated gas side mass transfer coefficient k_G of dichloromethane in pressured CO_2 as a function of temperature at different values of pressure. The droplet diameter is 30 μm and the velocity of droplet is 0.050 m s^{-1}. The k_G is calculated from modified Frössling Eq. (40).*

The change in the value of k_G is great just above the critical temperature and pressure of CO_2, therefore Reynolds number has a maximum above the critical point of CO_2. The values of Reynolds number have a maximum because the ratio of ρ/μ changes with pressure and temperature. To maximize mass transfer from the liquid to the gas phase and then to generate high supersaturation in droplets a near critical pressure and high temperature should be used. The typical value of k_G near critical pressure and high temperature was in the range of $3.5*10^{-3}$ m s^{-1} to $9*10^{-3}$ m s^{-1} in the typical range of process parameter values for the SAS processes. It is not always possible to use high temperatures because of the properties of the formed material, for example low melting point. The polymer may not solidify at high temperature in dense CO_2 and with liquid solvent.

4.5.3. LIQUID SIDE MASS TRANSFER COEFFICIENT

The results of calculated liquid side mass transfer coefficients in the SAS technique are presented by Rantakylä et al. [157]. The calculated liquid side mass transfer coefficient k_L at experiment conditions is in the range of $1.5*10^{-3}$ m s^{-1} to $4.8*10^{-3}$ m s^{-1}. The liquid side mass transfer coefficients at experimental conditions calculated by Eq. (42) are shown earlier in Table XV. The gas side mass transfer coefficient at the exit of the nozzle k_G is approxmately 6-11 times greater than the liquid side internal mass transfer coefficient k_L at experimental conditions. After 2 ms of droplet flying time the k_G has decreased so much that it is anymore only twice the k_L.

The dependence of liquid phase mass transfer coefficient k_L on temperature and pressure is shown in Fig. 34.

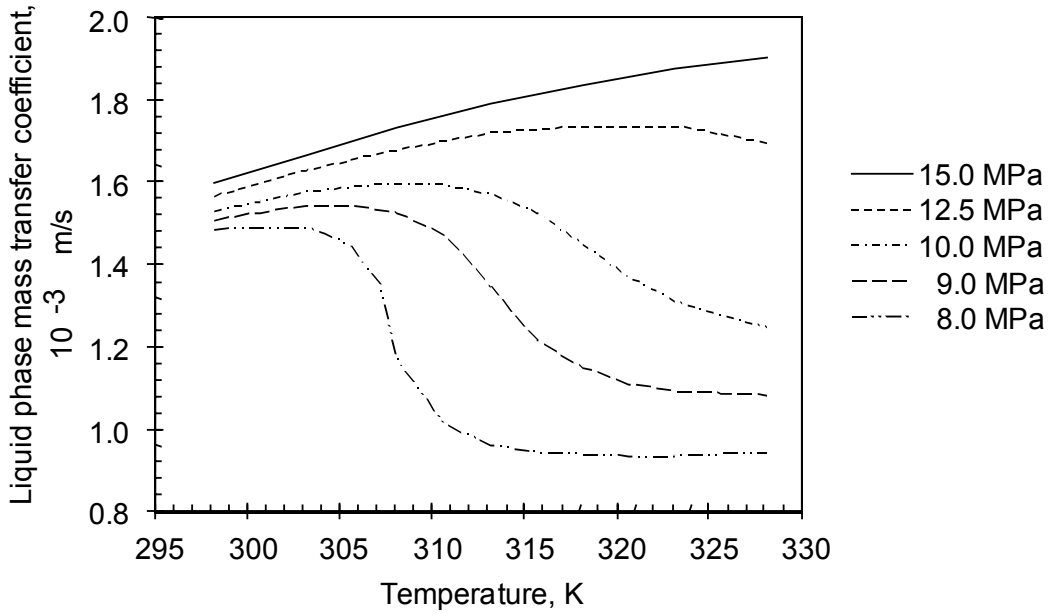

Fig. 34. *The calculated liquid side mass transfer coefficient k_L in CO_2 as a function of temperature in different values of pressure.*

At values just above the supercritical point of CO_2 the change of k_L is larger. The mass transfer coefficient increases with temperature and pressure above 12.5 MPa, but decreases with temperature below 12.5 MPa. Below the critical temperature and pressure of CO_2 the effect of pressure and temperature on value of k_L is less significant. Typical values of k_L below critical temperature and pressure are around $1.6*10^{-3}$ m s^{-1}. The smallest particles are observed near or below the critical point of CO_2 where the value of liquid mass transfer coefficient is highest. Under these conditions the gas side mass transfer coefficient is lowest. Carbon dioxide dissolves well in DCM and the liquid phase controls the mass transfer from gas phase to the droplet.

4.5.4. CORRELATION BETWEEN MASS TRANSFER COEFFICIENT AND PARTICLE SIZE

In this work we have shown that the model of initial droplet size correlated generally with the final particle size at near and supercritical temperature and pressure, but the model did not correlate with the effect of change in temperature and pressure for droplets and particles size (Chapter 4.4.). The results of the experiments show, that the effect of temperature and pressure (density of CO_2) is greater for particle size than the model of droplets shows. It is supposed that mass transfer controls particle sizes in the near critical and supercritical regions. The linear and nonlinear (only factors k_L, k_G and CO_2 density) correlations between some variables of mass transfer and particle diameter are shown in Table XVII. The results were calculated with the SPSS Diamond statistical program.

Table XVII *The correlation between variables of experimental particle diameter.*

Variable Pair	Correlation	R-square	Slope
Temperature - Diameter	0.955	0.913	1.4
Pressure - Diameter	0.853	0.727	2.2
Weber number - Diameter	0.227	0.052	0.85
Reynolds number - Diameter	-0.017	0.00029	-4.8
Velocity - Diameter	-0.281	0.079	-3.1
Viscosity CO2 - Diameter	-0.727	0.528	-800
Viscosity liquid - Diameter	-0.946	0.895	-220
Density CO2 - Diameter	-0.745	0.555	-5.0
Log(Density CO2) - Log(Diameter)	0.791	0.626	-8.3
k_L - Diameter	-0.848	0.720	-4.1
Log(k_L) - Log(Diameter)	0.998	0.997	-1.2
k_G - Diameter	-0.648	0.420	-0.81
Log(k_G) - Log(Diameter)	0.867	0.752	-1.5

The smallest particles are observed at subcritical point of CO_2, where the value of liquid mass transfer coefficient is the highest. In these conditions the gas side mass transfer coefficient is the lowest. The correlation between liquid mass transfer coefficient k_L and mean particle size d_p is nonlinear. The linear correlation between liquid mass transfer coefficient and mean particle size is only -0.85, but nonlinear correlation log(k_L)-log(d_p) is 0.998. The correlation of log(k_L)-log(d_p) is nearly perfect and the equation explains the generated particle size quite exactly. The result of the experiment in which the mean particle size is about 25 μm (Experiment 2, Table XIII), does not deviate from the other results in log(k_L)-log(d_p) correlation even there was strong agglomeration of particles. This is understandable since d_p does not stand for macro agglomerate size but for the size of 'elementary' particles (see Chapter 4.3.)

The linear correlation between temperature and particle diameter is over 0.95 and the correlation is positive. Previously Fig. 28 showed the effect of temperature on mean particle size. However, in crystallization techniques such as cooling/heating, solvent evaporation, flash/evaporative cooling, change of pressure and chemical reaction, temperature and the rate of change of temperature have an effect on crystallization.

The linear correlation between viscosity of liquid and particle diameter is also high, almost 0.95 and the correlation is negative. In this simple particle formation model the droplet viscosity is assumed to be the same as the viscosity of pure liquid solvent during the whole droplet flying time. Therefore the correlation is not as clear as the correlation values indicate. In fact, the viscosity of liquid decreased during droplet flying time because the amount of CO_2 increased in droplets. The content of polymer inside the droplet also decreased the mass transfer between droplet and CO_2 phase.

Previously it was shown in Chapter 4.4.4. that the particle size depends on the density of carbon dioxide. The linear correlation between density of CO_2 and particle diameter is not so high, only -0.75 and nonlinear correlation 0.79. Fig. 29 shows the effect of the density of CO_2 on mean particle size. The particle diameter decreased with increasing density of CO_2 in supercritical state. In supercritical state the linear correlation between particle diameter and density of CO_2 is 0.98.

4.5.5. DISCUSSION OF MASS TRANSFER COEFFICIENT

Earlier in this work it is shown, that it is not possible to largely adjust the initial droplet size by changing temperature, pressure and flow rate within the typical range in the SAS process with a similar nozzle. With small droplets a high supersaturation may be achieved more rapidly than with bigger droplets, because the small ones expand more rapidly and their density decreases quickly. The rate of supersaturation of heavy materials in droplets depends on the rate of mass transfer of CO_2 into droplets and the rate of mass transfer of liquid phase to the gas phase. CO_2 is very soluble in DCM and the liquid phase controls the mass transfer. In this application of the particle formation it is advantageous to use low temperature and high pressure, where the liquid side mass transfer is maximum. The mass transfer coefficient of the liquid phase should be maximized to obtain a fast and high supersaturation, when small particles with a narrow size distribution are desired. The problem is that the effect of temperature on k_L is competing with the effect on k_G. To produce high values of k_L and k_G there is a compromise on the value of temperature and pressure.

However, the solubility of polymer in the antisolvent phase increases with increased temperature and pressure. To maximize the mass transfer coefficient in order to produce a high rate of supersaturation it is important to optimize temperature and pressure so that the formed material doesn't dissolve too much in antisolvent phase decreasing the yield of polymer. Secondly, it is not always possible to use a high temperature because the formed materials have a low

melting point. Other effects including initial droplet diameter, liquid phase density, solubility of the heavy component in the fluid/solvent mixture also influence the particle formation and supersaturation, which makes the design of the process more difficult.

4.6. DROPLET PROPERTIES

4.6.1. VOLUMETRIC EXPANSION OF DICHLOROMETHANE

The volumetric expansion of the liquid carrier mainly controls the morphology of particles produced by GAS precipitation [2]. In the SAS processes, the liquid of a droplet is evaporated into the continuous supercritical fluid. At the same time the droplet is volumetrically expanding and the mole fraction of CO_2 in the liquid phase increasing. The mole fraction of CO_2 in liquid phase depends on temperature, pressure and the solvent. The results of calculated volumetric expansion of DMC droplet in the CO_2 is shown early by Rantakylä et al. [157]. The volumetric expansivity of liquid dichloromethane in CO_2 at different pressures and temperatures is shown in Fig. 35. The expansion curves have been obtained using a Peng-Robinson equation of state [92].

In Fig. 35 it can be seen that CO_2 in the vicinity of its critical point produces a large volumetric expansion of dichloromethane. Expansion curves move towards lower pressures when temperature decreases. Therefore the same volumetric expansion can be obtained at lower pressures. In other words, in a lower temperature not so high pressure is needed as in the higher temperature to obtain equal volumetric expansion.

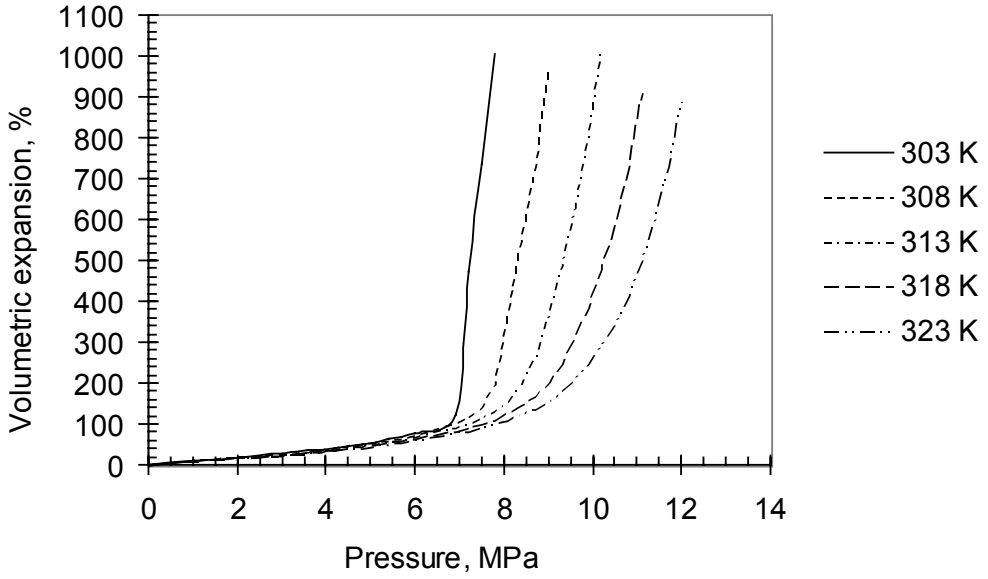

Fig. 35. *Volume expansion of dichloromethane in CO_2 at different pressures and temperatures. The expansion curves have been obtained using the Peng-Robinson equation of state [92].*

The mole fraction of CO_2 in liquid phase depends on temperature, pressure and the solvent. The volumetric expansion depends on the mole fraction of CO_2 in the liquid phase. In fact it has been presented that the plot of solvent expansion vs. mole fraction of antisolvent instead of pressure and temperature, reveals a striking similarity between various organic solvents [90]. Fig. 36 shows the volume expansion for several liquid solvents as the function of mole fraction of CO_2 [90] and the calculated volume expansion of DCM at several temperatures calculated with Peng-Robinson equations of state [92]. The calculated volumetric expansion of DCM in this work corresponds to the experimental results of Kordikowski et al. [90].

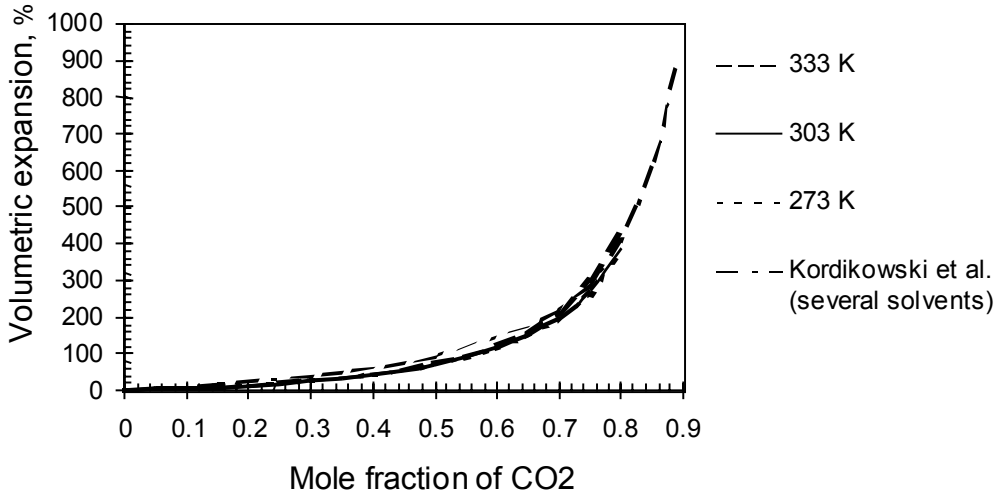

Fig. 36. *The volume expansion of several liquid solvents as a function of mole fraction of CO_2 (Kordikowski at al. [90]) and in this thesis calculated volume expansion of dichloromethane from Peng-Robinson equation of state [92]. The pressure range is 0.1 MPa to 12.0 MPa.*

Fig 36. shows that the expansion curves are almost indistinguishable in all temperatures at constant mole fraction of the CO_2 in the liquid phase. Various solvents coincide when the plot of the expansion is presented as function of mole fraction of CO_2 in the liquid phase. However, the rate of volume expansion of droplet and then the rate of supersaturation of heavy materials in droplets in SAS precipitation depends on the rate of the mass transfer of CO_2 into droplets.

4.6.2. SIZE AND DENSITY OF LIQUID DROPLET

Although the volumetric expansion of dichloromethane (DMC) in compressed CO_2 is large (see Figs. 35 and 36), the DMC droplet size increases slightly with droplet flying time in CO_2 ambient. The change of droplet expansion and size as a function of droplet flying time is shown in Fig. 37A and 37B. The data of calculation is as follows: temperature 313 K, pressure 9.0 MPa, average gas velocity 1.34 m s^{-1}, CO_2 density 487 kg m^{-3} and viscosity 0.0350 mPas, liquid

DCM liquid density 1316 kg m^{-3} and viscosity 0.355 mPas. It is assumed that the initial droplet doesn't disperse during flying time.

A)

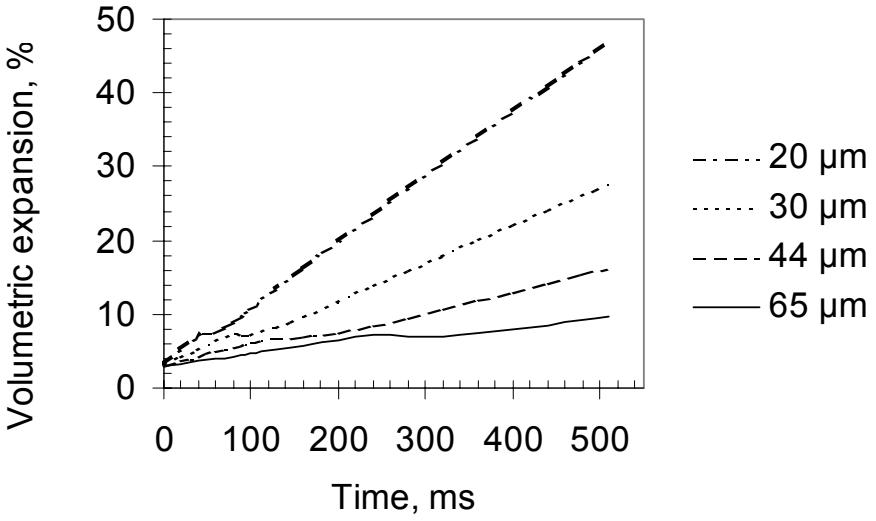

B)

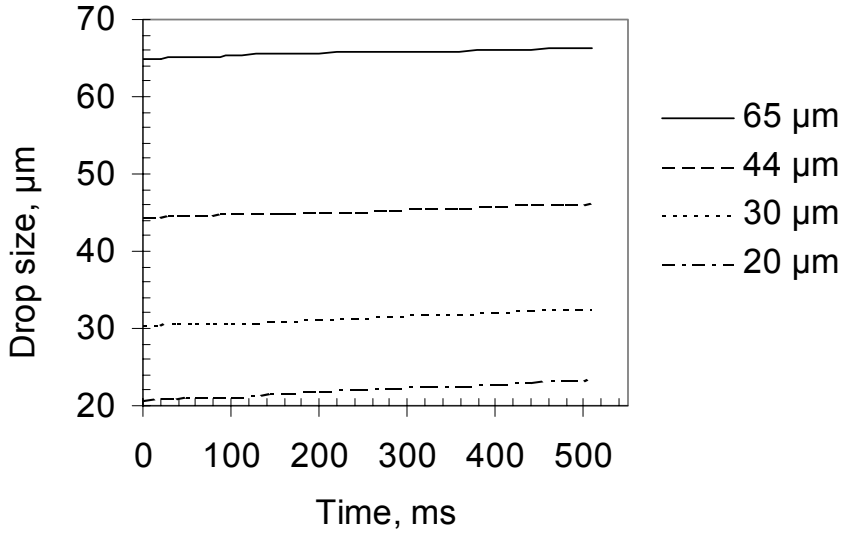

Fig. 37. *The change of volume expansion (Fig. A) and size (Fig. B) of dichloromethane droplet size as a function of droplet flying time in CO_2. The parameter is the droplet initial size. The pressure is 9.0 MPa and temperature 313 K.*

The change of droplet diameter is quite small as a function of flying time. The size of the small droplets increases more than that of the bigger droplets. The mass transfer rate between liquid and gas phase is a function of surface area. However, in a small droplet the surface area versus volume is greater than in a bigger droplet. The problem is that in SAS technique it is not possible to influence much the initial droplet size by using a single nozzle type and process parameters

temperature, pressure and flow rates in their typical operating range (see Rantakylä et al. [156] and Kröbel and Teibel [188]).

As the CO_2 is dissolved into the liquid phase, the liquid is dissolved into continuous CO_2 phase. At the same time, the density of the liquid is decreased. The solubility of heavy material in droplet depends on the density of the liquid. When the density of the liquid phase is decreased, the solubility of polymer in liquid phase is decreased at the same time. The concentration of CO_2 inside the droplets as the function of droplet flying time is dependent on the initial droplet size. The density of droplets as a function of droplet flying time is shown in Fig. 38. The input data of calculation is the same as used before in Fig 37. The density of droplet approaches the value of the density of CO_2 asymptotically. The density of small droplets decreases more quickly than the density of bigger droplets. In small droplets the polymer is formed earlier than in bigger droplets. When the available droplet flying time is short, for example because of the dimension of crystallization vessel, it is possible to produce dry particles by using small droplets.

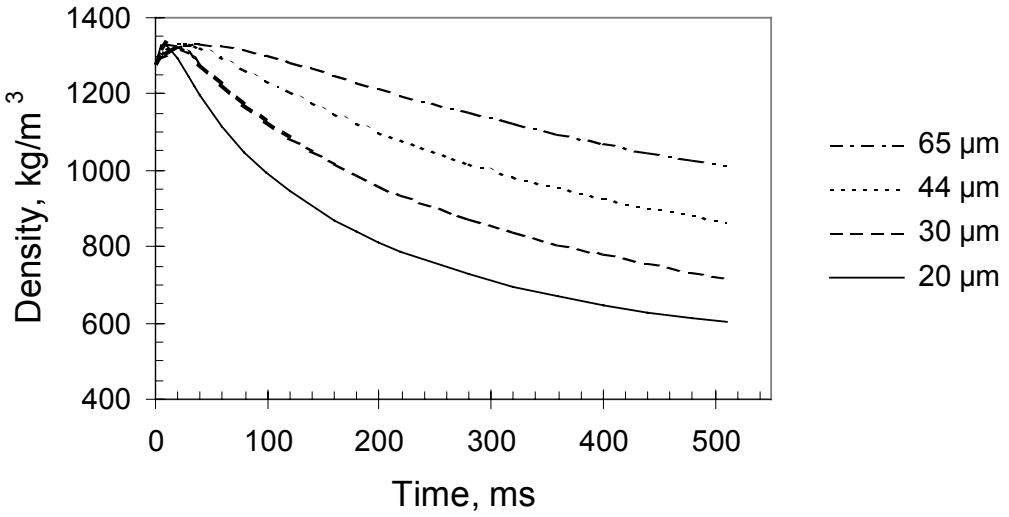

Fig. 38. *Dichloromethane/CO_2 droplet density as a function of droplet flying time in CO_2. The parameter is the droplet initial size. The pressure is 9.0 MPa and temperature 313 K.*

Other researchers have found following results: Werling and Debenedetti [8,147] presented a mathematical model for mass transfer between a droplet of organic solvent (toluene) and a compressed antisolvent (CO_2) which takes into account the two-way mass transfer both into the droplet and into the bulk antisolvent. The model includes the composition dependence of the diffusion coefficient, non-idealities in the liquid phase density due to addition of antisolvent and the corresponding changes in the droplet radius. The model is applicable to the SAS method of particle formation. They used Peng-Robinson EOS equation and the same mixing rules as in this thesis and presented that at the mixture critical point, droplet lifetime diverges. They showed also that the lower pressures and larger initial radii of droplets result in longer droplet lifetimes, and that lifetimes

increase sharply at near-critical conditions. Away from the critical point, the lifetime decreases as the pressure is increased, but shows a non-monotonic temperature dependence. Werling and Debenedetti [147,149] also calculated that the lifetime of a 50 μm size toluene droplet in CO_2 is around 1.5 s at pressure between 8.2-8.7 MPa and at temperature 313 K. This droplet lifetime is of the same order of magnitude as calculated in this work.

4.6.3. SOLUBILITY OF POLYMER

The solubility of heavy solute in liquid phase decreased as mole fraction of CO_2 increased in liquid phase. Fig. 39 shows the calculated solubility of L-PLA in DCM as a function of pressure at various temperatures. The solubility is calculated with the Peng-Robinson EOS, and the physical properties and the mixture parameters k_{ij} are shown earlier (see Table XII).

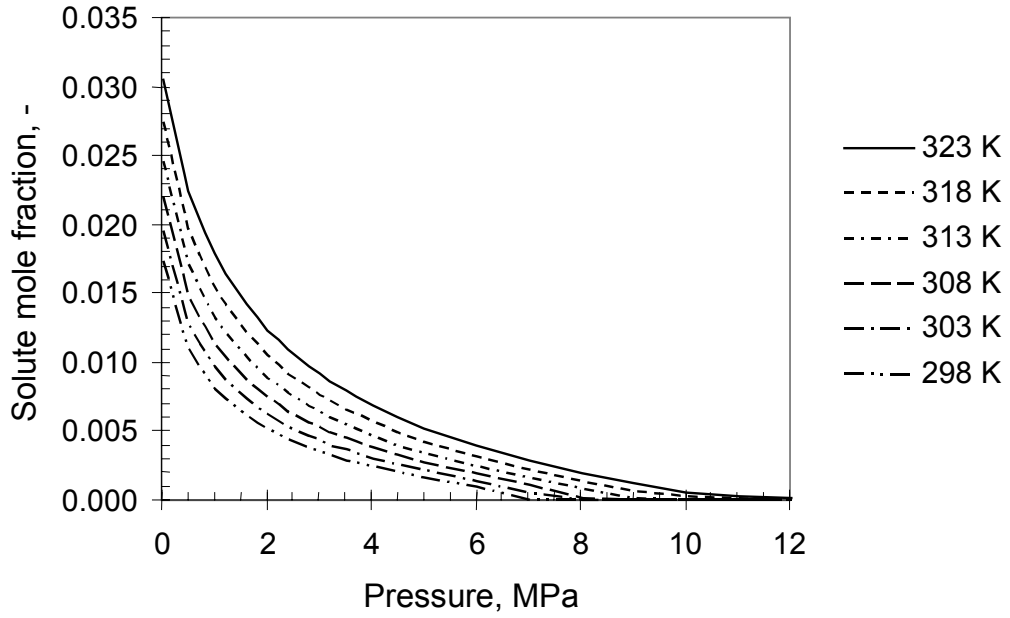

Fig. 39. *The calculated solubility of L-PLA in dichloromethane as a function of the pressure at various temperatures by using Peng-Robinson equation of state [92].*

In SAS particle formation processes of L-PLA the use of high temperatures (over 308 K) is not warranted. Neither will the use of a pressure over 10 MPa at near critical temperature guarantee a good result. It can be seen from Fig. 39, that the solubility of PLA decreases with increasing pressure and temperature. The lines seem to end at zero. At high values of pressure, beyond the critical point of CO_2, the decrease of solubility seems to be the same for high and low temperatures and lines are running parallel. The greater the change in the solubility of polymer in liquid phase from the feeding point to the liquid expansion in the particle

collection device, the bigger is the supersaturation ratio. However, it is advantageous to use a low temperature to achieved favourable conditions for supersaturation in a droplet.

In SAS processes, the maximum concentration of formed materials in solute is usually not used because it produces large particles. Fig. 40 shows the calculated solubility of L-PLA in DCM as a function of mole fraction of CO_2 in DCM solute at various temperatures. The solubility of L-PLA in liquid phase decreases as mole fraction of CO_2 increases in liquid phase. Above 0.35 mole fraction of CO_2 in DCM solute the polymer solubility does not decrease significantly. The solubility of polymer in DCM at high mole fractions of CO_2 approaches values of polymer solubility in CO_2 asymptotically. This means that the steepest decreasing of polymer solubility in DCM is achieved before 0.35 mole fraction of CO_2 in DCM. The temperature does not affect much the decreasing tendency of polymer solubility in DCM.

As mentioned before, a maximum L-PLA concentration is usually not used in the SAS process, but typically a 1…5 wt% solute concentration. This means that high mole fraction values of CO_2 in DCM are needed to produce high supersaturation rates. Figure 40 shows that over 0.8 mole fraction of CO_2 in solvent is needed to obtain a high supersaturation because the low initial concentration of solute concentration in droplet.

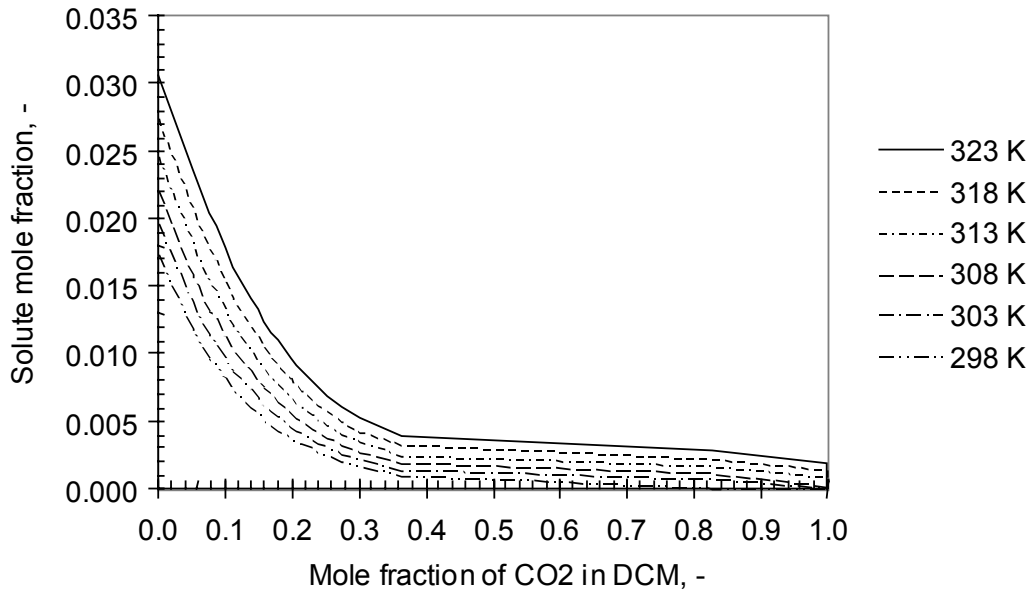

Fig. 40. *The calculated solubility of L-PLA in dichloromethane (DCM) as a function of mole fraction of CO_2 in DCM at various temperatures by using Peng-Robinson equation of state [92].*

4.6.4. DISCUSSION OF DROPLET PROPERTIES

In particle formation, it is sometimes advantageous to produce a supersaturation ratio as large as possible. For example if very small particles and a narrow distribution is needed a high supersaturation is necessary. The volumetric expansion and decreasing of density is more rapid for small droplets than for bigger droplets. In this case it will be possible to produce a high rate of nucleation and a high overall growth rate. The problem is that in the typical range of process parameter values for the SAS process (temperature, pressure and flow rate) it is not possible to largely adjust the initial droplet size with similar nozzles. In particle formation by SAS technique it is advantageous to use low temperature and high pressure, where the mass transfer effect and volumetric expansion of are favourable and the supersaturation is high as well. Not in all cases a high supersaturation is useful. When bigger particles or broad distributions are wanted, the SAS process can be operated at different saturation conditions. This is one of the advantages of this process.

5. SPECIAL APPLICATIONS OF CRYSTALLIZATION FROM CO_2

In this thesis two special applications of supercritical precipitation techniques are shown. Amorphous pharmaceutical particle production by supercritical antisolvent precipitation (SAS) [55] and selective extraction/crystallization of cholesterol from supercritical CO_2 [189] are presented. The later crystallization process is not antisolvent technique, but it is an interesting way to produce pharmaceutical product where no liquid solvents are needed.

5.1. PRODUCTION OF AMORPHOUS PHARMACEUTICAL PARTICLE

In this part of thesis, amorphous pharmaceutical particle production with supercritical fluids is presented [55]. The absorption rate of a pharmaceutical depends on the crystal structure of the drug. Amorphous materials are known to dissolve more rapidly than crystalline substances [97]. Therefore, the observation that it would be possible to produce controlled amorphous particles repeatedly would be significant. Perrut et al. [190] have presented the review of the results already published in literature and their own results on morphology changes and stability of particles generated by SCF processes.

The objective of our work was to develop a method to produce amorphous sodium cromoglycate with a narrow particle size distribution and in controlled particle form. Sodium cromoglycate is an anti-allergic agent, which is given by inhalation in the prophylactic control of asthma, and by nasal insufflation in the treatment and prophylaxis of allergic rhinitis. It acts mainly by inhibiting the release of inflammatory mediators [191]. A multi-purpose, easily transformable laboratory-scale equipment was constructed. Particles were prepared by using the SAS particle precipitation technique. Completely amorphous particles were obtained by spraying a methanol solution of sodium cromoglycate into supercritical carbon dioxide.

5.1.1. METHODS OF SODIUM CROMOGLYCATE PRECIPITATION

Sodium cromoglycate was obtained from Orion Corporation Fermion with the purity of at least 98%. Sodium cromoglycate is soluble in water, sparingly soluble in methanol and practically insoluble in ethanol and acetone. The molecule structure indicates (see Appendix II) that sodium cromoglycate does not dissolve in supercritical CO_2. It was tested in a variable volume view -cell apparatus (see Chapter 3.1). No dissolution of sodium cromoglycate in methanol modified CO_2 was observed. More details of the solubility results have been reported in our article [55].

The laboratory scale semicontinuous SAS apparatus is shown in Chapter 4.2.2 and in paper [55]. The vessel was warmed up and pressurized with CO_2. The CO_2 flow was calibrated with a gas meter. The solution of sodium cromoglycate in methanol was pumped together with CO_2 into the vessel where the precipitation

took place. The CO_2 ran continuously through the precipitation vessel carrying along methanol. The flow was led to the solvent collection vessel. After collecting precipitated particles for a pre-set time, the flow of the sodium cromoglycate solution was stopped and pure CO_2 was pumped through the vessel. By doing this methanol was partially rinsed from the particles. After the precipitation the particles were collected from the vessel and placed into an oven to dry for at least 20 hours in 378 K.

45 experiments were carried out. The process conditions were varied in these limits:

- solution flow 0.2–0.75 ml/min
- portion of water in methanol 0–6.0 wt-%
- CO_2 flow 11–15 ml/min
- pressure 100–200 bar
- temperature 313–346 K
- concentration of solid in methanol solution 2.5–7.5 mg/ml
- particle collection time 45–140 min
- rinsing time 40–80 min

A rough measurement of particle mean size and size distribution was done with Scanning Electron Microscopy (SEM). The particle fine structure was observed with High Resolution SEM. Crystallinity and crystal form was determined with X-Ray Powder Diffraction (XRPD) analyses in Orion Pharma. Purity was analyzed with High Pressure Liquid Chromatography (HPLC). The compounds were detected at 200-400 nm by a HP diode array UV-detector. Residual methanol in the particles was analyzed by Gas Chromatography with flame ionization detector.

5.1.2. RESULT AND CONCLUSION OF SODIUM CROMOGLYCATE PRECIPITATION

Paper [55] shows the result of sodium cromoglycate precipitation. Both crystalline and amorphous samples were obtained, and the results were successfully repeated. Fig. 41 shows one XRPD pattern diagram containing the curves of reference sample, the original raw material sample (Original) and one crystalline (KROL 41) and one amorphous (KROL 39) sample. The reference tells how close the curves of the samples are to the crystal form of the market product. The curve of the crystalline sample resembles the curve of the reference sample so closely that it is justified to classify them to the same polymorph class. The curve of the amorphous sample indicates complete amorphism.

The most significant parameter affecting the crystallinity was the residual methanol concentration in the particles. It could be reduced by adding a small amount of water into the methanol solution of sodium cromoglycate prior to pumping the solution to the precipitation vessel. The results varied in these limits:

- weight of collected particles 5 to 200 mg
- weight decrease in oven 2 to 70%

- crystallinity from amorphous to moderately crystalline
- size of particles 0.1-20 μm.

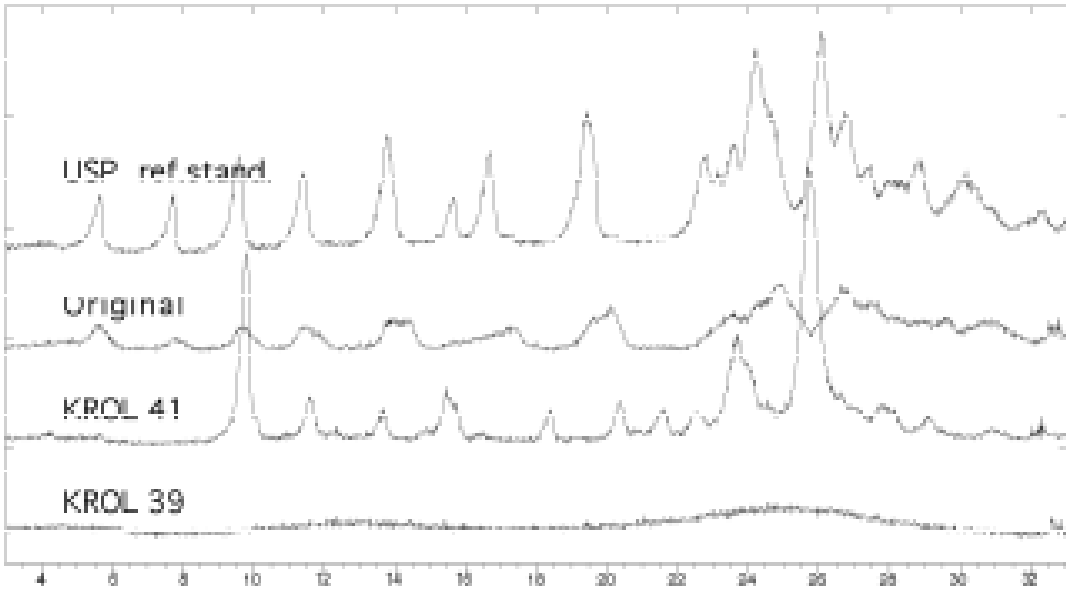

Fig. 41. *XRPD patterns of sodium cromoglycate samples [55].*

The experiments were made by letting the CO_2 stream to flow through the inner tube of the nozzle and the solution stream through the outer tube, and also in the opposite way. The order in the nozzle did not cause discernible transition in crystallinity. The HPLC analysis showed no impurities in the final product. The amorphous products did not show any crystallinity after five months' storage. More details concerning the particle form of produced sodium cromoglycate is presented in paper [55].

5.2. SELECTIVE CRYSTALLIZATION OF CHOLESTEROL

Cholesterol is used as one of starting materials for a number of semisynthetic steroid drugs, for examples vitamins D, sex hormones and corticosteroids. Important natural sources are the spinal cord of cattle, wool grease and egg yolk. Conventional separation methods include extraction with petroleum ether and recrystallization from alcohols. The purpose of the work [189] was to find out, if it is possible to extract industrially viable lipid matrices with supercritical CO_2 and then selectively precipitate cholesterol from the extraction flow. The phase behaviour of model system cholesterol/triglyceride/CO_2 - was studied in a static variable volume view cell (VVV –cell). Various non-bovine lipid raw materials were extracted with supercritical CO_2 and the extract fractionally precipitated in attempts to crystallize cholesterol.

5.2.1. METHODS OF CHOLESTEROLS PRECIPITATION

Static solubility measurements and preliminary precipitation studies of cholesterol/C20-iso-cholesretol/triglyceride/CO_2 were carried out in a static variable volume view cell. In Appendix II the structure of cholesterol, C20-iso-cholesterol and tripalmitin are shown. VVV-cell has been described in detail by Laitinen and Jäntti [137] and as well in Chapter 3.1. More details concerning the solubility methods is presented elsewhere [189].

The consecutive dissolution/crystallization studies were done using a flow system depicted in Fig. 42. A batch of cholesterol containing lipid material was placed in a pressure vessel and CO_2 was continuously pumped through it. The fluid from the extraction vessel was continuously led to another vessel, equipped with a window for observing the precipitation phenomena. The windowed cell was kept at lower temperature and/or lower pressure than the extraction vessel. The pressure in the precipitation vessel was controlled with a vibrating back pressure regulator. The flow from the precipitation vessel was led through the back pressure valve into extract collection vials. The cholesterol concentrations of the materials collected in the crystallization cell and in the extract collection vials were analyzed. More details concerning cholesterol analysis are presented elsewhere [189].

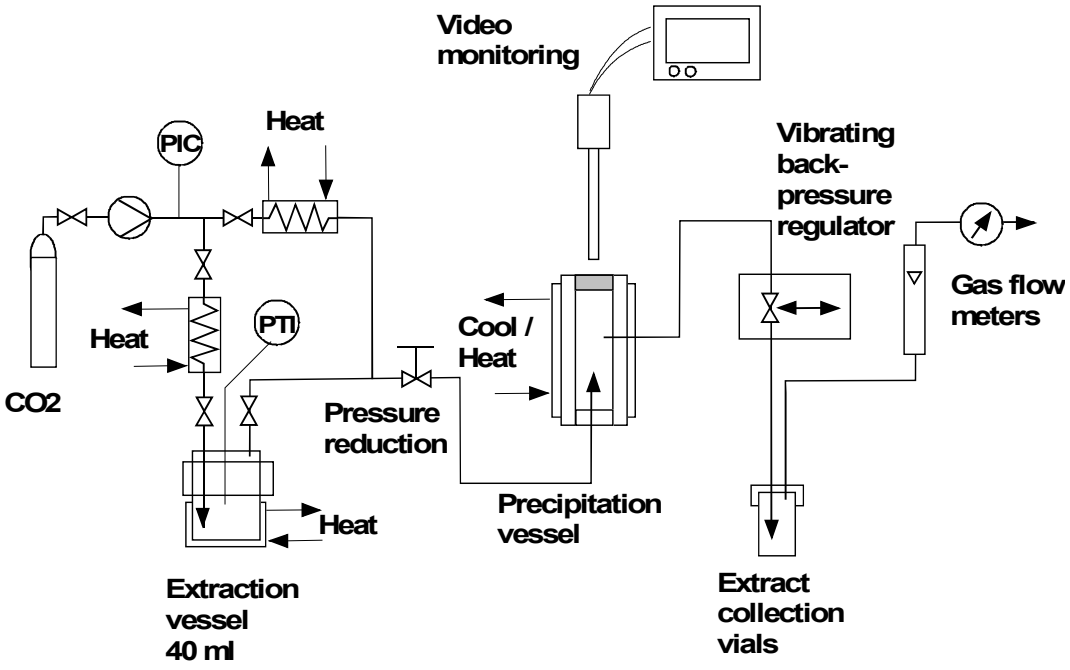

Fig. 42. *The experimental set-up for studying the extraction/fractional precipitation of lipids in a semibatch flow system [189].*

Four cholesterol containing lipid materials were extracted with supercritical CO_2 and the extract flow depressurized and/or cooled to achieve fractional precipitation and crystallization. The materials used were:

1) distilled woolwax alcohols from Croda (34 w-% cholesterol and 20 wt% isocholesterol)
2) egg yolk powder from Källbergs Industry (total fat min. 61 % of which approx. 5 % cholesterol
3) egg yolk powder extract (obtained with ethanol and dichloromethane, the extract contained about 5 wt% cholesterol)
4) phospholipid concentrate from egg yolk from Belovo (85 wt% phospholipids, 10 wt% triglycerides and 5 wt% cholesterol)
5) the cholesterol was from Merck and tripalmitin from Fluka.

5.2.2. CHOLESTEROL CRYSTALLIZATION RESULTS

The solubility of cholesterol in pure CO_2 and in CO_2 saturated with either tripalmitin (1 part cholesterol / 2 parts tripalmitin) or egg yolk oil (5 % cholesterol) is shown in our article [189]. Although cholesterol has affinity to triglycerides in supercritical CO_2, the static solubility results in this study do not indicate any significant increase of cholesterol solubility in CO_2 when it is modified with triglycerides. In carefully controlled conditions cholesterol crystallized from the one phase fluid mixture as fine needles by temperature and/or pressure reduction.

The results of the extraction/precipitation flow experiments with four starting materials are summarized in Table XVIII.

Pure, crystallized cholesterol was obtained by extracting an egg yolk phospholipid concentrate at sufficient pressure 50 MPa and 353 K to obtain at least 0.5 g cholesterol/kg CO_2 concentration in the fluid stream, and then cooling the fluid stream close to ambient temperature with simultaneous pressure reduction to 9-12 MPa. No solid precipitates were obtained when using egg yolk powder as starting material, probably because cholesterol content in this material is too low so that a sufficiently high cholesterol concentration in CO_2 could not be achieved.

We did not obtain pure cholesterol crystals despite of high cholesterol content of the distilled wool wax alcohols. The precipitation product apparently contains other sterols (e.g. lanosterol), which, along with the other constituents, prevent selective crystallization of cholesterol.

Table XVIII *Extraction and precipitation conditions and results from the semibatch flow experiments. Abbreviations: CHO is cholesterol, PL is phospholipid and TG is triglycerides [189].*

Exp.	Extraction conditions					Precipitation conditions			
	p max	T max	CO_2 flow	Solutes in CO_2	Cholesterol in CO_2	p	T	Visual observation of the precipitate	CHO in precipit.
No	MPa	K	g/min	g/kg CO_2	g/kg CO_2	MPa	K		wt-%
Egg yolk phospholipid concentrate, 85 % PI, 10 % TG, 5 % cholesterol									
1	50	353	1.6-4.8	6 -> 2	2 -> 0.7	20 -> 12	325 -> 303	**white needles**	100
2	40	350	7.2-8.4	2 -> 0.4	0.7 -> 0.1			no precipitate	
3a	50	361	3.7-1.4	2	0.7	14 -> 12	308	very slight precip.	
3b	50	361	1.8-0.4	1 -> 0.6	0.7 -> 0.5	9	301 - 304	**white needles**	100
4	50	358	3.2-4.1	1 -> 0.3		40	298 - 299	no precipitate	
Egg yolk powder, lipids > 61 %, 5 % cholesterol of lipids									
5a	45	367	4.3 - 2.7	5 -> 2	0.2 -> 0.1	7 -> 15	295 -> 288	oily	
5b	45	369	2.2	0.6	0.02	25 ->11	325 -> 286	oily	
6	50	356	2.3	11 ->2		40	294 -> 296	no precipitate	
Etract from egg yolk powder, 6 % cholesterol									
7a	44	365	2.0	8 -> 17	0.8	40	296	slight, needle -like	
7b	40	358	3.2 - 1.5	8 -> 2	0.6 -> 0.1	40	309 -> 296	oil droplets	
Distelled woolwax alcohols, 54 % cholesterol									
8	30	353	1.0	36	7	20 -> 16	313 -> 306	very slight precip.	35
9	30	354	1.2	27	7	17	314 -> 310	abundant, waxy	55
10a	50	369	2.9 - 2.4	32	11	12	294	abundant, two fract.	45/72
10b	50	363	2.1 - 1.9	17		13	291 -> 282	abundant, waxy	48
11	45	343	1.3	7 -> 13		40 - 45	294	abundant, waxy	
Cholesterol concentrate from distilled woolwax alcohols, 74 % cholesterol									
A residue from extraction by CO_2 at 13 MPa and 293 K									
12	45	355				12 -> 9	296 -> 284	white, waxy mass	37 - 68

5.2.3. CONCLUSIONS OF CHOLESTEROL CRYSTALLIZATION

The cholesterol can be selectively crystallized, at high purity, from a one-phase mixture, which contains lipids and cholesterol dissolved in pressured CO_2. The successful extraction/crystallization requires, that the concentration of cholesterol in CO_2 is adequate, the crystallization temperature and pressure are correct and there are no other sterols or other similar compounds present. The choice of conditions in the crystallization vessel is critical. The egg yolk phospholipid concentrate (containing about 5 % cholesterol) was the most suitable raw material for the tested method. Pure 100 % cholesterol was obtained directly from this raw material by using one extraction/crystallization sequence.

Because the concentration of cholesterol in the fluid stream is only 0.5 g/kg CO2, this method is not viable industrially in an economic way. However, this simple extraction/fractional precipitation process is interesting technique for producing pharmaceutical products where no liquid solvents are needed. Further development of the cholesterol crystallization process requires a more systematic determination of the phase behaviour of lipid matrices, cholesterol and supercritical CO_2, the determination of crystallization kinetics and the development of equipment for catching and separating the cholesterol crystals from supercritical CO_2 fluid flow.

6. THE SAS PARTICLE PRODUCTION PROCESS; THEIR ENGINEERING AND ECONOMICS

In this part of the thesis estimation of capital costs of a Supercritical Antisolvent (SAS) Particle Production Process [192] and a cost study of this type of plant [193] are discussed.

A limited number of papers have been published on the economic issues of supercritical fluid processes [194,195,196,197,198,199,200,201,202] compared to the number of papers on scientific principles. A common belief seems to be that supercritical fluid technology is more capital intensive than alternative, conventional techniques and the dense gas antisolvent precipitation processes are best suited to the specialty chemicals industry, where the market value of the products may be from hundreds to tens of thousands of Euro per gram. An annual production rate of some of these compounds may be in the order of 100 - 2000 kg per year [194], which means that the antisolvent mass flow would be 20 - 900 kg/h under the conditions, which we have been used in the base case of this work. With such production rate the SAS process would be pilot scale compared with the typical size of conventional processes in the chemical industry. A classification of supercritical extraction units based on size is shown in Table XIX [202].

Table XIX *A classification of supercritical extraction units based on size* [202].

	Extraction vessel volume (dm^3)	Design pressure (MPa)	Use
Laboratory units			
Bench-scale	0.2-0.5	< 40	Screening test
Research-scale	2-10	< 100	Enable quantity and quality analyses, required in optimization
Pilot-scale	200-100	< 70	For scale-up purposes recommended for use with new products
Medium scale unit	20-800	< 80	Production plant (spices and herbs)
Large-scale unit	even 5000	about 30	Production plant (decaffeination of coffee, for tobacco)

However, it may be more economical to invest capital in a larger antisolvent precipitation process and operate it as a multi-purpose unit for several products [194]. Therefore, we examined a considerably larger SAS process in this work. The SAS process equipment sizes, mass flows and energy consumption depend on the running time, production rate, concentration of solute, amount of CO_2 per

solute, the yield of the micronized material etc. Furthermore, the costs may drastically change according to the type of equipment, instrumentation and automation.

The aim of our work [192] was to develop a quick calculation tool for estimating the total battery limits capital costs of a SAS process. A further aim was to study the effect of production rate and feed concentration on the capital cost. In addition the aim was to develop a cost calculation tool and to study the micronization costs of particles in a large semi-continuous supercritical antisolvent precipitation process [193].

6.1. LARGE SCALE SAS PARTICLE PROCESS

Complete plants using compressed fluid technology are available from several companies [203], for example in Europe SEPAREX, Chematur Engineering AB and Natex. High-pressure components, laboratory scale and pilot equipment are available from Sitec Sieber Engineering AG [204]**.** In the year 2000 more than 70 supercritical fluid plants in pilot or industrial scale had been working on many applications and products [196]. This includes also some pilot-scale GMP particle precipitation equipment [205]. In addition, a development companies exist which possess proprietary formulation and particle design technologies with supercritical fluids, for example Lavipharma Corporation [206] and Thar Technologies [207]. Nektar Therapeutics [208] help pharmaceutical and biotechnology partners realize the full potential of their molecules by solving complex development challenges to create breakthrough therapeutics, extend product franchises, and fuel product pipelines.

Reverchon et al. [209,210] have been published papers on the pilot or large-scale supercritical fluid precipitation. They presented, that the SAS process has been performed prevalently in laboratory scale apparatus. Therefore, process limitations that are significant on the large scale, have not been studied yet. These limitations may even lead to the failure of translating the process into a commercial dimension. Further Reverchon et al. present, that the change of nozzle arrangement and diameter from the laboratory to the pilot scale does not affect significantly the particle size and distribution. Muher et al. [211] aim to analyze the effect antisolvent addition rate and initial solute concentration on product quality, and to verify the possibility of scaling-up the process. Changing the initial solute concentration at constant antisolvent addition rate yields populations of particles, whose particle size distributions are qualitatively identical and quantitatively not very different. This shows that on the contrary to the antisolvent addition rate, initial solute concentration cannot be used effectively to adjust the final product quality.

Jun et al. [205] have presented, that most parts of supercritical fluid drug formulation plants are similar to those used in classical SCF operations such as extraction, fractionation, reactions, chromatography etc. Similarly, equipment such as fluid pumps, heat exchangers, separators, control and relief valves,

instrumentation are identical to those used on earlier plants designed at any scale (lab to pilot and very large commercial scale). Jun et al. [205] focused the characteristics specific to particle design plants:

- Atomization nozzles; a pure geometric scale-up does not work.
- Particle collection and harvesting; this is probably the most acute problem, when very fine particles (below 5 μm) are formed, because they have to be collected without losses and without re-agglomeration.
- Fluid recycle; most organic solvents are volatile and the total separation from the fluid is not possible, if operated at a pressure permitting an easy fluid recycling (a few tens of bars).

Some continuous precipitate separation techniques was described [194,212,213] in laboratory scale. A truly continuous antisolvent precipitation process, that allows a continuous removal of precipitate from a pressurized vessel on a production scale, has not yet been development [194].

Jun et al. [205] have presented an equipment design for supercritical fluid micronization in compliance with GMP for pharmaceutical applications. They have presented some equipment requirements:

- Safety, which is obtained by applying the high pressure vessel and equipment standards enforced in the country of operation, but also by incorporating the constructor know-how on both hardware and software (process control system)
- Reliability as for all industrial system, demanding the right choice of all components and a sophisticated control system to help operation, mean while a preventative maintenance is applied.
- Manufacture, design, construction and operation shall be in compliance with GMP rules, specifically to equipment used for drug formulation either for clinical lots preparation etc. For example for GMP compliance a special difficulty is related to cleaning of high pressure systems that must be designed to permit a total cleaning without dismounting all tubing's and vessel; for example no dead volumes are allowed, draining points are needed for liquid solvent used for cleaning.
- The operator wishes to benefit of a great flexibility, permitting to operate one particle design process over the wider range of parameters (pressure, temperatures, flow rates, co-solvents etc.), which dramatically complicates the task of the designer and constructor.

The conceptual flowsheet of the particle production process discussed in more detail in this chapter is shown in Fig. 43.

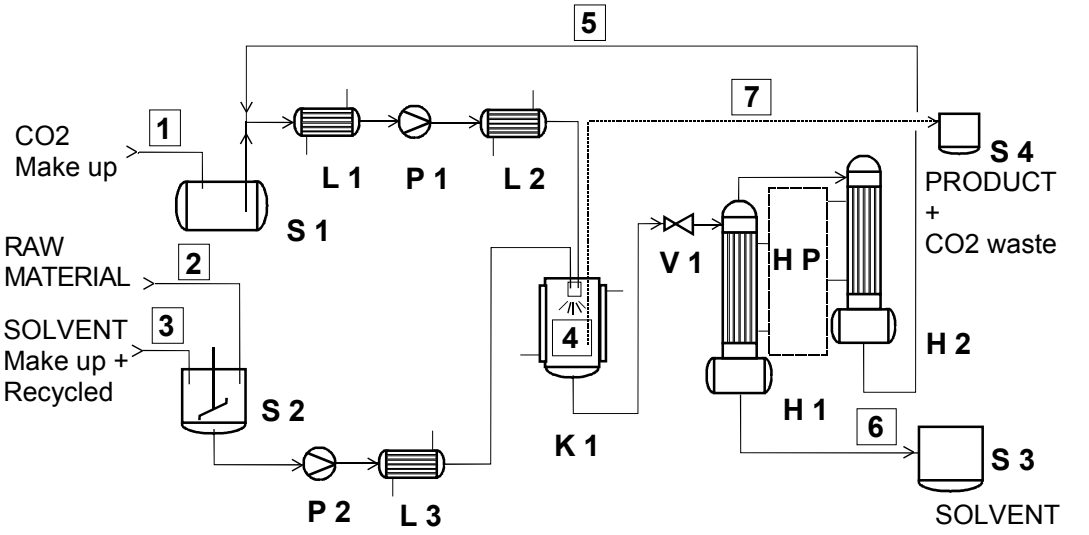

S 1 Feed tank, CO2	L 1 Cooler, CO2	P 1 Pump, liquid CO2
S 2 Mixing tank, solvent/raw material	L 2 Heater, CO2	P 2 Pump, solution
S 3 Solvent receiver tank	L 3 Heater, liquid	V 1 Pressure reducer
S 4 Product receiver	H 1 Evaporator, CO2/liquid	K 1 Precipitation vessel
	H 2 Liquefier, CO2	H P Heat pump

Fig. 43. *Conceptual flowsheet of the particle production process [192].*

In the example process [192] the CO_2 stream is cooled (L1) to 5 °C, compressed (P1) to process pressure 100 bar, heated (L2) to process temperature 40 °C, and led together with the solution stream into the precipitation vessel (K1). In this case, two units K1 and K2 are used alternatively. Raw material is mixed with solvent in the mixing tank (S2) and pumped (P2) via heater (L3) into the vessel where the precipitation takes place. CO_2 and solvent are led through pressure reducer (V1) into the evaporator (H1). In this unit, CO_2 is separated from the solvent and then recycled via the liquefier (H2) in 14 °C and 50 bar back to feed the tank (S1). The produced particles are recovered semi-continuously through the bottom of the precipitation vessel (S4). From solvent receiver tank (S3) the solvent is distilled and recycled back to the mixing tank (S2). Energy consumption in CO_2 evaporation and liquefaction system is reduced by connecting the operations with a conventional heat pump (HP). The maximum operating pressure of CO_2 feed tank, evaporator and liquefier is 70 bar. The operating pressure of the other high-pressure units is 250 bars. Solvent/raw material mixing tank, solvent receiver and product receiver tanks are in atmospheric pressure. The maximum operating temperature is 70 °C.

The required size of the major equipment at different production rates is calculated from mass and energy balances. The ratio of CO_2 to solvent has an effect on the size of equipment and raw material mass flows. In this scheme, the CO_2 per solvent ratio is 20 kg/kg, which is commonly used in SAS techniques. The filling factor of CO_2 tank and solvent/raw material mixing tank is 70 %. The overall heat-transfer coefficient of CO_2 cooler, CO_2 heater, liquid heater, CO_2 evaporator and liquefier is estimated as 300 W/m^2 °C. The size of CO_2 feed tank S1 corresponds to 10 min production time and the size of solvent/raw material

mixing tank S2 and product receiver S4 corresponds to 8 h of production time. The precipitation vessel is depressurized and emptied twice a day. The yield of product from feed is 90 %. CO_2 loss is 3 % of circulation and the loss of solvent is 1 % of precipitation process circulation and 3 % of regeneration distillation. The CO_2 pumping energy requirement is calculated from the change of enthalpy assuming that the temperature difference of CO_2 between inlet flow and outlet flow is 10 °C. The pump and the heat pump mechanical efficiency is assumed to be 80 % and that of liquid pump 90 %.

The mass flows and energy consumptions were calculated using MS Excel spreadsheet. The density, entropy and enthalpy of CO_2 were calculated using a DLL-module, programmed with Fortran. The properties of CO_2 were calculated using correlations from the IUPAC thermodynamic tables [75].

The mass flows and energy consumption of the SAS example process are presented in Table XX [192]. The mass and energy flows correspond to those of a large scale SAS precipitation process. In this example, the production rate is 4500 kg/year, running time 975 hours/year, concentration of solid in solvent 5 wt% and CO_2 / solvent ratio 20 kg/kg. It can be seen that the size of a SAS process resembles more a pilot-scale unit than a typical process in the chemical industry.

Table XX *The mass flows and energy consumptions of a large scale SAS precipitation process. In this example, the production rate is 4500 kg/year, running time 975 hours/year, concentration of solid in solvent 5 wt% and CO_2/solvent ratio 20 kg/kg. The flow numbers are same as in Fig. 43. [192].*

Flow	1	2	3	4	5	6	7
Temperature, K	293	293	293	313	387	303	393
Pressure, MPa	5.7	0.1	0.1	10.0	5.0	5.0	0.1
Total mass flow, kg/h	67.8	5.1	97.4	2089	1919	106	64.1
CO2, kg/h	67.8	0	0	1949	1881	9.6	58.2
Solvent, kg/h	0	0	97.4	135	37.6	96.1	1.3
Product material, kg/h	0	5.1	0	5.1	0	0.5	4.6

Description	Tag no	Power	
Cooler, CO2	L1	29	kW
Heater, CO2	L2	31	kW
Heater, liquid	L3	1.3	kW
Pump, liquid CO2	P1	42	kW
Pump, solution	P2	0.4	kW
Evaporator, CO2/solute	H1	70	kW
Liquefier, CO2	H2	97	kW
Heat pump	HP	34	kW

6.2. CAPITAL COST ESTIMATION

The battery limits plant comprises of equipment and systems directly associated with operation. The capital costs of chemical plants can be estimated from the purchased cost of major equipment using factorial or exponential methods [214]. These methods are used in initial feasibility studies and for choices between design alternatives. The potential accuracy of methods is ±30 to 40 %.

Single factor methods collect the various items of expenditure into one factor, which is usually used to multiply the total cost of delivered equipment to give the fixed-capital cost for plant within the battery limits. This so called Lang factor includes for example equipment erection, piping, instrumentation, electrical and utilities. The typical value of Lang factor for fluid processing is 4.8 [214].

An other way to estimate the plant capital cost is to use the known cost of the same process but with different capacity and to scale the costs using capacity exponent expression method (49).

$$CE_2 = CE_1\left(\frac{SC_2}{SC_1}\right)^n \tag{49}$$

CE_2 is the capital cost of equipment or process with capacity SC_2 and CE_1 is the capital cost with capacity SC_1. The value of exponent n depends on the type of equipment. Typical capacity exponents for equipment are given in chemical engineering handbooks. The scaling exponent n is usually between 0.5 and 0.85. As a rule-of-thumb 0.6 - 0.7 is often used for scaling the cost with plant capacity [214].

A calculation tool was developed for estimating the capital costs of a semicontinuous supercritical antisolvent precipitation process (SAS). The battery limits capital costs were calculated as a function of CO_2 mass flow in two independent ways:

1) by scaling the equipment cost using an exponent appropriate for each equipment type and
2) by fitting the exponent of the total plant cost scaling equation to plant costs known from previous projects.

The main capital costs of a SAS processes consist of antisolvent recycling equipment like in an industrial supercritical fluid extraction plant: CO_2 tank, CO_2 pump, evaporator and condenser [192]. Figure 44 shows the total battery limits capital cost of SAS precipitation process as a function of CO_2 mass flow at production rate from 1000 to 8000 kg/year, when the reference cost is based on an industrial supercritical fluid extraction plant. The total battery limits cost versus CO_2 flow was fitted to data obtained from Chematur Engineering [215] and from Separex [196,197]. The reference point (0.95 million € and CO_2 flow 2160 kg/h) is from Clavier et al. [197], who presented an economical estimation of an industrial supercritical fluid extraction plant. Their data is used in the capacity

exponent equation (50) for the total battery limits capital cost of the SAS precipitation process. Once the reference point was fixed we fitted the exponent was fitted so that the cost/CO_2 curve went through both of the known cost points. The best fit was obtained with capacity exponent 0.7. The cost equation is then:

$$BC = 0.96 * \left(\frac{m_{CO2}}{2160} \right)^{0.7} \tag{50}$$

where BC is the total battery limits capital cost (million Euro) and m_{CO2} is the recycled CO_2 flow (kg/h).

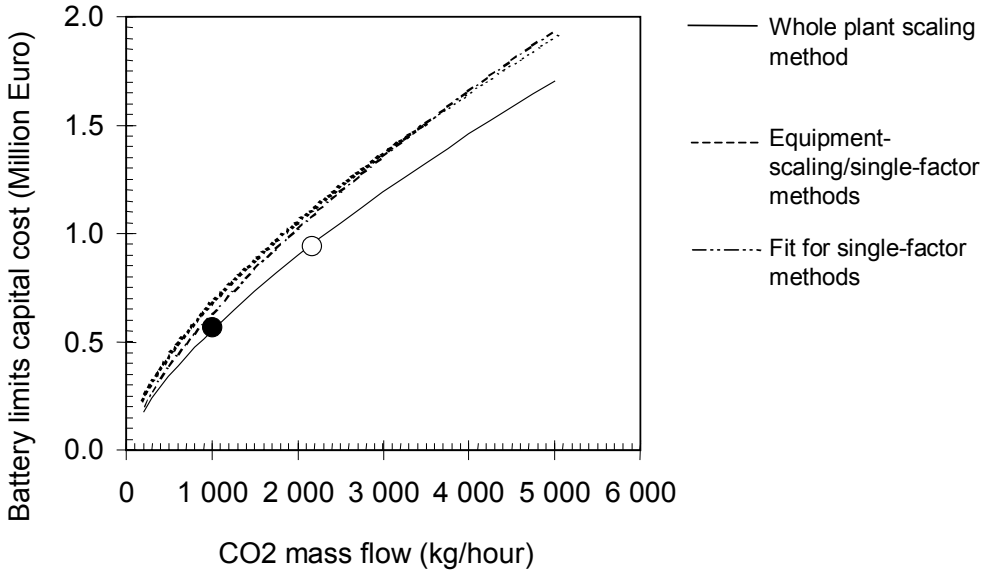

Fig. 44. *Total battery limits capital cost of SAS precipitation processes as function of recirculated CO_2 mass flow [192]. Comparison of costs calculated by different methods (see text). Reference points: white bullet [197] and black bullet [215].*

The battery limits capital costs calculated by the equipment capacity exponent scaling / single-factor method and by the whole plant capacity exponent method were almost equal. Figure 44 also shows a capital cost curve calculated using the result of the single-factor example case (Table XX) as reference point and using exponent 0.7 for scaling the whole plant cost with CO_2 flow.

We have shown earlier [192] that the battery limit capital cost of a SAS process can be estimated from the cost of a process of certain CO_2 mass flow by multiplying the known capital cost with the CO_2 mass flow ratio of the two processes raised to the power of 0.7. The capacity exponent cost equation is then:

$$BC_2 = BC_1 * \left(\frac{G_{2,CO2}}{G_{1,CO2}} \right)^{0.7} \tag{51}$$

where BC_i is the total battery limit capital cost and $G_{i,CO2}$ is the CO_2 mass flow for the process i. Estimation of the SAS process battery limit capital costs based on the CO_2 mass flow is more reliable than using the production rate, because the total battery limits capital cost is sensitive to the feed concentration (see Chapter 6.3).

The problem of using the capacity exponent method Eq. (50) for calculating the plant cost is that capital cost information is needed for a plant with a reference capacity. Capital cost estimations for industrial scale supercritical fluid extraction plants have been presented in literature, but there are only few data available in the literature for economic evaluation for a special plant such as the SAS [192,194,198]. Rantakylä et al. [192] presented how the total battery limit cost of a SAS process depends on the CO_2 flow rate for an industrial supercritical fluid extraction plant. The comment of a commercial supercritical fluid plant producer at the 4th International Symposium on High Pressure Technology and Chemical Engineering was, that they believed that capital cost of the plant presented in the publication [192] would be 2.0 ± 0.3 millions Euro plus the profit of the plant supplier and the cost of GMP compliance, which is at least + 25 %. Our estimate based on equipment costs and Lang factor 4.8 was 1.05 millions Euro [192].

Figure 45 shows the total battery limit capital cost of SAS precipitation process as a function of CO_2 mass flow at production rate from 1000 to 8000 kg/year based on two different reference points representing different types of processes. The broken line (0.95 million Euro and CO_2 flow 2160 kg/h) is for an industrial supercritical fluid extraction plant presented by Clavier et al. [197]. The solid line (2.5 million Euro and CO_2 flow 1719 kg/h) stands for a known cost of GMP compliance. In both cases the scaling exponent is 0.7

Fig. 45 shows the area between the solid and broken lines, where the total battery limit capital cost of SAS precipitation processes lies. The solid line correspond to the total battery limit capital cost of a SAS precipitation processes complying GMP regulations. It seems to be closer to feasible cost of a SAS precipitation processes than broken line, which is calculated from supercritical extraction plant data GMP process.

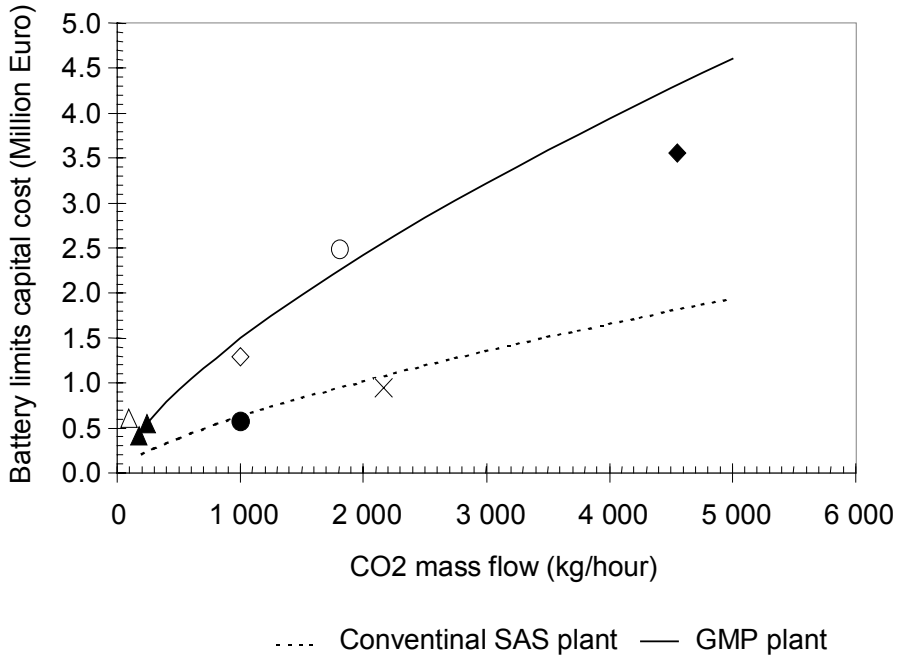

Fig. 45. *Total battery limit capital cost of SAS precipitation processes by using a capacity exponent function (Eq.49). Reference points: broken line and asterisk Clavier et al. [197] and solid line and white bullet from with a commercial supercritical fluids plant producer (see text). Others data: black square [201], white square [198], black bullet [215], black triangle [215] and white triangle [194].*

In this work the estimated total battery limit capital cost of the SAS precipitation process complying with GMP regulations is quite equal to that given by Weber et al. [198]. They estimated the investment cost of a PCA plant to be 1.26 Million Euro with CO_2 mass flow 1000 kg/h (see Fig 45; white square). The plant consists of four vessels, a crystallizer (volume 250 l/max 150 bar), a separator (250 l/ max 80 bar), a solvent recovery tank (260 l/1 bar) and an antisolvent storage tank (500 l/max 100 bar).

6.3. COST STUDY OF SAS PARTICLE PRODUCTION PROCESS

Rantakylä et al. [193] have presented a cost study of a Supercritical Antisolvent (SAS) Particle Production Process. The aim of this work was to develop a cost calculation tool and to study the micronization costs of SAS. Battery limit capital costs were estimated by a capacity exponent method with an exponent appropriate for each type of equipment. The battery limits capital costs and operating costs were calculated for 1000 to 8000 kg/year production and for 2-10 wt% concentration of the starting material in an organic solvent. The organic solvent and CO_2 are regenerated and recirculated in the process. Costs were calculated for one shift (975 hours/year) and two shift (1950 hours/year) effective production

times. One person/shift is needed. The effective process running time is assumed to be 65 % from total working day and the rest is reserved for start up and shutdown, maintenance, reparation and cleaning time. Employer's labour cost is 42 €/h with taxes and employer's contribution etc. The interest rate of annuity loan is only 6 %, which includes only bank rate. The depreciation time of capital is 10 years. The start up cost is 10 % and design & management cost is 5 % from fixed capital. The rent of premises is 17 Euro/m^2. The cost of raw materials was not considered. More details are presented in paper [193].

In the above example [193] the process cost represented an favorable situation (the low estimated total battery limits capital, one person/shift, the interest rate of annuity loan 6 % etc.). When the production rate is 4000 to 8000 kg/year and the concentration of the starting material in organic solvent is 5-10 wt%, the total micronization cost ranges from around 50 € to 100 € per kg product without feedstock price for a non-GMP SAS micronization process. The manufacturing cost decreases much with increasing raw material concentration in feed solvent, because less solvent and CO_2 volume is needed and the equipment becomes smaller. Paper [193] shows that it is favorable to use over 5 wt% feed concentration. The manufacturing cost difference between one- and two-shift work is small at a same production rate. An effective way to decrease the manufacturing cost is to increase the feed material concentration in solvent. More details concerning the cost structure and manufacturing cost of large scale SAS processes as a function of production rate and feed material concentration are presented in paper [193].

In Figure 46 the micronization cost in large SAS processes is presented as the function of production rate at two different cases. The broken line represents the cost in a more conventional SAS process (such as non-GMP or supercritical solvent extraction plant as in the example above). The solid line represents a GMP and other more challenging SAS process. In the latter case the calculation was made on the following basis: Total battery limit capital cost for a GMP plant (CO_2 flow 1719 kg/h, 2.5 million Euro), two persons per shift, rent of premises 42 Euro/m^2 and the rate of return on capital is 20%.

The area between lines in Fig. 46 shows the manufacturing cost variation of SAS precipitation processes. Line correspond the total battery limit capital cost of SAS processes complying with GMP regulations. In this GMP case the total manufacturing cost will be around 150 € to 200 € per kg product without feedstock price, when the production rate is 4000 to 8000 kg/year and feed concentration 7.5 wt%. A commercial supercritical fluids plant representative commented in the 4th International Symposium on high Pressure Technology and Chemical Engineering in 2002 that, they believe that 200 €/kg is acceptable manufacturing cost for some pharmaceuticals product by SAS techniques. From the results presented by Rantakylä et al. [193] and the Figure 45 we can conclude, that it is favourable to design a process of production rate over 2000-3000 kg/year. Below this production rate, the manufacturing cost increases dramatically.

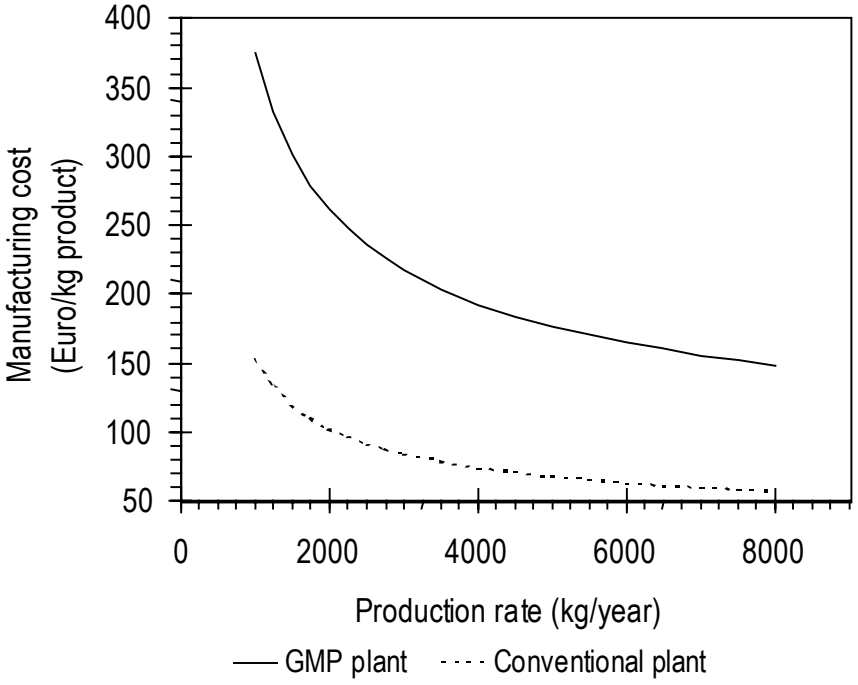

Fig 46. *The micronization cost in a large SAS processes as a function of production rate at two different cases; broken line for more conventional conditions [193] and solid line for GMP and other demanding conditions (see text). The raw material concentration in solvent is 7.5 wt%, one shift needed and effective production time is 975 hours/year.*

Fig. 47 shows the micronization cost structure of a large scale SAS processes as a function of the production rate for GMP and other demanding conditions. In Paper [193] the cost is calculated for more conventional (non-GMP) conditions.

Figures 47 shows that the capital cost is the largest contributor in manufacturing (i.e. micronization) cost (if raw material are not considered). Above 4000 kg/year production rate, the proportion of capital cost in manufacturing cost is nearly constant at constant feed concentration. The proportion of labour decreases with increasing production rates. In SAS technique, the starting material streams are dilute and this means large volumes of solvent and CO_2 are handled. This results to large equipment sizes. A way to reduce the share of capital cost in manufacturing cost is to increase raw material feed at constant raw material concentration and at constant CO_2 flow. In this case, the concentration of organic solvent in CO_2 increases.

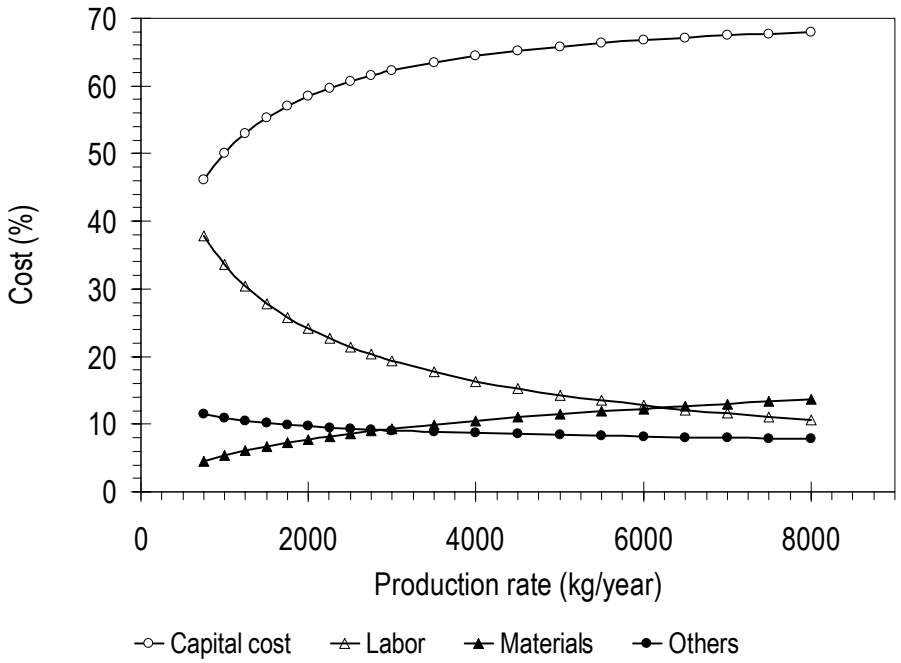

Fig. 47. The micronization cost structure in large scale GMP SAS processes as function of production rate without raw materials. Reference plant CO_2 flow is 1719 kg/h and cost 2.5 million Euro, two people required per shift and return on capital 20%.

Another effective way to decrease the manufacturing cost is to increase the feed material concentration in solvent. Fig. 48 shows the manufacturing cost as a function of feed material concentration in the solvent. The parameters are the production rate and the number of shifts used. The manufacturing cost is estimated for a total battery limit capital of a GMP plant (reference plant CO_2 flow 1719 kg/h and cost 2.5 million Euro), two persons are required per shift and a 20% return on capital is needed. It is not always possible to use a high raw material concentration, because the particle size is increased in the precipitation process. Therefore the optimization of the technology (temperature, combinations of the solvent / antisolvent / product, pressure, flow rates, concentrations etc.) is essential before scale up of the process.

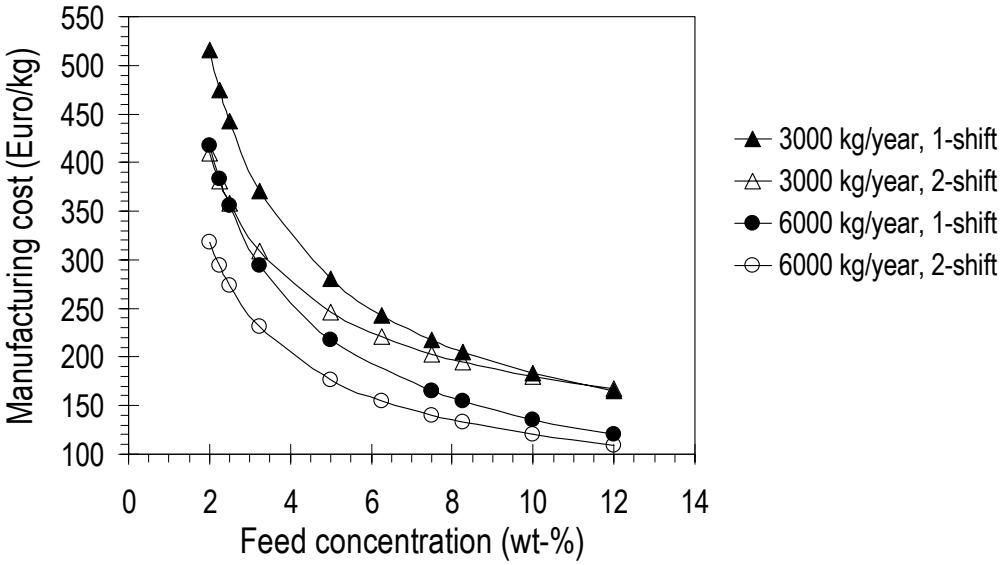

Fig. 48. *Manufacturing costs in large scale SAS processes as a function of feed material concentration and production rate. The manufacturing cost is estimated for the total battery limit capital of GMP plant.*

Presented results in Figure 48 and in paper [193] show that the manufacturing cost decreases much with an increasing raw material concentration in feed solvent, because less solvent and CO_2 is needed. Therefore the equipment becomes smaller. Figures 48 shows that it is favourable to use over 5 wt% feed concentration. However, it is not always possible to use a high raw material concentration, because the particle size is increased in the precipitation process. The 1-shift and 2-shift lines intersect as a function of feed concentration. The intersection point depends on production rate. In GMP plant under 8 % feed concentration 1-shift work is more economical than 2-shift work. Over the 10 % feed concentration of the starting material, the 1-shift work and 2-shift work is almost equally economical.

Weber at al. [198] calculated the processing cost of a production plant for PCA considering the energy consumption needed in the compression and temperature stabilization of vessels, payoff of the equipment and labour costs of the staff. The antisolvent to solution ratio is from 2 kg CO_2/solvent to 3 kg CO_2/solvent, capacity from 125 kg/hour to 250 kg/hour, crystal yield 90%, solid concentration in feed 10 %, operation the batch time 9 hours considering a operating time of 300 days a year and 24 hour/day. Product quantity is from 68 t/year to 117 t/year. They presented, that gas antisolvent crystallization is an attractive process for high quality solid e.g. pharmaceutical products, polymer, cosmetics or nutritional products where demands on low residual solvent content are high and processing costs of 5 Euro/kg to 10 Euro/kg product are acceptable. Those costs are much less than the values calculated in this work (50-300 Euro/kg products) because of the high antisolvent to solution ratio and feed concentration in their study, which means smaller plant and high production capacity.

Also Bertucco et al. [194] evaluated the SAS particle process manufacturing costs. The antisolvent to solution ratio is 15 CO_2/solvent, capacity 0.35 kg/hour, solid concentration in feed 6 %. Then product quantity is 2740 kg/year. Operating time is 330 days a year and 24 hour/day. Three shifts and three employees / year are required. They estimated the fixed capital cost of this SAS processes 0.60 million Euro (see Fig. 44), when the CO_2 mass flow is about 90 kg/h. They showed, that the SAS particle processes would be industrially interesting, when the product price is at least 150-220 Euro/kg for 20% return on capital required before income taxes. This provides an added value of a least 100 Euro/kg over the raw-material price, which they assumed to be 49 Euro/kg. Therefore they concluded that only high-value products can be manufactured through supercritical CO_2 anti solvent processes. The costs shown by Bertucco et al. [194] are less than in this work because higher effective operation time and a smaller plant.

Also in this work it is shown that to recrystallize fine particles with SAS techniques the price of the products must be high, as it is the case with some chemical intermediates and many biological and pharmaceutical compounds. The manufacturing cost is around 50-300 Euro/kg products without feedstock cost, when the production rate is 4000 to 8000 kg/year and the feed concentration of the starting material in organic solvent is 5-10 wt%. On the other hand, if the compound properties are waxy or soft and/or the products are thermally unstable and therefore difficult to process in other ways, the use of continuous gas antisolvent techniques provides a technical advantage in the production of fine particles although the production cost is high.

7. CONCLUDING REMARKS

The thesis discusses the feasibility of the supercritical antisolvent (SAS) particle production process. The specific aims were to study the applicability of the variable volume view cell (VVV–cell) for finding the appropriate combinations of the solvent and the gaseous antisolvent for a given solid, to describe models for the SAS technique and to examine, which factors control particle sizes in the near critical and supercritical regions, to study the applicability of two special supercritical antisolvent precipitation techniques for particle production, to develop calculation tools for estimating the capital and manufacturing costs and to study the cost structure of large scale SAS processes.

A static variable volume view -cell is a useful and fast way to find an appropriate combination of the solvent and the gaseous antisolvent for a given solid. In this work four different pharmaceuticals compounds were examined; nalmefene HCl, oxybutynine HCl, clonidine base and clonidine HCl. Based on the behaviour in the view-cell nalmefene HCl, clonidine base and clonidine HCl appear to be good candidates for particle production with CO_2-antisolvent techniques. Often pharmaceutical materials are expensive and not available in large quantities, which makes the phase separations studies by laboratory or production scale SAS techniques impossible. In VVV-cell experiments it is possible to use small amounts of materials, examine fast with one material re-fillable many recrystallization temperatures, pressures and concentrations. However it is not possible to conclude from the VVV-cell produced particles, what the particle properties such as particle size, size distribution, crystal habit and morphology would be in the SAS technique because of the differences in conditions and residence time in the formation.

The present study showed that the changing of process parameters (temperature, density, pressure, interfacial tension between liquid and gas and velocity of gas) has a small calculated effect on the initial droplet size in the SAS process. The results of the experiments showed that the effect of density of CO_2 and temperature in supercritical state have a greater influence on the particle size than the model of droplets predicts. It was noticed that the model of initial droplet size correlated broadly with the final particle size. The liquid side mass transfer seems to control the particle size.

It is advantageous to use a low temperature and a high pressure, since the mass transfer effect and volumetric expansion of droplets to produce high supersaturation are favourable in these conditions. The effect of temperature on liquid side mass transfer coefficient k_L is competing with the effect of temperature on gas side mass transfer coefficient k_G near the CO_2 critical pressure. Near the CO_2 critical pressure k_L will decrease with increasing temperature and will increase with increasing temperature. To obtain a high value of k_L and k_G there is a compromise in the value of temperature. By using a typical range of process parameter values of the SAS process (for example temperature, pressure, flow rate) it is not possible to largely adjust the initial droplet size with similar nozzles.

Therefore, the mass transfer coefficient of the liquid phase should be maximized to produce a high supersaturation fast.

Supercritical fluid technology is considered an innovative and promising way to design particles. In this thesis, also the applicability of two special supercritical precipitation techniques was studied. In the first case the results show, that it is possible to produce completely amorphous particles by supercritical the antisolvent processing technique by spraying a methanol solution of sodium cromoglycate into supercritical carbon dioxide. The most significant parameter affecting the crystallinity was the residual methanol concentration in the particles. In the second case the results show, that cholesterol can be selectively produced by extraction/fractional precipitation, at high purity, from a one phase mixture, which contains lipids and cholesterol, dissolved in pressured CO_2. The egg yolk phospholipid was the most suitable raw material for the tested method. Because the concentration of cholesterol in the fluid stream is dilute, this method is not viable industrially because of economics. However, this simple extraction/fractional precipitation process is interesting technique to produce pharmaceutical products, where no liquid solvents are needed.

The work clearly demonstrated that to recrystallize fine particles with SAS techniques the price of the products must be high, as it is the case with some chemical intermediates and many biological and pharmaceutical compounds. The manufacturing (i.e. micronization) cost is around 50-300 Euro/kg products without feedstock cost, when the production rate is 4000-8000 kg/year and the feed concentration of the starting material in organic solvent 5-10 wt%. The manufacturing cost was calculated for a GMP plant by first estimating the total battery limit capital cost and operating costs. The manufacturing cost of SAS process is capital intensive. An effective way to decrease the manufacturing cost is to increase the feed material concentration in solvent. It is favourable to design a process with a production rate over 2000-3000 kg/year and to use over 5 wt% feed concentration. Below those values, the manufacturing cost increases dramatically. A way to reduce the share of capital cost in manufacturing cost is to increase raw material feed at constant raw material concentration and at constant CO_2 flow. In this case, the concentration of organic solvent in CO_2 increases. Another effective way to decrease the manufacturing cost is to increase the feed material concentration in solvent. It is not always possible to use a high raw material concentration, because the particle size is increased in the precipitation process. Therefore the optimization of the technology (temperature, combinations of the solvent / antisolvent / product, pressure, flow rates, concentrations etc.) is essential before scaling up of the process.

REFERENCES

1. Sze, T., Dehghani, F., Dillow, A., Foster, N., Applications of Dense Gases in Pharmaceutical Processing, *Proceedings of the 5th Meeting on Supercritical Fluids*, Materials and Natural Products Processing, M. Perrut and P. Subra (Eds.), Tome 1: Materials, Nice, 1998, 263-269.
2. Gallagher, P., Coffey. M., Krukonis, V., Klasutis, N, Gas Antisolvent Recrystallization: *New Process to Recrystallize Compounds Insoluble in Supercritical Fluids*, ACS Symposium Series 406, Supercritical Fluid Science and Technology, K. Johnston and J. Penninger (Eds.), American Chemical Society, Washington, DC, 1989, 334-354.
3. Reverchon, E., Supercritical Antisolvent Precipitation: Its Application to Microsparticle Generation and Products Fractionation, *Proceedings of the 5th Meeting on Supercritical Fluids*, Materials and Natural Products Processing, M. Perrut and P. Subra (Eds.), Tome 1: Materials, Nice, 1998, 221-236.
4. Weber, A., Tschernjaew, J., Kümmel, R., Coprecipitation with Compressed Antisolvents for the Manufacture of Microcomposites, *Proceedings of the 5th Meeting on Supercritical Fluids*, Materials and Natural Products Processing, M. Perrut and P. Subra (Eds.), Tome 1: Materials, Nice, 1998, 243-248.
5. Jung, J., Perrut, M., Particle Design Using Supercritical Fluids: Literature and Patent Survey, *Journal of Supercritical Fluids*, 20(2001) 179.
6. Debenedetti, P., Tom, J., Yeo, S.-D., Lim, G.-B. Application of Supercritical Fluids for the Production of Sustained Delivery Devices, *Journal of Controlled Release*, 24(1993) 27-44.
7. Bleich, J., Kleinebudde, P., Muller, B, Influence of Gas Density and Pressure on Microparticles Produced with the ASES Process, *International Journal of Pharmaceutics*, 106(1994) 77-87.
8. Werling, J., Debenedetti, P., Mass Transfer and Phase Equilibrium in the Supercritical Antisolvent Process, *Proceedings of AIChE 1998 Meetings*, November 15-20. Miami Beach, Florida, 1998.
9. Reverchon, E., Porta, G., Trolio, A., Pace, S., Supercritical Antisolvent Precipitation of Nanoparticles of Superconductor Precursors, *Ind. Eng. Chem. Res.*, 37(1998) 952-958.
10. Randolph, T. Randolph, A., Mebes, M., Yeung, S., Sub-Micrometer-Sized Biodegradable Particles of Poly(L-Lactid Acid) via the Gas Antisolvent Spray Precipitation Process, *Biotechnol. Prog.*, 9(1993) 429-435.
11. Eggers, R., Wagner, H., Jaeger, P., Extraction of Spray-Particles with Supercritical Fluids, *High Pressure Chemical Engineering*, R. Rohr and Ch. Trepp (Eds.), Elsevier Science, Amsterdam, 1996, 247-252.
12 . Steinhagen, V., Bork, M., Koerner, J.-P., Application of Supercritical Fluids in Pharmaceutical Industry, *Proceedings of the 4th International Symposium on High Pressure Technology and Chemical Engineering,* A. Bertucco (Ed.), Venice, Vol. 2, 2002, 235-240.
13. Jessop, C., Leitner, W. (Eds.), *Chemical Synthesis Using Supercritical Fluids,* Wiley-VCH, Weinheim, 1999.

14. Rantakylä, M., Alkio, M., Aaltonen, O., Stereospecific Hydrolysis of 3-(4-methoxyphenyl)glycidic Ester in Supercritical Carbon Dioxide by Immobilized Lipase*, Biotechnology Letters*, 18(1996) 1089-1094.
15. Rantakylä, M., Aaltonen, O., Enantioselective Esterification of Ibuprofen in Supercritical Carbon Dioxide by Immobilized Lipase, *Biotechnology Letters*, 16(1994) 825-830.
16. Aaltonen, O., Enzymatic Catalysis, In: Chemical Synthesis Using Supercritical Fluids, P.G. Jessop and W. Leitner (Eds.), Wiley-VCH, Weinheim, 1999. 414
17. Kamat, S., Beckman, E., Russel, A., Enzymatic Activity in Supercritical Fluids, *Crit. Rev. in Bitechnology,* 15(1995) 41.
18. Aaltonen O., Alkio, M., Lundell, J., Ruohonen, S., Arvinen, L., Suoninen, V., Polypeptide Purification with Industrial-Scale Supercritical Fluid Chromatography, *Pharmaceutical Technology Europe,* 1998.
19. Alkio M., Rantakylä, M., Simulation of Chiral SFC-prosess Using a PC-worksheet Model, Proc. 3rd Int. Symp. Supercritical Fluids, Strasbourg, 1994, Tome 3, 471-476.
20. D'Aquino, R., Pumped up on Nutraceuticals, *Chemical Engineering*, 107(2000), 41-45.
21. Vajdy, M., O'Hagan, *Advanced Drug Delivery Reviews*, 51(2000) 127-141.
22. Elvassore, N., Vezzù, K., Bertucco, A., Cecchi, A., Caliceti, P., Protein Loading in Biodegradable Polymeric Micro-Particles Produced by Compressed Gas Antisolvent Techniques, *Proceedings of the 4th International Symposium on High Pressure Technology and Chemical Engineering,* A. Bertucco (Ed.), Venice, 2002, Vol. 2, 827-832.
23. Wang, Y., Dave, R., Pfeffer, R., Polymer Coating/Encapsulation of Nanoparticles Using a Supercritical Anti-Solvent Process, *The Journal of Suprcritical Fluids*, 28(2004) 85-99.
24. Knez, Ž, Weidner, Precipitation of Solids with Dense Gases, Alberto Bertucco and Gerhard Vetter (Eds.) *High Pressure Process Technology: Fundamentals and Applications,* Elsevier Science, Amsterdam, 2001, 587-611.
25. Miranda, S., Yaeger, S., Homing in on the Best Size Reduction Method, *Chemical Engineering*, 105(1998) 102-110.
26. Matson, D., Petersen, R., Shmith, R., Formation of Silica Powders from the Rapid Expansion of Supercritical Solutions, *Adv. Ceram. Mater.*, 1(1986) 242-246.
27. Matson, D., Fulton, J. Petersen, R., Shmith, R., Rapid Expansion of Supercritical Fluid Solutions: Solute Formation of Powders, Thin Films, and Fibers, *Ind. Eng. Chem. Res.*, 26(1987) 2298-2306.
28. Vasukumar, K., Bansal, A., Supercritical Fluid Technology in Pharmaceutical Research, *Crips*, 4(2003) 8-12.
29. Tom, J., Debenedetti, P., Particle Formation with Supercritical Fluids - A Review, *J. Aerosol Sci.*, 22(1991) 555-584.
30. Thiering, R., Charoenchaitrakool, M., Sze, L., Dehghani, F., Dillow., A., Foster, N., Crystallization of Para-Hydroxybenzoic Acid by Solvent Expansion with Dense Carbon Dioxide, *Proceedings of the 5th Meeting on*

Supercritical Fluids, Materials and Natural Products Processing, M. Perrut and P. Subra (Eds.), Tome 1: Materials, Nice, 1998, 291-296.

31. Weidner, E., Steiner, R., Knez, Z., Powder Generation from Polyethylene Glycols with Compressible Fluids, in *High Pressure Chemical Engineering*, R. von Rohr and Ch. Trepp (Eds.), Elsevier Science, 1996, 223-228.
32. Weidner, E., Knez, Z., Novak, Z., PGSS (Particles from Gas Saturated Solutions) - a New Process for Powder Generation, *Proceedings of the 3rh International Symposium on Supercritical Fluids*, G. Brunner and M. Perrut (Eds.), Tome 3, Strasbourg, 1994, 229-234.
33. Palakodaty, S., York, P., Hanna, M., Pritchard, J., Crystallization of Lactose Using Solution Enhanced Dispersion by Supercritical Fluids (SEDS) Technique, *Proceedings of the 5th Meeting on Supercritical Fluids*, Materials and Natural Products Processing, M. Perrut and P. Subra (Eds.), Tome 1: Materials, Nice, 1998, 275-280.
34. Debenedetti, P., Supercritical Fluids as Particle Formation Media: From Fundamentals to Applications, *Proceedings of the 3rd Internat. Symp. on Supercritical Fluids*, M. Perrut, and G. Brunner (Eds.), Tome 3, Strasbourg, 1994, 213-216.
35. Hanna, M., York, P. *Method and Apparatus for the Formation of Particles*, *WO 95/01221*, International Publication Date 12. 01.1995.
36. Sze, T., Dehghani, F., Dillow, A., Foster, N., Applications of Dense Gases in Pharmaceutical Processing, *Proceedings of the 5th Meeting on Supercritical Fluids*, Materials and Natural Products Processing, M. Perrut and P. Subra (Eds.), Tome 1: Materials, Nice, 1998, 263-269.
37. Yeo, S., Debenedetti, P., Patro, S., Przybycien, T., Secondary Structure Characterization of Microparticle Insulin Powders, *Journal Pharm. Sci.*, 38(1994) 1651-1656.
38. Berends, E., Bruinsma, O., de Graauw, J., van Rosmalen, G., Crystallization of Phenanthrene from Toluene with Carbon Dioxide as the Anti-Solvent by the GAS-Process, *Proceedings of the 3rh International Symposium on Supercritical Fluids*, G. Brunner and M. Perrut (Eds.), 1994, Tome 3, 223-228.
39. Berends, E., Bruinsma, O., de Graauw, J., van Rosmalen, G., Crystallization of Phenanthrene from Toluene with Carbon Dioxide by the GAS Process, *AIChE J.*, 42(1996) 431.
40. Schmitt, W., Finely Divided Solid Crystalline Powers via Precipitation into an Antisolvent, Patent Application, *WO 90/03782,* 1990.
41. Gallagher P., Coffey, M., Krukonis, V., Klausustis, Gas Antisolvent Recrystallization: New Process to Recrystallize Compounds Insoluble in Supercritical Fluids, *Supercritical Fluid Science and Technology*, ACS Symposium Series 406, Chap. 33, 1988, 334-354.
42. Gallagher, P., Krukonis, V., van de Kieft, L., Gas Anti-Solvent Recrystallization: Application to the Separation and Subsequent Processing of RDX and HMX, *Proceedings of the 2nd International Symposium on Supercritical Fluids*, M. McHuch (Ed.), Boston, 1991, 45-48.
43. Gao, Y. Mulenda, T., Shi, Y.-F., Yuan, W.-K., Fine Particles Preparation of Red Lake C Pigment by Supercritical Fluid, *The 4th International*

Symposium on Supercritical Fluids, S. Saito and K. Arai (Eds.), Sendai, 1997, Vol. A, 31-34.

44. Wubbolts, F., Kersch, C., van Rosmalen, G., Semi-Batch Precipitation of Acetaminophen from Ethanol with Liquid Carbon Dioxide at a Constant Pressure, *Proceedings of the 5th Meeting on Supercritical Fluids, Materials and Natural Products Processing*, M. Perrut and P. Subra (Eds.), Tome 1: Materials, Nice, 1998, 249-256.
45 Cai, J.-G., Liao, X.-C., Zhou, Z.,-Y., Microparticle Formation and Crystallization Rate of HMX Using Supercritical Carbon Dioxide Antisolvent Recrystallization, *The 4th International Symposium on Supercritical Fluids*, S. Saito and K. Arai (Eds.), Sendai, 1997, Vol. A, 23-26.
46. Robertson, J., King, M., Seville, J., Merrifield, D., Buxton, P., Recrystallization of Organic Compounds Using Near Critical Carbon Dioxide, *The 4th International Symposium on Supercritical Fluids*, S. Saito, K. Arai (Eds.), Sendai, 1997, Vol. A, 47-50.
47. Tan, C.-S., Chang, W.-W., Precipitation of Polystyrene from Toluene with HFC-134a by the GAS Process, *Ind. Eng. Chem. Res.*, 37(1998) 1821-1826.
48. Reverchon, E., Portta, G., Di Troloi, A., Pace, S., Supercritical Antisolvent Precipitation of Nanoparticles of Superconductor Precursors, *Ind. Eng. Chem. Res.*, 37(1998) 952-958.
49. Yeo, S.-D., Debenedetti, P., Radosz, M., Schmidt, H.-W., Supercritical Antisolvent Process for Substituted Para-Linked Aromatic Polyamides: Phase Equilibrium and Morphology Study, *Macromolecules*, 26(1993) 6207-6210.
50. Randolph, T., Randolph, A., Mebes, M., Yeung, S., Sub-Micrometer-Sized Biodegradable Particles of Poly(L-Lactid Acid) via the Gas Antisolvent Spray Precipitation Process, *Biotechnol. Prog.*, 9(1993) 429-435.
51. Dixon, D., Johston, K., Bodmeier, R., Polymeric Materials Formed by Precipitation with a Compressed Fluid Anti-solvent, Materials, Interfaces and Electrochemical Phenomena, *AIChE Journal*, 39(1993) 127-139.
52. York, P., Hanna, M., Particle Engineering by Supercritical Fluid Technologies for Powder Inhalation Drug Delivery, *Proceedings of the 5th Respiratory Drug Delivery*, Phoenix, 1996, 231-240.
53. Hanna, M., York, P., Rudd, D., Beach, S., A Novel Apparatus for Controlled Particle Formation Using Supercritical Fluids, *Pharmaceutical Res.*, 12(1995) 5141.
54. Wubbolts, F., Bruinsma, O., de Graauw, J., Continuous Gas Anti-solvent Crystallisation of Hydroquinone from Acetone Using Carbon Dioxide, *The 4th International Symposium on Supercritical Fluids*, S. Saito, K. Arai (Eds.), Sendai, 1997, Vol. A, 63-66.
55. Jaarmo, S., Rantakylä, M., Aaltonen, O., Particle Tailoring with Supercritical Fluids: Production of Amorphous Pharmaceutical Particles, *The 4th International Symposium on Supercritical Fluids*, S. Saito and K. Arai (Eds.), Sendai, 1997, Vol. A, 263-266.

56. Yeo, S.-D., Lim, G.-B., Debenedetti, P., Bernstein, H., Formation of Microparticulate Protein Powders Using a Supercritical Fluid Antisolvent, *Biotechnology and Bioengineering*, 41(1993) 341-346.
57. Yeo, S.-D., Debenedetti, P., Radosz, M., Schmidt, H.-W., Supercritical Anti-Solvent (SAS) Process for a Series of Substituted Para-Linked Aromatic polyamides, *Macromolecules,* 28(1995) 1316.
58. Bodmeier, R., Wang, H., Dixon, D., Mawson, S., Johnston, K., Polymeric Microspheres Prepared by Spraying into Compressed Carbon Dioxide, *Pharmaceutical Research,* 12(1995) 1211-1217.
59. Dillow, A., Dehghani, F., Foster, N., Production of Polymeric Support Materials Using a Supercritical Fluid Gas Anti-Solvent Process, *The 4th International Symposium on Supercritical Fluids*, S. Saito, K. Arai (Eds.), Sendai, 1997, Vol. A, 247-250.
60. Rantakylä, M., Jäntti, M., Aaltonen, O., Modelling Droplet- Gas Interaction and Particle Formation in Gas-Anti-Solvent System (GAS), *Proceedings of the 5th Meeting on Supercritical Fluids, Materials and Natural Products Processing*, M. Perrut and P. Subra (Eds.), Tome 1: Materials, Nice, 1998, 333-338.
61. Tom, J., Lim, G.-B., Debenedetti, P., Prud´homme, R., Applications of Supercritical Fluids in Controlled Release of Drugs, in J.F. Brennecke and E. Kiran (Eds.) *Supercritical Fluid Engineering Science*, ACS Symp. Ser. 514, American Chemistry Society, Washington, DC, 1993, 238-257.
62. Debenedetti, P., Lim, G.-B., Prud'Homme, R., Formation of Protein Microparticles by Anti-Solvent Precipitation, *European Patent, 0 542 314 B1*, 1998.
63. Johnston, K., Luna-Barcenas, G., Dixon, D., Mawson, S., Polymeric Materials by Precipitation with a Compressed Fluid Anti-Solvent, *Proceedings. of the 3rd International Symposium on Supercritical Fluids*, M. Perrut, and G. Brunner (Eds.), Tome 3, Strasbourg, 1994, 359-364.
64. Luna-Barcenas, G., Kanakia, S., Sanchez, I., Johnston, K., Semi-Crystalline Microfibrils and Hollof Fibers by Precipitation with a Compressed Fluid Antisolvent, *Polymer,* 36(1995) 3173-3182.
65. Benedetti, L., Bertucco, A., Pallado, P., Production of Micronic Particles of Biocompatible Polymer Using Supercritical Carbon Dioxide, *Biotech. Bioeng.,* 53(1997) 232.
66. Schmitt, W., Salada, M., Shook, G., Speaker, S, Finely-Divided Powders by Carrier Solution Injection in to a Near or Supercritical Fluid, *AIChE J.*, 41(1995) 2476.
67. Reverchon, E., Della Porta, G., Celano, C., Di Trolio, A., Pace, S., Processo di Formazione di Microparticelle di Composti precursori di Supercon Duttori per Precipitazione Indotta da Fluidi Supercritici, *Ital. Patent SA97A/10*, 1997.
68. Reverchon, E., Della Porta, G., Celano, C., Pace, S., Di Trolio, A., Supercritical Antisolvent Precipitation: a New technique for Preparing Submicronic Yttrium Powder to Improve YMBO Superconductors *J. of Material. Res.*, 13(1998) 284.

69. Palakodaty, S., York, P., Hanna, M., Pritchard, J., Crystallization of Lactose Using Solution Enhanced Dispersion by Supercritical Fluids (SEDS) Technique, *Proceedings of the 5th Meeting on Supercritical Fluids, Materials and Natural Products Processing*, M. Perrut and P. Subra (Eds.), Tome 1: Materials, Nice, 1998, 275-280.
70. Sloan, R., Hollowood, M., Humpreys, G., Ashraf, W., York, P., Supercritical Fluid Processing: Preparation of Stable Protein Particles, *Proceedings of the 5th Meeting on Supercritical Fluids, Materials and Natural Products Processing*, M. Perrut and P. Subra (Eds.), Tome 1: Materials, Nice, 1998, 301-306.
71. Hanna, M., York, P., Shekunov, Y., Control of Polymorphic Forms of a Drug Substance by Solution Enhanced Dispersion by Supercritical Fluids (SEDS), *Proceedings of the 5th Meeting on Supercritical Fluids, Materials and Natural Products Processing*, M. Perrut and P. Subra (Eds.), Tome 1: Materials, Nice, 1998, 325-330.
72. Chou, Y.-H., Tomasko, D., GAS Crystallization of Polymer-Pharmaceutical Composite Particles, *The 4th International Symposium on Supercritical Fluids*, S. Saito and K. Arai (Eds.), Vol. A, Sendai, 1997, 55-57.
73. Dixon, D., Luna-Barcenas, G., Johnston, K., Microcellurar Microspheres and Microballoon by Precipitation with a Vapour-Liquid Compressed Fluid Antisolvent, *Polymer*, 35(1994) 3998.
74. Winters, M., Knutson, A., Debenedetti, P., Sparks, H., Przybycien, T., Stevenson, C., Prestelski, S., Precipitation of proteins in Supercritical Carbon Dioxide, *J. Pharm. Sci.* 85(1996) 586.
75. Angus, S., Armstrong, B., de Reuck, K., (Eds.), *International Thermodynamic Tables of the Fluid State*, Vol. 3., *Carbon Dioxide,* IUPAC, Division of Physical Chemistry, Pergamon Press, Oxford, 1976.
76. de Filippi, R., CO_2 as a Solvent: Application to Fats, Oil and Other Materials, *Chemistry and Industry*, (1982), no 6, 390-394.
77. Laitinen, A., *Remediation of Contaminated Soil by Carbon Dioxide Extraction*, Licentiate's Thesis, Helsinki University of Technology, Department of Chemical Technology, Espoo, 1998.
78. Hanna, M. York, P. Method and Apparatus for the Formation of Particles, WO 95/01221, 1995.
79. Aaltonen, O., Rantakylä, M., Biocatalysis in Supercritical CO_2, *CHEMTECH*, (1991), no 4, 240-248.
80. Bartmann, D., Scneider, M., Experimental Results and Physicochemical Aspects of Supercritical Fluid *J. Chromatogr.* 83(1973) 135-145.
81. Stahl, E., Schilz, W., Schütz, W., Willing, E., A Quick Method for the Microanalytical Evaluation of the Dissolving Power of Supercritical Gases, *Extraction with Supercritical Gases*, E. Stahl, G. Wilke (Eds.), Verlag Chemie, Weinheim, 1980, 94-114.
82. Bartle, K., Clifford, A., Jafar, S., Shilstone, G., Solubility of Solids and Liquids of Low Volatility in Supercritical Carbon Dioxide, *J. Phys. Chem. Ref. Data*, 20(1991) 713-756.

83. Suzuki, T., Tsuge, N., Nagahama, K., Solubilities of Ethanol, 1-Propanol , 2-Propanol and 1-Butanol in Supercritical Carbon Dioxide at 313 K and 333 K, *Fluid Phase Equilibria*, 67(1991) 212-226.
84. Panagiotopoulos, A., Reid, R., High-Pressure Phase Equilibria in Ternary Fluid Mixtures with a Supercritical Component, *Supercritical Fluids, Chemical and Engineering Principles and Applications*, ACS Symposium Series 329, Washington, DC, 1989, 155-129.
85. Staby, A., *Application of Supercritical Fluid techniques on Fish Oil and Alcohols*, Doctoral Thesis, Technical University of Denmark, Department of Chemical Engineering, Lyngby, 1993, 14.
86. Van Konynenburg, P., Scott, R., Critical Lines and Phase Equilibria in Binary van der Waals Mixtures, *Roy. Soc., Phil. Trans*. A298, 1442, 495-540.
87. Street, W., Phase Equilibria in Fluid and Solid Mixtures at High Pressure, In *Chemical Engineering at Supercritical Fluid Conditions*, M. E. Paulaitis, J. M. Penninger, R. D. Gray Jr. and P. Davidson (Eds.) Ann Arbor Science, Collingwood, 1983, Chap.1, 3-30.
88. McHuch, M., Krukonis, V., *Supercritical Fluid Extraction*, Second Edition, Butterworth-Heinemann, Boston, 1994, 27-85.
89. Schneider, G., Physicochemical Principle of Extraction with Supercritical Gases, in *Extraction with Supercritical Gases*, E. Stahl, G. Wilke (Eds.), Verlag Chemie, Weinheim, 1980, 45-81.
90. Kordikowski, A. Schenk, R. van Nielen, C. Peters, Volume Expansions and Vapor-Liquid Equilibria of Binary Mixtures of a Variety of Polar Solvents and Certain Near-Critical Solvents, *The Journal of Supercritical Fluids*, 8(1995) 205-216.
91. Kikic, I., Lora, M., Bertucco, A., A Thermodynamic Analysis of Three-Phase Equilibria in Binary and ternary Systems for Applications in Rapid Expansion of a Supercritical Solutions (RESS), Particles from Gas-saturated Solutions (PGSS), and Supercritical Antisolvent (SAS), *Ind. Eng. Chem. Res.*, 36(1997) 5507-5515.
92. Peng, D.-Y., Robinson, D., A New Two-Constant Equation of State, *Ind. Eng. Chem. Fundam.*, 15(1976) 59.
93. Gibbs, J. *The Collected Works of J. W. Gibbs,* Vol. I, Thermodynamics, Yale University Press, New Haven 1957, 322.
94. Adamson, A., *Physical Chemistry of Surfaces,* Interscience Publishers, Easton 1963, 288-298.
95. Hallas, N., *Crystallization Course*, Separation Processes Service, Harwell, 1990.
96. Yeo, S.-D., Choi, J.-H., Lee, T.-J., Crystal Formation of $BaCl_2$ and NH_4Cl Using a Supercritical Fluid Antisolvent, *The Journal of Supercritical Fluids*, 16(2000) 235-246.
97. Sebhatu, T., Angberg, M., Ahlneck, C., Assessment of the Degree of Disorder in Crystalline Solids by Isothermal Microcalorimetry, *Int. J., Pharm.*, 104(1994) 135-144.

98. Jaeger, P., von Schnitzler, J., Eggers, R., Interfacial Tension of Fluid Systems Considering the Nonstationary Case with Respect to Mass Transfer, *Chem. Eng. Technol.*, 19(1996) 197-202.
99. McCabe, W., Smith, J., Harriot, P., *Unit Operations of Chemical Engineering*, Fourth Edition, McGraw-Hill Book Company, Singapore, 1985, 605.
100. Schiemann, H., Weidner, E., Peter, S., Interfacial Tension in Binary Systems Containing a Dense Gas, *The Journal of Supercritical Fluids*, 6(1993) 181-189.
101. Jasper, J. The Surface Tension of Pure Liquid Compounds, *J. Phys. Chem. Ref. Data*, 1(1972) 841-984.
102. Moser, M., Pietzonka, W., Trepp,C. Interfacial Tension Measurements between α-Tocopherol and Carbon Dioxide at High Pressures. *High Pressure Chemical Engineering*, R. von Rohr and Ch. Trepp (Eds.), Elsevier Science, Amsterdam, 1996, 655-660.
103. Chun, B.-S., Wilkinson, T., Interfacial Tension in High-Pressure Carbon Dioxide Mixtures, *Ind. Eng. Chem. Res.*, 34(1995) 4371-4377.
104. Weast, R., *CRC Handbook of Chemistry and Physics*, 64th Edition, CRC Press, Inc., Florida, 1984, f-33.
105. A. Negiz, E. Lagergren, A. Cinar, Mathematical Models of Cocurrent Spray Drying, *Ind. Eng. Chem. Res.*, 34(1995) 3289-3302.
106. Mukhopadhyay, M., Dalvi, S., Prediction of Ternary Solid-Liquid-Vapor Equilibrium from PMVF of Solvent in Binary (CO_2-solvent) Mixture, Submitted to *Journal of Supercritical Fluids,* 2003.
107. Tan, C. Liang, S., Liou, D., Fluid-Solid Mass Transfer in a Supercritical Fluid Extractor, *The Chem. Eng. J.*, 38(1988) 17-22.
108. Jaeger, P., Eggers, R., Interfacial Properties and Mass Transfer in Supercritical Fluid Exteraction, *The 4th International Symposium on Supercritical Fluids*, S. Saito and K. Arai (Eds.), Volume B, 1997, Sendai, Japan, 11-14 May, 711-714.
109. Seibert, A., Moosberg, J., Bravo, H., Johnston, K., Spray, Sieve Tray and Packed High Pressure Extraction Columns-Design and Analysis, *Proceedings of International Symposium on Supercritical Fluids,* M. Perrut (Eds.), Tome 2, Nice, 1988, 561-570.
110. Simoes, P., Matos, H., Carmelo, P., de Azevedo, E., de Ponte, M., Mass Transfer in Countercurrent Packed Columns: Application to Supercritical CO_2 Extraction of Terpenes, *Ind. Eng. Chem. Res.*, 34(1995) 613-618.
111. Ferreira, S., Meireles, M., Nikolov, Z., Mass Transfer Coefficient Correlation's for SCFE of Black Pepper Essential, *The 4th International Symposium on Supercritical Fluids*, S. Saito and K. Arai (Eds.), Volume B, Sendai, 1997, 731-734.
112. Reda, M., Diffusion and Mass Transfer of Organic Solids in Supercritical CO_2, Part II: Diffusion Coefficients, *2nd International Symposium High Pressure Chemical Engineering*,. G. Vetter (Ed), 24-26 September 1990, Erlangen, 293-304.
113. Catchpole, O., Simoes, P., King, M., Bott, T., Film Mass Transfer Coefficients for Separation Processes using Near-critical CO_2, *2nd*

International Symposium High Pressure Chemical Engineering, G. Vetter (Ed.), Erlangen, 1990, 293-304.
114. Baker, J., Trebble, M., Development of an Apparatus for Mass-Transfer Studies in Supercritical Fluids, *Ind. Eng. Chem. Res.*, 37(1998) 1991-1997.
115. Debenedetti, P., Reid, R., Diffusion and Mass Transfer in Supercritical Fluids, *AIChE Journal*, 32(1986) 2034-2046.
116. Lim, G.-B., Holder, G., Shah, Y., Solid-Fluid Mass Transfer in a Packed Bed Under Supercritical Conditions, ACS Symposium Series 406, *Supercritical Fluid Science and Technology*, K. Johnston and J. Penninger (Eds.), American Chemical Society, Washington, DC, 1989, 379-395.
117. Bertucco, A., Vetter G., *High Pressure Process Technology: Fundamentals and Applications,* Elsevier Science, Amsterdam, 2001, 114-130.
118. Laitinen, A., Kaunisto, J., Supercrtical Fluid Extraction of 1-Butanol from Aqueous Solutions, *The Journal of Supercritical Fluids,* 15(1999) 245-252.
119. Hughmark, G., Liquid-Liquid Spray Column Drop Size, Holdup, and Continuous Phase Mass Transfer, *Ind. Eng. Chem. Fundam,* 6(1967) 408.
120. McCabe, W., Smith, J., Harriot, P., *Unit Operations of Chemical Engineering*, 5th Edition, McGraw-Hill Book Company, New York, 1993.
121. Liong, K., Wells, P., Foster, N., Diffusion in Supercritical Fluids, *The Journal of Supercritical Fluids*, 4(1991) 91-108.
122. Coulson, J., Richardson, J., *Chemical Engineering*, vol. 1, Third edition (SI Units), Wheaton & Co. Ltd, Exeter 1984, 279.
123. Sassiat, P., Mourier, P., Caude, M., Rosset, R., Measurement of Diffusion Coefficients in Supercritical Carbon Dioxide and Correlation with the Equation of Wilke and Chang, *Anal. Chem.*, 59(1987) 1164-1170.
124. Cassanello, M., Larachi, F., Laurent, A., Wild, G, Midoux, N, Gas-Liquid Mass Transfer in High Pressure Trickle-Bed reactors: Experiments and Modelling, *High Pressure Chemical Engineering*, R. von Rohr and Ch. Trepp (Eds.), Elsevier Science, Amsterdam, 1996, 493-498.
125. Roy, B., Goto, M., Hirose, T., Extraction of Ginger Oil with Supercritical Carbon Dioxide: Experiments and Model, *Ind. Eng. Chem. Res.*, 35(1996) 607-612.
126. Lai, C.-C., Tan, C.-S., Measurement of Effective Diffusivities of Toluene in Activated Carbon in the Presence of Supercritical Carbon Dioxide, *Ind. Eng. Chem. Res.*, 32(1993) 1717-1722.
127. Shenai, V., Hamilton, B., Matthews, M., Diffusion in Liquid and Supercritical Fluid Mixtures, *Supercritical Fluid Engineering Science: Fundamentals and Applications*, Editors, Kiran, E., Brennedke, J., ACS Symposium Series 514, American Chemical Society, Washington, DC, 1993, 92-103.
128. Silva, C., Macedo, E., Diffusion Coefficients of Ethers in Supercritical Carbon Dioxide, *Ind. Eng. Chem. Res.*, 37(1998) 1490-1498.
129. Wells, T., Fosters, N., Chaplin, R., Diffusion of Phenylacetic Acid and Vanillin in Supercritical Carbon Dioxide, *Ind. Eng. Chem. Res.*, 31(1992) 927-934.
130. Riazi, M., Whitson, C., Estimating Diffusion Coefficients of Dense Fluids, *Ind. Eng. Chem. Res.*, 32(1993) 3081-3088.

131. Reda, M., Diffusion and Mass Transfer of Organic Solids in Supercritical CO_2, Part II: Diffusion Coefficients, *2nd International Symposium High Pressure Chemical Engineering*, G. Vetter (Ed.), Erlangen, 1990, 293-304.
132 . Wilke, C., Chang, P., Correlation of Liquid Diffusion Coefficient, *AIChE J.,* 1(1955) 264-270.
133. Marrazzo, W., Merson, R., McCoy, B., Enzyme Immobilized in a Packed-Bed Reactor: Kinetic Parameters and Mass Transfer Effects, *Biotechnology and Bioengineering*, 17(1975) 1515-1528.
134. Elvassore, N., Cozzi, F., Bertucco, A., Mass Transport Modelling in Gas Antisolvent Process, *Ind. Eng. Chem. Res.,* in press, 2003.
135. Vignes, A. , Diffusion in Binary Solutions, Variation of Diffusion Coefficient with Composition, *Ind., Eng. Chem. Fundam,* 5(1966) 189.
136. Lengsfeld, C., Delplanque, J., Barocas, V., Randolph, W.T., Mechanism Governing Microparticle Morphology during Precipitation by a Compressed Antisolvent: Atomization vs. Nucleation and Growth, *J. Phys. Chem.* B104 (2000) 2725-2735.
137. Laitinen, A., Jäntti, M., Solubility of 6-Caprolactam in Supercritical Carbon Dioxide, *Journal of Chemical & Engineering Data,* 41(1996) 1418-1420.
138. Debenedetti, P., Tom, J., Kwank, X., Yeo, S, Rapid Expansion of Supercritical Solutions (RESS): Fundamentals and Applications, *Fluid Ph. Eq.*, 82(1993) 311.
139. Kwauk, X., Debenedetti, P., Mathematical Modelling of Aerosol Formation by Rapid Expansion of Supercritical Solutions in a Converging Nozzle, *J. Aerosol Sci.*, 24(1993) 445.
140. Debenedetti, P., Homogeneous Nucleation in Supercritical Fluids, *AIChE J.*, 36(1990) 1289.
141. Lele, A., Shine, A., Morphology of Polymers Precipitated from a Supercritical Solvent, *AIChE J.*, 38(1992) 724.
142. Bertucco, A., Guarise, G., Pallado, P., Corain, B., Solution Deposition in Porous Polymer Matrix from Rapid Expansion of a Supercritical Solution, *Chem. Biochem. Eng.*, 8(1994) 11.
143. Ksibi, H., Effect of Small Capillaries on the Hydrodynamic Conditions in the RESS Process, *Proceedings of the 5th Meeting on Supercritical Fluids*; Materials and Natural Products processing, M. Perrut and P. Subra (Eds.), Tome 1: Materials, Nice, 1998, 319-324.
144. Shaub, G., Brennecke, J., McCready, M., Radial Model for Particle Formation from the Rapid Expansion of Supercritical Solutions, *The Journal of Supercritical Fluids*, 8(1995) 318.
145. Reverchon, E., Pallado, P., Hydrodynamic Modelling of the RESS Process, *The Journal of Supercritical Fluids,* 9 (1996) 216.
146. Badilla, J., Peters, C, De Swaan, A., Selection of the Appropriate Combination Solvent, Antisolvent and Process Conditions for the GAS-Antisolvent Process, *Proceedings of the 5th Meeting on Supercritical Fluids;* Materials and Natural Products Processing, M. Perrut and P. Subra (Eds.), Tome 1: Materials, Nice, 1998, 237-242.

147. Werling. J., Debenedetti, P., Numerical Modelling of Mass Transfer in the Supercritical Antisolvent Process, *The Journal of Supercritical Fluids,* 16(1999) 167-181.
148. Elvassore, N., d'Aquino, S., Bertucco, A., Mass Transfer in Supercritical Antisolvent Processes: Experiments and Modelling, *Proceedings of the 4th International Symposium on High Pressure Technology and Chemical Engineering,* A. Bertucco (Ed.), Venice, Vol. 2, 2002, 815-820.
149. Werling, J., Debenedetti, P., Numerical Modelling of Mass Transfer in the Supercritical Antisolvent process: Miscible Conditions, *Journal of Supercritical Fluids,* 18(2000) 11-24.
150. Elvassore, N., Cozzi, F., Bertucco, A., Modelling of Particle Formation in Supercrtical Antisolvent Processes: Diluted and Concentrated Regime. In: *Proceedings of the 6th International Symposium on Supercritical Fluids*, Tome 3, Versailles, 2003, 1853-1858.
151. Lora, M., Bertucco, A., Kikic, I., Simulation of the Semicontinuous Supercritical Antisolvent Recrystallization Process, *Ind. Eng. Chem. Res.,* 39(2000) 1487-1496.
152. Kikic, I., Bertucco, A., Lora, M., Thermodynamics and Mass Transfer for the Simulation of Recrystallization Processes with a Supercritical Solvent, In: E. Reverchon (Ed.), *Proc. Proc. Fourth Italian Conf. On Supercritical Fluids and their Applications*, 1997, 299.
153. Shekunov, B.Y., Badylga, J., York, P., Particle Formation by Mixing with Supercritical Antisolvent at High Reynolds Number, *Chemical Engineering Science*, 56 (2001) 2321-2433.
154. Mukhopadhyay, M., Dalvi, S., Mass and Heat Transfer Analysis of SAS: Effects of Thermodynamic States and Flow rates on Droplet Size, *Journal of Supercritical Fluids,* in press, 2004.
155. Rantakylä, M., *Particle Formation in Supercritical Antisolvent Processing*, *Licentiate's Thesis*, Helsinki University of Technology, Department of Chemical Technology, Espoo, 2000.
156. Rantakylä, M., Jäntti, M., Aaltonen, O., Hurme, M., The Effect of Initial Drop Size on Particle Size in the Supercritical Antisolvent Precipitation (SAS) Technique, *Journal of Supercritical Fluids* 24(2002), pp. 251-263.
157. Rantakylä, M., Jäntti, M., Aaltonen, O., Hurme, M., The Effect of Mass Transfer on Droplet Properties in the Supercritical Antisolvent Precipitation (SAS) Technique, submitted to *Journal of Supercritical Fluids*, 2003.
158. Coulson, J., Richardson, J., *Chemical Engineering*, vol. 6, (SI Units), Pergamon, Oxford 1985, 765-769.
159. Altunin, V., Sakhabetdinov, M., Viscosity of Liquid and Gaseous Carbon Dioxide at Temperatures 220-1300 K and Pressure up to 1200 bar, *Teploenergetika,* 8(1972) 85.
160. Negiz, A., Lagergren, E., Cinar, A., Mathematical Models of Cocurrent Spray Drying, *Ind. Eng. Chem. Res.*, 34(1995) 3289.
161. Lucien, F., Foster, N., Influence of Matrix Composition on the Solubility of Hydroxybenzoic Acid Isomers in Supercritical Carbon Dioxide, *Ind. Eng. Chem. Res.*, 35(1996) 4686-4699.

162. Yaws, C., Chen, D., Yang, H.-C., Tan, L., Nico, D., Critical Properties of Chemicals, *Hydrocarbon Processing*, 68(1989), no 7, 61-64.
163. Press, W., Teukolsky, S., Vetterling, W., Flannery, B., Numerical Recipes in C, 2nd Ed., Cambridge University Press, New York, 1992.
164. Chai, J.-G., Liao, X.-C., Zhou, Z.-Y., Microparticle Formation and Crystallization Rate of HMX Using Supercritical Carbon Dioxide Antisolvent Recrystallization, *The 4th International Symposium on Supercritical Fluids*, S. Saito, K. Arai (Eds.), Sendai, 1997, Vol. A, 23-26.
165. Sovová H., Procházka, J., Calculations of Compressed Carbon Dioxide Viscosities, *Ind. Eng. Chem. Res.*, 32(1993) 3162-3169.
166. Vesovic, V., Wakeham, W., Olchowy, G., Sengers, J., Watson, J., Millat, J., The Transport Properties of Carbon Dioxide, *J. Physic. Chem. Ref. Data*, 19(1990) 763-808.
167. Steinmayer, D., Use Power/Mass to Estimate Drop Size in Gas/Liquid Contactors, *Chem. Eng. Prog.*, 91(1995) 72-80.
168. El-Shanawany, M., Lefebvre, A., Airblast Atomization: Effect of Linear Scale on Mean Drop Size, *J. Energy*, 4(1980) 184.
169. Jasuja, A., Airblast Atomization of Alternative Liquid Petroleum Fuels Under High- Pressure Conditions, *Trans. Am. Soc. Mech. Engr.*, 103(1981) 514.
170. Steinmayer, D., Gas Absorption and Gas-Liquid System Design, *Perry's Chemical Engineers, Handbook*, R. H. Perry and D. W. Green (Eds.), 7th Ed., McGraw Hill, New York 1997, 14-63 - 14-66.
171. Coulson, J., Richardson, J., *Chemical Engineering*, vol. 2, Third edition (SI Units), Pergamon, Oxford, 1985, 736.
172. Burkholder, H., Berg, J., Effect of Mass Transfer on Laminar Jet Breakup: I. Liquid Jets in Gases; II. Liquid Jets in Liquids, *AIChE Journal*, 20(1974) 863-880.
173. Coyle, R., Berg, J., Niwa, J., Liquid-Liquid Jet Breakup Under Conditions of Relative Motion, Mass Transfer and Solute Adsorption, *Chem. Eng. Sci.*, 36(1981) 19-28.
174. Hinze, J., Fundamentals of the Hydrodynamic Mechanism of Splitting in Dispersion Processes, *J. Am. Inst. Chem. Eng.*, 1(1953) 289-295.
175. Dudewicz, E., Mishra, S., *Modern Mathematical Statistics*, John Wiley, New York, 1988.
176. Coulson, J. Richardson, J., *Chemical Engineering*, Vol. 2, Third edition (SI Units), Pergamon, Oxford 1985, 610-611.
177. Lo, T., Baird, M., Hanson, C., *Handbook of Solvent Extraction*, John Wiley and Sons, 1983, 102.
178. Liu, H., Rangel, R., Lavernia, E., Modelling of Droplet-Gas Interactions in Spray Atomization of Ta-2.5W Alloy, *Material Science and Engineering*, A191(1995) 171-184.
179. Tom, J., Debenedetti, P., Formation of Bioerodible Polymer Microspheres and Microparticles by Rapid Expansion of Supercritical Solutions, *Biotechnol. Prog. 7(1991) 403-411.*

180. Bewlay, B., Cantor, B., Modelling of Spray Deposition: Measurements of Particle Size, Gas Velocity, Particle Velocity, and Spray Temperature in Gas-Atomized Sprays, *Metallurgical Transactions,* 21B(1990) 899-912.
181. Bewlay, B., Cantor, B., Gas Velocity Measurements from a Close-coupled Spray Deposition Atomizer, *Materials Science and Engineering,* A118(1989) 207-222.
182. Lefebvre, A., *Atomization and Sprays*, Hemisphere Publishing, New York 1989.
183. Mawson, S., Kanakia, S., Johnston, K., Coaxial Nozzle for Controlled of Particle Morphology in Precipitation with a Compressed Fluid Antisolvent, *J. Appl. Polym. Sci.*, 64 (1997) 2105-2118.
184. Thies, J., Müller, B., Size Controlled Production of Biodegradable Microparticles with Supercritical Gases, *Eur. J. Parm. Biopharm*., 45 (1998) 67-74.
185. Tu, L.S., Dehghani, F., Foster, N., Micronization and Microencapsulation of Pharmaceuticals Using a Carbon Dioxide Antisolvent, *Powder Technology*, 126 (2002) 134-149.
186. Taki, S., Badeus, E., Charbit, G., Controlled Release System Formed by Supercritical Antisolvent Coprecipitation of a Herbicide and a Biodegradable Polymer, *J. Supercrit. Fluids*, 21 (2001) 61-70.
187. Goa, Y., Mulenda, T., Shi, Y.-F., Yuan, W.-K., Fine Particles Preparation of Red Lake C Pigment by Supercritical Fluid, *Journal of Supercritical Fluids*, 13(1998) 369.
188. Kröber, H., Teipel, U., Materials Processing with Supercritical Antisolvent Precipitation: Process Parameters and Morphology of Tartaric Acid, *Journal of Supercritical Fluids*, 22(2002) 229-235.
189. Aaltonen, O., Rantakylä, M., Alkio, M., Selective Crystallization of Cholesterol from SC-CO_2, *Proceedings of the 6th Conference on Supercritical Fluids and Their Applications*, E. Reverchon (Ed.), Maiori, 2001, 35-40.
190. Perrut, M., Jung, J., Leboeuf, F., Solid State Morphology of Particles Prepared by a Supercritical Fluid Process, *Proceedings of the 4th International Symposium on High Pressure Technology and Chemical Engineering,* A. Bertucco (Ed.), 2002, Venice, Vol. 2, 711-716.
191. Reynolds, J., Sodium Cromoglycate and Related Anti-Allergic Agents*, The Extra Pharmacopoeia*, 29th editon, The Pharmaceutical Press, London 1989, 1419-1422.
192. Rantakylä, M., Aaltonen, O., Hurme, M., The Estimation of Capital Costs of a Supercritical Antisolvent (SAS) Particle Production Process*, Proceedings of the 8th Meeting on Supercritical Fluids*, Chemical Reactivity and Material Processing in Supercritical Fluids, M. Mesnard and F. Cansell (Eds.), Bordeaux, 2002, Tome 2, 793-798.
193. Rantakylä, M., Aaltonen, O., Hurme, M., Cost Study of a Supercritical Antisolvent (SAS) Particle Production Process, Proceedings of the 4th International Symposium on High Pressure Process Technology and Chemical Engineering, A. Bertucco (Ed.), *Chemical Engineering Transactions*, Vol. 2, AIDIC, Milano, 2002, 525-530.

194. Bertucco, A., Striolo, A., Zanette, F., Precipitation by Supercritical Anri-solvent, Alberto Bertucco and Gerhard Vetter (Eds.) *High Pressure Process Technology: Fundamentals and Applications,* Elsevier Science, Amsterdam, 2001, 460-471.
195. Thiering, R., Dehghani, F., Foster, N., Current Issues Relating to Anti-solvent Micronisation Techniques and Their Extension to Industrial Scales, *Journal of Supercritical Fluids*, 21(2001) 159-177.
196. Perrut, M., Supercritical Fluid Applications: Industrial Developments and Economic Issues, *Ind. Eng. Chem. Res.,* 39(2000) 4531-4535.
197. Clavier, J., Majewski, W., Perrut, M., *High Pressure Chemical Engineering*, R. Rohr and C. Trepp (Eds.), Elsevier Science, 1996, 639-644.
198. Weber, A., Tschernjaew, J., Berger, T., Bork, M., A Production Plant for GAS Antisolvent Crystallization, *Proceedings of the 5th Meeting on Supercritical Fluids;* Materials and Natural Products Processing, M. Perrut and P. Subra (Eds.), Tome 1: Materials, 1998, Nice, 1997, 281-285.
199. Nieuwouldt, J., Crause, M., Rand, M., Supercritical Fractionation vs. Competing Processes: an Operating Cost Comparison, *Proceedings from 6th Conference on Supercritical Fluids and Their Applications*, E. Reverchon (Ed.), 2001, 69-74.
200. Chordia, L., White, C., Process Economics for De-Oiling Lecithin, *The 4th International Symposium on Supercritical Fluids*, S. Saito and K. Arai (Eds.), Sendai, 1997, Vol. A, 489-492.
201. Novak, R, Robey, R., Supercritical Fluid Extraction of Flavoring Material, Design and Economics, *Supercritical Fluid Science and Technology*, ACS Symposium Series 406, Chap. 33, 1988, 511-524.
202. Lack, E., Seidlitz, Economics of High Pressure Processes, Alberto Bertucco and Gerhard Vetter (Eds.) *High Pressure Process Technology: Fundamentals and Applications,* Elsevier Science, Amsterdam, 2001, 437-440.
203. Aaltonen, O., VTT Processes*, http://www.vtt.fi/pro/pro6/compressed/indappl.htm*, 11.6.2003.
204. SITEC-Sieber Engineering AG, *http://www.sitec-hp.ch/SITEC/index.htm,* 25.3.2004.
205. Jung, J., Leboeul, F., Francais, E., Clavier, J.-Y., Perrut, M., Equipment Design for Supercritical Fluid Micronization in Compliance with GMP for Pharmaceutical Applications, Chemical Engineering Transactions, *Proceedings of the 4th International Symposium on High Pressure Technology and Chemical Engineering,* A. Bertucco (Ed.), Venice, 2002, Vol. 2, 459-464.
206. Lavipharm Corporation, *http://www.lavipharm.com/us/home_com.html*, 25.3.2004.
207. Thar Technogies, Inc*., http://www.thartech.com*, 16.10.2004.
208. Nektar, Inc., *http://www.nektar.com/index.php,* 25.3.2004.
209. Reverchon, E., De Marco, I., Caputo, G., Della Porta, G., Pilot Scale Micronization of Amoxicillin by Supercritical Antisolvent Precipitation, *Journal of Supercritical Fluids*, 23(2003) 1-7.

210. Reverchon, E., Caputoa, G., Correrab, S., Cestic, P., Synthesis of Titanium Hydroxide Nanoparticles in Supercritical Carbon Dioxide on the Pilot Scale, *Journal of Supercritical Fluids*, 26(2003) 253-261.
211. Muhrer, G., Mazzotti, M., Müller, M., Gas Antisolvent Recrystallization of an Organic Compound. Tailoring Product PSD and Scaling, *Journal of Supercritical Fluids,* 27(2003) 195-203.
212. Thiering, R., Hofland, G., Foster, N., Witkamp, G., van de Wielen, L., Fractionation of Soybean Proteins with Pressurised Carbon Dioxide as a Volatile Electrolyte*, Biotech. Bioeng*, 73 (2001) 1-11.
213. Weider,E., Steiner, R., Knez, Z., Powder Generation from Polyethylene with Compressible Fluids, in: P. Rodolf von Rohr, C. Trepp (Eds.), *High Pressure Chemical Engineering,* Process Technology Proceeding, Vol. 12, Elsevier Science, Oxford 1996, 223-228.
214. Perry, J.H., *Chemical Engineering Handbook*, Seventh ed., McGraw-Hill Book Company, Inc., New York 1997, 9-68.
215. Parvinen, L., Chematur Engineering Oy, 1999, in: Rouhiainen, L, *Purification of a Drug by Using Supercritical Chromatography*, Master's Thesis, Helsinki University of Technology, Department of Chemical Technology, Espoo 1999.

APPENDIX I

The structural formulas of nalmefene HCl, oxybutynine HCl, clonidine base and clonidine

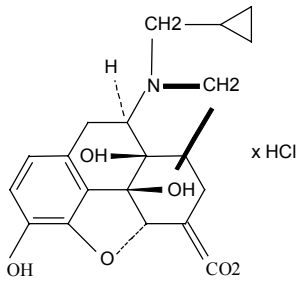

Nalmefene HCl
Mw = 375.9 g/mol

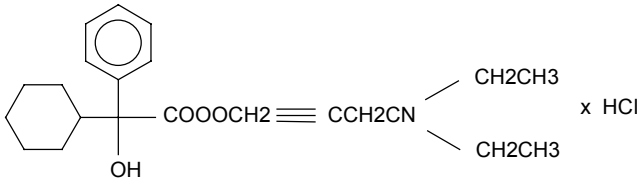

Oxybutynine HCl
Mw = 393.97 g/mol

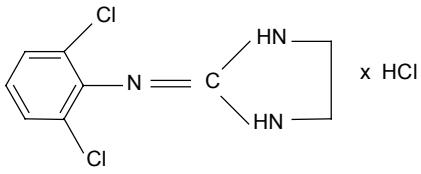

Clonidine HCl
Mw = 266.56 g/mol

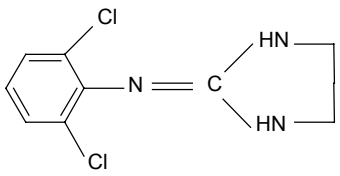

Clonidine base
Mw = 230.10 g/mol

APPENDIX II

The structural formulas of sodium cromoglycate, cholesterol, C20-iso-cholesterol and tripalmitin.

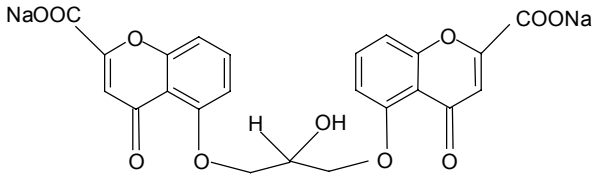

Sodium cromoglycate
Mw = 512.3 g/mol

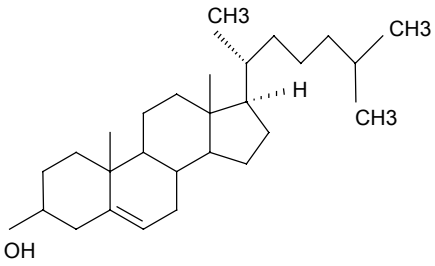

Cholesterol
Mp = 422 K

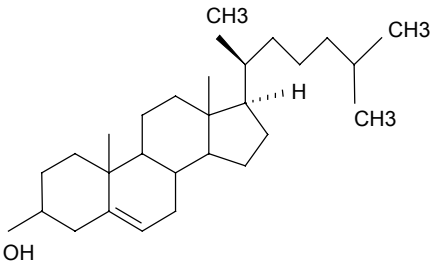

C20-iso-cholesterol
Mp = 422 K

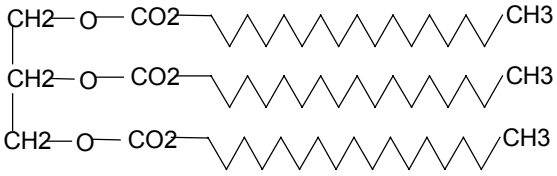

Tripalmitin
Mp = 339 K